Universidade de Lisboa
Faculdade de Ciências
Departamento de Física

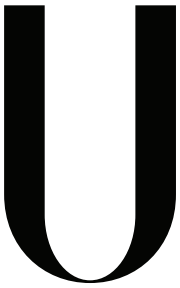

Development of a beamline high speed atomic force microscope and tuning of a mechanical oscillator via a force feedback strategy

Miguel Vargas Vitorino

Dissertação
Mestrado Integrado em Engenharia Física

2014

Universidade de Lisboa
Faculdade de Ciências
Departamento de Física

Development of a beamline high speed atomic force microscope and tuning of a mechanical oscillator via a force feedback strategy

Miguel Vargas Vitorino

Dissertação
Mestrado Integrado em Engenharia Física

Orientador: Doutor Mário Rodrigues

2014

Contents

List of Figures

Abstract

The Atomic Force Microscope (AFM) has had a predominant role in the exploration of the nano world. It has profited from several technical and theoretical improvements to become present across the study of soft matter. There are, however, still some non-visited possibilities such as the combination with other nanoscale analysis techniques, specifically, X-ray characterization.

This Thesis concerns the work done in an internship performed at the European Synchrotron Radiation Facility.

Its main task relates to the project of a new type of AFM, targeting the fusion of the microscope with X-ray scattering techniques. The AFM also addresses the analysis of matter at time scales compatible with many biological phenomena (1s).

The first chapter introduces the AFM and X-ray analysis, justifying and motivating the construction of this new instrument. In the second chapter are explained the challenges associated with the combination of high speed AFM and X-Rays techniques, such as the extremely small sample space or high mechanical stability. In the third chapter the commissioning of the microscope is presented, and also some tests, calibrations and different measurements. It is shown that the microscope can successfully do *ex-situ* images of soft matter samples at high speed.

The fourth chapter concerns the second task performed during the internship. It is shown that the strategy of force feedback can be used to tune the dynamic properties (resonance frequency and quality factor) of nano- and micromechanical oscillators. The tuning ranges obtained surpass the ones achieved through other techniques.

Finally, the fifth chapter presents a revision of the beamline high speed AFM. It details the next stages of development with the purpose of making *in-situ* experiments. A reflection is made over the different choices taken throughout the project.

Keywords: Atomic Force Microscopy, X-Ray Spectroscopy, Soft Matter, Instrumentation.

Sumário

O microscópio de força atómica (AFM) tem tido um papel preponderante na exploração de fenómenos à escala do nanómetro. Alvo de diversas melhorias, o microscópio tornou-se transversal no estudo da matéria mole. No entanto, existem ainda potencialidades não exploradas no uso deste instrumento como a combinação com outras técnicas de análise à nano escala, nomeadamente, técnicas de caracterização com Raios-X.

Esta Tese trata o trabalho realizado num estágio no Instituto Europeu de Radiação de Sincrotrão.

A principal parte da mesma visa o projecto de um novo tipo de AFM, que alia o microscópio com técnicas de difracção de Raios-X. Promete ainda a capacidade de analisar a matéria a escalas de tempo da ordem do segundo.

O primeiro capítulo introduz o AFM e as técnicas de Raios-X, e motiva a construção deste novo instrumento. No segundo capítulo são explicados os desafios introduzidos pela combinação dos instrumentos, como o espaço para amostra extremamente pequeno ou a elevada estabilidade mecânica. No terceiro capítulo são apresentadas a montagem do instrumento, seus testes e adaptações necessárias. Comprova-se o seu bom funcionamento mostrando-se que o microscópio é capaz de fazer imagens de matéria mole a alta velocidade.

O quarto capítulo concerne outra investigação executada durante o estágio. Nele mostra-se que o mecanismo de retroacção em força pode ser usado para controlar as propriedades dinâmicas (frequência de ressonância e factor de qualidade) de micro- e nano-osciladores mecânicos. A gama de controlo alcançada ultrapassa aquela obtida através de outras técnicas para desenvolvidas para o mesmo efeito.

Finalmente, no quinto capítulo é feita uma revisão do AFM de alta velocidade, elencando as próximas etapas que o levarão à utilização na linha de feixe. São enumerados os diversos pontos a melhorar e é feita uma reflexão sobre as opções tomadas ao longo do trabalho.

Palavras-Chave: Microscopia de Força Atómica, Espectroscopia de Raios-X, Matéria Mole, Instrumentação

Resumo

A popularização das técnicas de análise de fenómenos à escala do nanómetro tem beneficiado fortemente dos avanços tecnológicos e científicos nesta área. Por exemplo, a microscopia de força atómica tem sofrido melhorias constantes da sua performance desde a sua introdução. A optimização da sua sonda, do método de detecção ou da sistematização teórica do seu funcionamento contribuíram para a sua disseminação pela indústria especializada e pela ciência. Em especial na área da Biologia, a microscopia de força atómica constitui uma das poucas técnicas de análise não-invasiva à nano escala.

Nos últimos anos, o desenvolvimento do microscópio de força atómica (AFM) não tem abrandado. Podem-se destacar três destes domínios de expansão que irão ser abordados nesta Tese. O aumento da velocidade de medida do microscópio, que permite investigar fenómenos inacessíveis com o AFM convencional. A combinação da microscopia de força atómica com as técnicas de caracterização por Raios-X permite colmatar as deficiências das duas técnicas correlacionando as suas medidas. Por fim, a tecnologia de retroacção em força, que oferece uma resolução em força superior à do microscópio convencional e permite o estudo das características mecânicas da amostra em função da frequência de excitação da sonda do AFM. Estes configuram, pela sua novidade, protótipos de novos e melhorados AFMs.

Esta tese, orientada pelo Dr. Mário Rodrigues, concerne o trabalho desenvolvido ao longo de um estágio de sete meses e meio no seio do *Surface Science Laboratory*, pertencente ao *European Synchrotron Radiation Facility*. O estágio teve o acompanhamento do Dr. Fabio Comin e pelo Dr. Luca Costa.

O trabalho concerne a expansão das capacidades da microscopia de força atómica para aplicação ao estudo de fenómenos inacessíveis com o microscópio convencional. Neste contexto, pode ser dividido em dois temas. Por um lado foi objectivo criar um microscópio de força atómica que fosse capaz de ser integrado numa linha de feixe específica do Sincrotrão, a ID13, e que realizasse imagens a alta velocidade. Esta é uma linha de feixe especializada na análise de matéria mole. Por outro, o trabalho abordou a utilização da

metodologia da microscopia de retroacção em força para controlar as propriedades dinâmicas de diferentes osciladores mecânicos.

Apesar do gigante impacto que os Raios-X tiveram na ciência e tecnologia ao longo do último século, estas carecem ainda de um carácter de análise local que só será possível obter tornando os feixes cada vez mais pequenos. Um esforço para os reduzir tem sido levado a cabo nas últimas décadas, mas a resolução espacial de uma experiência com este tipo de radiação ainda não ultrapassa as centenas de nanómetros. Este valor não se compara à resolução recorrentemente obtida com outras técnicas baseadas nos microscópios por varrimento de sonda ou pelo microscópio electrónico de varrimento, que conseguem obter de forma rotineira uma resolução melhor que a do nanómetro. As técnicas de Raios-X também não oferecem geralmente a capacidade de manipulação mecânica da amostra. Surge assim a necessidade de levar a cabo uma combinação com um outro instrumento capaz de obter este tipo de informação. Um instrumento perfeito para obter caracterização de superfícies e de manipulá-las à nano escala é o AFM. Esta combinação, o X-AFM, tem sido já tentada ao longo dos últimos anos, tendo obtido resultados interessantes. No entanto, os X-AFMs apresentados não abordam a dinâmica das amostras em estudo, um campo aberto pela primeira vez pelo AFM de alta velocidade. Este é o único instrumento que permite inspeccionar directamente à nano escala fenómenos biológicos com escalas de tempo inferiores ao segundo, de forma não-invasiva,. Torna-se portanto interessante incorporar a tecnologia de alta velocidade no X-AFM, perfazendo assim o tema central desta tese, o *High Speed X-AFM* (HSX-AFM). Identificam-se três áreas-chave em que o novo instrumento poderá ser útil a curto-prazo. O estudo dos efeitos da radiação em amostras de matéria mole em tempo real (da ordem do segundo), o uso do novo instrumento como localizador de um feixe de Raios-X e a sua utilização para fins de nano manipulação sob iluminação deste tipo de radiação.

O ponto de partida da construção do instrumento é o enquadramento técnico dos requisitos de cada componente que dele faz parte. O HSX-AFM, sendo um instrumento complexo que irá ser instalado num ambiente exigente como uma linha de feixe, tem um conjunto de parâmetros que terão que ser respeitados no seu desenho. Primeiro, as consequências do ambiente da linha de feixe no AFM: o microscópio terá que ser leve, extremamente fino na direcção de propagação dos Raios-X e terá que acomodar a propagação do feixe desde o último elemento óptico até aos detectores, através da amostra. Em seguida, os elementos a ser tomados em conta para atingir um AFM de alta velocidade: é necessário empregar cantilevers pequenos, *scanners* ultra rápidos, dispositivos de focagem de laser específicos e esquemas de controlo, leitura e geração sinais electrónicos a alta velocidade.

Estes parâmetros de desenho são aplicados no projecto do microscópio. A estratégia de desenho consistiu em dividir o instrumento em três elementos funcionais (sistema de varrimento da amostra, sistema de detecção do cantilever e base do AFM) e aplicar os diferentes constrangimentos. Uma série de opções de desenho tiveram que ser tomadas, como a adopção do esquema de detecção por interferometria ou a opção por um *scanner* simétrico que garantisse estabilidade quando o microscópio fosse utilizado na linha de feixe. Na presente Tese todas as partes do microscópio são abordadas, e são mostrados os desenhos gerados através de *software* de projecto 3D, posteriormente enviados para manufactura.

Após o fabrico das partes desenhadas procedeu-se à montagem, calibração e uso *ex-situ* do instrumento. As variáveis de medida numa experiência de AFM foram detectadas, seguindo-se várias optimizações, adaptações e calibrações. Aumentou-se progressivamente a dificuldade da medida feita, fazendo estudos sobre diferentes amostras biológicas (DNA e monocamadas lipídicas), a diferentes velocidades. Depois de obtido um funcionamento aceitável do microscópio foi feito um estudo comparativo de uma amostra biológica, entre um microscópio comercial e o HSX-AFM. O objectivo do projecto foi atingido: o microscópio é capaz de gerar imagens de matéria mole a alta velocidade e cumpre as especificações necessárias à sua introdução na linha de feixe ID13.

O funcionamento do HSX-AFM à data da conclusão do estágio pode ser considerado satisfatório. Mas, apesar de ser possível a realização de imagens a alta velocidade, podem ser identificados diversos vectores a trabalhar para melhorar a sua performance, numa primeira fase de *upgrade*. Incluem-se aqui a instalação do conjunto de motores em falta à data da conclusão do trabalho, uma calibração completa do *scanner* e a optimização do sistema de focagem do laser. Após esta fase, o instrumento poderá ser introduzido na linha de feixe para realização de diversas experiências, como a investigação do efeito da radiação em tempo real em tecidos biológicos ou a nano manipulação de uma amostra sob incidência de Raios-X. Pode também ser considerada uma segunda fase de *upgrade* das capacidades do instrumento, a realizar num futuro de médio prazo. Nesta incluem-se o desenho de um *scanner* com características complementares, a adaptação de sistemas de controlo mais eficazes ou a construção de uma câmara reguladora da humidade. O instrumento deverá ser, quando este planeamento for executado, uma ferramenta importante de análise científica de matéria mole à nano escala.

No entanto, o projecto de um instrumento acarreta sempre interrupções no fluxo de trabalho. Durante os períodos de pausa na construção houve tempo suficiente para fazer uma investigação paralela, aproveitando as capacidades do autor previamente desenvolvidas no domínio da microscopia de

retroacção em força. Este tipo de microscopia apresenta diversas valências que melhoram o funcionamento do AFM. Por exemplo, a melhor resolução em força, a medição simultânea da força, do seu gradiente e da dissipação numa medida de AFM, ou a possibilidade de a fazer com frequências de excitação diferentes das associadas aos modos de vibração do cantilever. Um mecanismo subjacente a estas capacidades é a possibilidade de alterar artificialmente a frequência de ressonância e o factor de qualidade de osciladores mecânicos, o que pode ser interessante para um conjunto bastante diverso de aplicações não restringido à microscopia. Por esta razão durante o estágio foi feita uma sistematização das capacidades da metodologia FFM neste domínio. O método foi testado para diferentes tipos de osciladores (com variados tamanhos e frequências de oscilação), com diferentes tipos de actuação (capacitiva e fototérmica) e em diferentes ambientes (ar e líquido). Quando comparados com resultados de outros métodos, esta abordagem fornece uma capacidade de ajustar a frequência de ressonância e factor de qualidade num intervalo muito maior. Devido aos resultados entusiasmantes encontrados, esta investigação deu origem a um manuscrito que se encontra em revisão para publicação na revista científica *Scientific Reports*. A motivação, procedimentos e resultados deste trabalho encontram-se nesta Tese.

Acknowledgments

A time to acknowledge and thank the ones involved in this project is due. Firstly, I wish to thank my supervisor, teacher and guide, Mário Rodrigues, who taught me and showed me what is to be a true scientist in the last two years, and showed me that to explore Nature you have to get your hands dirty, burn "piezos", inhale a good amount of glue and that ultimately it will be both painful and pleasurable. To Fabio Comin, whose advice and guidance proved to be always insightful. His confidence in me was always inspiring and ultimately fundamental to the project, and I think my future too. Luca Costa, with who I worked directly on the HSX-AFM, proved to be an amazing teacher and kept pushing on me to excel myself in whatever I was doing. To all of the scientists and engineers that participated in the project, Alain Panzarella, Pascal Bernard, Olivier Hignette and the crew of ID13. A special thanks to the whole Surface Science Lab crew, for the stimulating environment and open discussions about the project, Science, and Life. Many thanks to the European Synchrotron Radiation Facility and Centro da Física da Matéria Condensada, Universidade de Lisboa, institutions that participated, shaped and sponsored my short scientific career from its beginning. Without their support all the work done here would be simply impossible. To all of the Teachers who in one way or the other contributed to my academic formation, especially to Margarida Godinho, who in my view accompanied me closely throughout most of the period that ends now. The rigour, hard work capability and psychological and physical resistance, which I acquired during my years in the Faculty will remain with me forever and I hope will prove valuable in the future.

To my Father, Mother, Brother and Sisters, that always supported me even when I was thousands of kilometers away, and never let me feel alone.

And, last but not least, to the ones who put up with my craziness: Ana, Isabel, André and Laura.

I don't know anything,
but I do know that
everything is interesting
if you go into it deeply enough.

RICHARD P. FEYNMAN

Chapter 1

Introduction

Throughout time, the history of the humankind has been immersed and influenced by a convoluted mixture of different characters, behaviors, happenings, different events caused by Man or not, and, certainly important, by pure chance. But, we can say, that no other entity has influenced more the destiny of the species, since its dawn, than the particular characteristic of humans to pursuit the comprehension of its surroundings, pushing the frontier of the unknown further and further. This behavior, objectified by different attempts and approaches like Religion, Philosophy, Science or Politics, has been present in the origin of crucial aspects of our "culture", like Language, Technology and Engineering, Social Constructions and Art.

Science has had, among the mentioned approaches, the most visible impact in the recent millennia. Since the Ancient Greeks pondered about the nature of the bright objects in the skies, it has been linked with every revolution in human thought and behavior, and it permitted the dominance of the species over the environment like no other. And in every discovery, theorization, thought or work in the history of Science, this pleasure of finding things out, like Richard P. Feynman would put it, has been present: from Newton's thoughts on the behavior of the objects above, to Darwin's explanation of the origin of the species, covering every branch of Science, whether it be in Biology, Chemistry, Physics, Psychology or the Social Sciences.

Evolution in Science has had a clear trend in regard to this principle. Because Science is ultimately an activity of observation, the first phenomena analyzed and explained were at the human scale of length and time. But along the history of scientific discovery, one can see that the quantity and quality of Science output increases substantially in some specific periods of history (the Renaissance, the late 19th and early 20th centuries and other periods of enlightenment). These, in my view, correspond to periods where a new tool enables the study of a whole new range of phenomena. These

new phenomena tended to be naturally on the frontiers of human reach: what would happen to Galileo and Newton without a telescope, where would modern Biology go without the development of X-Ray diffraction, would quantum phenomena be accessible without the interest over gas discharge tubes? The pursuit of new, unexplained phenomena has always been accompanied by the invention of new methods and instruments, and these are, and must be, a more and more important part of scientific research in the current age of Science, and will be even more in the years to come.

1.1 A little giant called Atomic Force Microscope

One of the trends over the last centuries in Science has been to investigate the very small. An example can be found in the evolution towards Particle Physics or Microbiology, evidencing the continuous miniaturization of Physics and Biology in the latest years. In these "fights", the obvious questions have been addressed since the beginning: what is the fundamental unit (of matter, of life, etc) and how does this fundamental unit explain the macroscopic phenomena already observable? In regards to Physics, this unit of intense study has been the atom.

The study of the atom, what is its composition, how does it interact with other atoms, has been without a doubt one of the more important and prolific subjects of Physics in the last two centuries, producing the most important technological advancements in the history of Mankind. To verify this, one can look at the changes in quality of living of the average person over the period of these most recent investigations and compare it with any other period in history.

It is therefore no wonder that scientists have been developing techniques and instruments in this period to study the very small better and better. The development of microscopy was a result of this, with new techniques being explored to observe matter at a small scale. The "departure" on this "trip" was the Optical Microscope and, by perfecting our understanding and expertise of optics, mankind reached new worlds. Many other followed, like the Electron Microscope. Feynman predicted, in his lecture "Plenty of Room at the Bottom" [4] that the fundamental questions and problems of Biology (and others) at the time could be solved if physicists and engineers dedicated themselves to inventing new ways to see and manipulate the very small. He predicted a revolution in this field of, how he baptized it, the small world. Twenty years later, in 1982 and four years after in 1986, Binnig et al. invented

the instruments that would revolutionize Science for the next decades: the Scanning Tunneling Microscope (STM) [5] and the Atomic Force Microscope (AFM) [6].

Both instruments fall in the general designation of the Scanning Probe Microscope (SPM). The name comes from the detection mechanism: a probe, usually a very sharp tip, is approximated very close to the sample object of the measurement. This probe interacts with the atoms of the surface of the sample in some way, and this interaction is recorded. It is exactly the conception of this probe that allowed for the detection of single atoms: while in other microscopy techniques the resolution would be limited by the wavelength of the radiation used, by employing a very sharp tip we are effectively limiting the object of measurement to the interaction of the sample surface with only a few atoms of this tip. The type of interaction is detailed in the name of the instruments: in STM it is measured the tunneling of electrons between a flat conductive sample and the tip, with a certain voltage applied between them. Correlating this measurement with the position of the tip over the surface, the topography of the sample is obtained.

What makes the AFM so special, and promising, is precisely the object of study it offers to an user: the force at the atomic scale. In an AFM, the sensor is a cantilever, a beam that is fixed in one end and left free in the other. In this free end of the cantilever is attached the very sharp tip. When the tip approaches the sample, a force between the atoms of the sample and the atoms of the tip will cause the cantilever to bend. For a cantilever with a rectangular cross-section, an applied force, F, will cause a deflection, Z_c [7, 8]:

$$F = k_{\mathrm{c}} Z_{\mathrm{c}} = \frac{E w t^3}{4L^3} Z_{\mathrm{c}} \tag{1.1}$$

being E the Young Modulus of the cantilever, w its width, t its thickness and L its length (see Figure 1.1 for a sketch with these quantities). This deflection can be detected in several ways, but originally it was detected using an STM measuring the displacement of the cantilever. Measuring the behavior of the cantilever while scanning the tip over the sample it is possible to obtain a direct measurement of the profile of the sample, since this force will depend on the distance between the two bodies [9]. But not only for inspecting the topography the AFM is used: the concept of force, has been in the foundation of Modern Science and the force between two atoms is at the basis of our understanding of a gigantic number of phenomena [10, 11, 7]. With the invention of the AFM, a multitude of experiments were made possible and carried on by the community in the most diverse fields of Science. Today it is a recurrent tool in Surface Science, Condensed Matter, Magnetism, Biology,

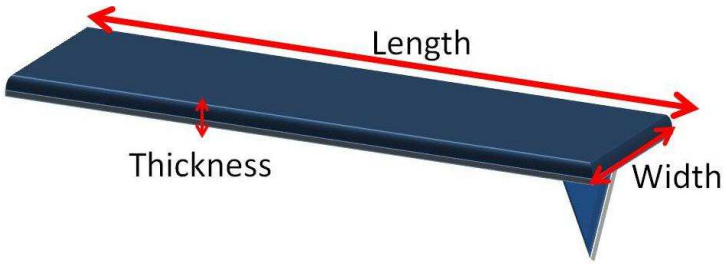

Figure 1.1: Representation of a cantilever used in an AFM measurement.

Chemistry and many more [11, 12, 13, 14].

Over the last thirty years AFM has gone from being a promising, but uncertain technique, to being fully established in the community as a central instrument in the lab. Its history, in my view, can be divided in three main periods, somehow overlapping, but each with a clear distinguishing character: a period of conception and development; a period of both a diversification of its use in different areas and a full conceptual understanding of the instrument; and, finally, a period where several approaches of improving its performance were attempted and achieved.

The first period starts with the invention of the microscope. The main interest that drove investigations at this time was the observation of atomic resolution, particularly on Silicon, since this proved to be a particularly difficult challenge. One year after the introduction of the AFM to the community, Martin et al. [15] introduced the dynamic operation of the cantilever with the Amplitude-Modulation Mode (AM-AFM) and years later Albrecht et al. proposed another type of dynamic actuation, known as Frequency-Modulation Mode (FM-AFM)[16]. Different technical improvements, like the use of an optical beam deflection detection scheme and micro-fabricated cantilevers, allowed for an increasing dissemination of the AFM across Science, and the first measurements in liquids and with biological samples started to appear. Atomic resolution on Silicon was firstly obtained in 1995 by Giessibl [17], using the Frequency Modulation technique in ultra-high vacuum.

It is important to properly introduce this measurement modes, as they will be used recurrently throughout this text. In the dynamic modes the cantilever is excited by a sinusoidal, time-periodic force. An usual approximation to describe the behavior of the cantilever in an experiment is made by assuming the cantilever a point mass-spring system with damping. The cantilever motion, when in absence of any tip-sample forces, can be somewhat approximated by that of an harmonic oscillator [8, 18]:

$$m\ddot{x} + \gamma\dot{x} + kx = F_0 \cos(\omega t) \tag{1.2}$$

with m, γ and ω respectively, the effective mass of the cantilever, its damping coefficient and the frequency of this periodic force. The harmonic oscillator can be described in terms of its natural frequency and quality factor, defined respectively as $\omega_0 = \sqrt{k/m}$ and $Q = \sqrt{mk}/\gamma$. The steady state solution of 1.2 takes the form of:

$$x = Acos(\omega t - \phi) \tag{1.3}$$

with amplitude

$$A = \frac{F_0}{\sqrt{(k - m\omega^2)^2 + \gamma^2\omega^2}} = \frac{F_0/m}{\sqrt{(\omega_0^2 - \omega^2)^2 + (\omega\omega_0/Q)^2}} \tag{1.4}$$

and phase given by

$$\tan\phi = \frac{\gamma\omega}{k - m\omega^2} = \frac{\omega\omega_0/Q}{\omega_0^2 - \omega^2} \tag{1.5}$$

The maximum amplitude will occur for the new resonant frequency, that will be given by:

$$\omega_r = \sqrt{\frac{k}{m} - \frac{\gamma^2}{2m^2}} = \omega_0\sqrt{1 - \frac{1}{2Q^2}} \tag{1.6}$$

In air or vacuum, the resonance frequency coincides with the natural frequency of the oscillator, due to the low damping in this media. This is not, however, the case in liquids [8].

To account for the tip-sample interaction one needs to add a term F_{ts} on the right side of equation 1.2 describing its change with the tip-sample distance. However, this dependence can be quite complex. The most simple description is the Lennard-Jones potential, describing the interaction between two atoms [9], but it is not a complete description of the system. Several types of interaction have to be accounted for: electrostatic, magnetic, van der waals, chemical and short range repulsion forces are all ultimately electromagnetic based. One can also detail capillary forces or viscous interactions, and that is just for an experiment done in air. For experiments in liquid like it is usual for the analysis of biologic matter, interactions with the media must also be considered. Finally, the geometry of the interacting bodies also plays a key role.

Despite this complexity, one can make the assumption that the total force will depend linearly with the distance, provided the tip oscillation amplitude is kept low enough. This is usually called the small oscillation regime. In this

case, the interaction force can be written as the first order Taylor expansion around a particular point z_0, where it is evaluated:

$$F_{ts}(z) = F_{ts}(z_0) + \left(\frac{dF_{ts}}{dz}\right)_{z_0} x \tag{1.7}$$

where x here represents the small movement around z_0. Thus we have

$$m\ddot{x} + \gamma\dot{x} + kx = F_0\cos(\omega t) + F_{ts}(z_0) + \left(\frac{dF_{ts}}{dz}\right)_{z_0} x \tag{1.8}$$

This will lead in practice to a new dynamical behavior characterized by a new resonance frequency that can be captured by equations 1.4 and 1.5 if we admit an effective spring constant $k_{\text{eff}} = k - (dF_{ts}/dz)_{z_0}$. If one oscillates at a certain fixed frequency, since with the approximation of the sample to the tip this gradient will change, the resulting oscillating amplitude will also change, to greater or smaller values depending on the interaction and the frequency chosen. It is this effect that is used in the dynamic modes of AFM: in AM-AFM, the value of the amplitude is monitored and fed to a controller that regulates the distance between the sample and the tip. To keep the amplitude constant throughout a measurement, the position of the sample (or the tip) is changed. The output of the feedback loop is the resulting displacement that, arranged point by point, will form a 3D image of the sample topography. In FM-AFM it is the shift in resonant frequency that is measured and controlled to form the image. One should note that this simple description of an AFM measurement can and should be improved by dropping some assumptions made up to here, namely the fact that there is no energy transferred to the sample in each oscillation. This can be accounted by including a damping factor that depends on the speed of the movement, $\gamma_i\dot{x}$, and applying the same reasoning for an effective damping coefficient γ_{eff}. Nevertheless, most of the experiments done in AFM, and all the ones presented in this thesis, are not made in this regime of low amplitude. When oscillating with higher amplitudes the first order Taylor approximation made will no longer be valid, and a more complex description is needed. The interaction force will also drive the cantilever at higher modes, and the information of the tip-sample interaction will also manifest in these modes. The reconstruction of the force in these cases cannot be done just from the frequency shift. However, the basis of the measurement procedure stays the same.

In what I like to think as the adolescence of AFM (the second period) scientists employed the microscope to explore the depths of science not available with the STM before, imaging atomic defects [19], studying DNA molecules [20], nanomanipulating different systems [21], and several other applications

in Condensed Matter Physics, Chemistry, etc. Particularly, the amplitude modulation mode gained an immense popularity [18]. By the turning of the century the full understanding of the dynamic operation of the AFM was needed. Theoretical descriptions started to appear in literature, at first with some resistance [18]. García [22], Butt [8], Giessibl [23] and several others contributed to a clear view and understanding of what was physically happening in an AFM experiment.

With the full power of theory, different groups across the community started to develop more complicated and complex techniques that further contributed to the full implementation of AFM in Science, addressing the remaining problems and issues, corresponding to my understanding of the third (and current) period of development of the microscope. I mention here 3 important advances made recently (in the last 6-7 years), that establish this trend, in my view: Culminating 15 years of research since Hansma, Ando, and a bit later Miles initiated independently their research, the three groups successfully developed AFMs capable of acquiring images at high speed [24], solving the serious disadvantage of AFM in comparison to other types of microscopy. These AFMs reduce the imaging speed of conventional microscopes, about 1 image/minute, to sub-second imaging. Multifrequency techniques were developed by many authors, to measure the behavior of the cantilever in higher-order modes. This allows to study the force in the regime of large amplitude, being this a rising trend in AM-AFM measurements [25, 26]. Very recently a simple solution proposed by Rodrigues et al. [10] introduced the technique of Force Feedback Microscopy (FFM), allowing for the first time ever the full measurement of force, force gradient and dissipation, for very soft cantilevers [10]. This technique has originated a series of possible new measuring modes for dynamic AFM unachievable before, for instance the direct measurement of short-ranged attractive forces. Furthermore, this technique allows the user to work at any frequency, and not just the ones associated with the modes of the cantilever [11, 27]. All of these recent advancements prospect a bright future for the field.

Fifty years after Feynman's predictions, scientists and engineers seem to have just grasped the limits of his mind. But no doubt the advances in the last decades have been enormous. More than ever physicists and engineers are following his suggestions and making an impact on the diverse fields of Science. But what does the future hold for technology at the nanoscale, and what part the AFM will take in it?

1.2 "Bringing light into the nanoworld"

Perhaps the greatest example of the revolution one instrument or experimental technique can precipitate in Science is not (yet) the Atomic Force Microscope, but the use of X-Rays in the last 100 years.

The history of this technique, starts with Röntgen's discovery of this type of radiation about 120 years ago. It immediately gained popularity with the general public for its possible applications. Also, within the scientific community the interest sparked over the radiation's somewhat mysterious character. A case was made for their particle-like behavior since it didn't exhibit diffraction, like it was known to happen for waves. In the middle of this particle-wave character of matter debate, Von Laue in 1912 discovered (inferring that the X-Rays if they were waves should have a wavelength comparable to interatomic distances) that this radiation would diffract in a specific way on a crystal. It was the same behavior already observed for different types of radiation with diffraction gratings. Based on this result Bragg published the famous law with his name.

These discoveries rocked the scientific world. For the first time in history scientists could look at what was happening at the atomic scale. The impact was enormous and it spread over several areas of research. It served as a basis for investigations in quantum physics, having influenced the first atomic and chemical bonding models [28]. It became the basic tool of chemists around the world and it was crucial in the studies of biology. It was at the basis of the discovery of the DNA structure and many more biologic molecules [29]. With the development of modern X-Ray sources like the synchrotron, the X-Ray beams were made ten orders of magnitude more collimated and intense than before, allowing for a broader spectrum of energies and handy pulse structures [30]. Several techniques were invented to study matter and extract information in different ways, and they became the premier source for chemical analysis in Science. Its impact can be directly seen looking at the list of Nobel prizes (not the most fair indicator, but it is good enough for a start) associated with X-Rays, from Röntgen (the first ever Nobel Prize winner in Physics), to an impressive number of awards in Physics, Chemistry and Medicine [31]. According to the source, since the year 2000 X-Rays have been directly or partially involved in half of the findings that led to these prizes. Consequently, synchrotron radiation sources have become gigantic centers for research across the world in the most diverse fields of knowledge and industry.

With the popularity of X-Ray techniques and the advent of Scanning Probe Microscopy, there was interest in combining the two techniques. The first sparse attempts were done based on the realization that the tunneling

current in a STM was dependent on the photoemitted electrons from a sample under illumination by X-Rays [32]. It was envisioned that the STM could serve as a very useful local probe for photoemission. However, it was only in recent years, with the maturity achieved by SPM techniques, that experiments combining STM or AFM and synchrotron radiation (SR) became more frequent and successful.

The idea is very simple: for their nature, X-Rays provide us with determined information, for instance concerning the chemical character of matter, but also of crystal dynamics, ferroelectricity, magnetism, and others. However, for the X-ray focusing devices available to scientists nowadays, this is always a measure averaged around many atoms [30]. Currently, a lot of work is addressing nanofocusing techniques [33], but the best efforts allow scientists to get spot sizes on the order of tens of nanometers, which puts a limit on the local character of the information acquired. Another important consideration is that in X-Ray experiments the manipulation of the samples cannot easily be made, which makes their characteristics under movement or stress complicated to inspect. These limitations severely affect the information obtainable in a experiment. SPM, on the other side, are by definition local probe instruments: atomic resolution is now routinely obtained with the most modern instruments. It is also an important tool in nanomanipulation. However, the precise chemical characterization power of X-Ray diffraction (XRD) is not comparable with the one offered by the SPM, particularly in non-conductive samples (meaning, with AFM) [30]. Combining the two approaches seems to be a potentially prolific endeavor, in terms of the new information such an instrument would make available.

In 2005, Saito et al. [34] presented a STM to use in *in-situ* SR experiments. The STM took advantage of the change in the local electron density with X-Rays illumination to analyze the chemical character of the sample. By varying the energy of the incident beam, they were able to detect the absorption spectra of the different materials composing the sample (Ge and Si), at the nanoscale, using the STM tip as the detector for X-Ray spectroscopy. Around the same time Suzuki et al. [35, 36] used the same approach to construct an AFM and integrate it in a beamline. Suzuki measured a change in the cantilever's resonance frequency over the change of the incident beam's energy, obtaining this way the wanted chemical nanoresolution. Other authors also presented similar instruments and results [37]. Despite the effort, these approaches were very limited in regards to what kind of information they were set to obtain, limiting themselves to observe the effects of X-Rays in a determined sample and use them to achieve chemical contrast at the nanoscale.

The following years Rodrigues et al. [38] presented a revised version of

the instrument that also permitted the combination of X-Ray techniques with Atomic Force Microscopy *in-situ*. This instrument, unlike the previous ones, permitted a true combination of AFM and X-Rays, in the sense that the AFM tip itself would work as a detector for different SR experiments, using a quartz tuning fork to detect both the force and photoemitted electrons without the need for any optics [30]. Like the author says, this was literally "bringing light into the nanoworld". Besides combining diffraction and absorption experiments with AFM, the author also explored the manipulation possibilities offered by an AFM. Compressing the sample with the tip and watching the change in diffraction peaks one is capable of obtaining, for instance, the Young modulus of the nanosample. Rodrigues et al. [39] and Sheler et al. [40] successfully tried this approach with microsized SiGe islands leaving prospects for trying with nanoscale objects, if the tip-sample contact model was improved.

Meanwhile Schmid et al. [41] developed the Scanning X-Ray Transmission Microscopy. This approach allowed the deconvolution of different types of X-Ray absorption mechanisms through topographic information. They also addressed another very interesting feature of the AFM, the capability to measure and investigate the different characteristics of the sample by the "selection" of the force measured: the built instrument was able to work as a Magnetic Force Microscope and as a Kelvin Probe Force Microscope, while X-Ray experiments were performed at the same time, addressing the magnetic, electronic and chemical character of the sample. Pilet et al. [42] testified the effect of radiation damage on a particular experiment by measuring the friction with the AFM. They did not, however, investigate the manipulation of these samples at the nanoscale under X-Ray illumination. AFM has also been coupled with other techniques, like Scanning Electron Microscopy [43] or Raman Microscopy [44].

It is clear that a closer look at the recent history of AFM and SR experiments shows an increasing effort to achieve combined and simultaneous operation of the instruments, and to improve the existing ones to new settings and measurements needed to characterize different types of research subjects. These integrated approaches are, at least, very promising, and as such, the advantages and setbacks of these instruments should be analyzed and addressed, to expand their applicability to a higher variety of samples and sample environments.

1.3 The High Speed X-AFM

As AFM technology matures, more and more research is being addressed towards the study of biological matter. The unique capabilities of AFM allow for studies of biological and soft matter, and what started as a technique mainly directed towards imaging shifted to be a much more powerful investigation tool [45, 46, 47, 27]. By performing imaging and force versus distance mapping experiments and also taking advantage of diverse tip functionalizations it is now possible to study the structure, function, mechanics and chemical behavior of different biologic specimens.

However, all of these studies fail to address one fundamental characteristic of living matter: their dynamics. Typical AFMs have, at best, a sub-minute time resolution, which means that all of the phenomena occurring at shorter time scales are averaged out. Other techniques are incapable to provide spatial and temporal resolution together with low invasiveness [24]. This problem was partially solved in the last years by the achievement of the High Speed Atomic Force Microscope (HS-AFM). A broad spectra of time-resolved (sub-second) measurements with the HS-AFM has been published in the last years, showing a progressive increase in the use of this microscope. Particularly impressive is the amount of scientific publications following from the development of the instrument by Ando et al. [1, 24].

But not only biological processes have timescales in the second or sub-second range. With regards to material science, little research has been done with the HS-AFM [48]. This probably has to do simply with the difficulty in constructing such kind of microscopes, which makes them almost commercially nonviable, and thus not spread throughout the community. Despite this, one can point out different experiments where the possibilities offered by an HS-AFM would be ideal. For instance, taking into account that radiation damage to surfaces is still, and has been for a long time, an important topic in modern SR facilities, there is still a need to provide *in-situ* topography measurements in real time, as there is no instrument that can do this at the nanoscale in a broad band of experiments, samples and environments.

There is therefore, in my opinion, a need for new X-Ray instrumentation. The integration of SR techniques and AFM can only be made by a coherent combination of the two instruments, specifically designed to study phenomena currently unexplored. For this reason, the focus of this thesis is the project, commissioning and operation of a novel instrument, which can surpass the current setbacks of a several experimental techniques, and serve as a primary tool in the field. I advance that the only way to have a complete understanding of soft and biological matter is to integrate the time and spatial resolution imaging, nanomanipulation and force spectroscopy offered by

AFM and the chemical and structural characterization power of the X-Rays. The High Speed AFM to be used in normal-incidence X-Ray experiments, the HSX-AFM, is meant to be an approach this goal.

Such instrument would have at least three immediate and main applications:

- Serve as a primary tool to study the effects of radiation on soft samples, with real time topography measurements *in-situ*.
- Would be an optimal tool to allow exact localization of the X-Ray beam on a macroscopic sample, increasing the effectiveness of an X-Ray experiment.
- Would also present itself as the perfect nanomanipulating tool to be used *in-situ*.

A prototypical version of this instrument has been developed: the Grazing-Incidence High Speed X-AFM was conceived in the Surface Science Lab of the European Synchrotron Radiation Facility [49]. The instrument was tested on a beamline, and is currently prospected to be used in several experiments. In grazing incidence geometry, the experiment accesses mainly the information at the surface of the sample, being averaged over a somewhat large area.

The project of Isabella (how the HSX-AFM described in this work was baptized) expands this approach making it possible normal incidence experiments, exploiting synchrotron radiation characterization in all the three dimensions of space. The inherent consequences on the design of the AFM will be explored after.

The main objective of the project is the construction of the AFM. This will provide the author a broad knowledge of all the steps necessary to build an AFM. From its inception and conceptualization, that implied a complete knowledge of the practical consequences of the required performance characteristics, passing through the designed phase, which meant the extensive use of several project and simulation tools, including different types of software, and to the last steps of testing and manipulation, that required a correct understanding of the operation of the instrument.

There is, however, one other issue addressed during this thesis. In the project of the HSX-AFM there were several time periods in which the work had to be outsourced to people outside the lab. For instance, the manufacturing time of the parts of the AFM took about one month. During this time the author, using previous experience in the field, took part in another investigation concerning the methodology of FFM to tune the dynamic properties

of a mechanical oscillators. This investigation led in the end to the writing of a scientific publication that is now currently in review at a scientific peer-reviewed journal. The theory, experiments and results that comprise the work that led to this publication will be addressed in a dedicated chapter in the end of this manuscript.

It is of the utmost importance to provide new tools for scientists to look at the unknown. I argue, due to the potential and history of both experimental techniques, that the combination of X-Rays and Atomic Force Microscopy seems to fill a gap in current experimental instruments. Like Tyson would put it "Science is a cooperative enterprise spanning the generations. It's the passing of the torch from teacher to student to teacher. A community of minds reaching back to antiquity and forward to the stars." We must "stand in the shoulders of the giants", the very giants that make it possible for us to even dare to think about the undiscovered. We must, with them, attempt the foolishness. And how fool it is to build "the hardest AFM that has ever been built?"

This work has been performed at the Surface Science Laboratory of the European Synchrotron Radiation Facility.

Chapter 2

The Project of the High Speed X-AFM

The design of a custom-made AFM is not a common task. Because of the availability of commercial AFMs available, only a handful of groups throughout the world continue to custom-made and develop their own instruments, tailoring their measuring characteristics to their own specific investigations. One of such groups is that of Toshio Ando, which developed and perfected the high speed AFM for almost two decades and dedicated to investigate the properties of matter at time scales below the second.

The objective of this work was to incorporate the know-how of high speed AFM and of X-AFM into one instrument. The project consisted of a coalescence of many fields of expertise, which had to be analyzed, and applied, in a relatively short time. For this, different cooperations were carried out between European Synchrotron Radiation Facility (ESRF) labs. The project of the HSX-AFM is a collaboration between the Surface Science Laboratory (SSL) and the beamline ID13. Thus, the project of the microscope profited from input from the beamline scientists, in order to accommodate the different constraints of the experimental setup. Besides this, several other specialists were consulted, to perfect the initial designs into a complete and integrated instrument.

In this chapter a theoretical review of the different aspects and constrictions taken into account in the project will be done. The needs of high speed microscopy and the consequences of bringing an AFM to a beamline will be detailed. An overview of the entire project will be made, where the different options made in the design of the microscope as well as the final assembly drawings will be shown.

2.1 What does it mean to go on a beamline?

A beamline of a synchrotron is a detail-oriented, extremely complex instrument. To perform all the necessary tailoring of the X-ray beam and also to direct it to the sample and finally to readout the results of the experiment, a vast amount of different instruments and stages have to be assembled and aligned. The beamlines of the ESRF undergo an almost continuous upgrade, to perfect more and more their experimental performance. They are usually composed of two different parts: the optics hutch and the experimental hutch(es). These hutches are long containers (tens of meters), usually made of lead to preventing any radiation to escape, where the different instruments necessary for the experiments are located. In regards to ID13, there are three experimental hutches, each one of them serving a different purpose. From the nature of the measurements of the HSX-AFM, it was decided that this instrument would be integrated in the hutch providing the smaller beamsize: the nano-focus hutch. This is one of the beamlines with the smallest beamsize in the whole ESRF and, thus, the world. For reference, ID13 reports regular beamsizes of about 250 nm and projects, after a future upgrade, beamsizes smaller than 100 nm. The accessible energy range is 6-24 keV.

With the current trend of miniaturization, the challenge of focusing an X-Ray is becoming more and more important. This is a procedure that often balances a number of opposite parameters: for instance a smaller beam size and higher flux means that most samples will be damaged after an experiment. Another consequence is that, since the refractive index for X-Rays in most materials is close to 1, usually many refractive lenses are combined to focus the beam, in what is called compound refractive lenses. To achieve spot sizes less than 100 nm, however, special nanofocusing lenses are built, with an extremely small radius of curvature. No matter the technology used, the limiting factors of the focus size are the source size (provided by the synchrotron itself), the demagnification (which depends on the focal length of the system) and finally, the diffraction limit: this limit imposes that a reduction in spot size must be accompanied with an increase of the numerical aperture, which in turn requires a smaller focal length ($N_A \propto D/f$). In practice the beamlines of the ESRF with the smaller spots, and in particular the nano-branch of ID13, have an extremely small sample environment surrounding space.

For simplicity, unless stated otherwise, the directions mentioned in this work will be in respect to the X-Ray beam as follows: x represents the direction of the X-Ray beam; the sample is positioned in the plane perpendicular to this direction, comprised by directions z, vertical in regards to the laboratory frame of reference, and y.

The working space of ID13 can be regarded as the main constraint for the design of the HSX-AFM. There are several parameters detailed by the ID13 scientists indicated in the schematics that can be seen in Figure 2.1. They can be summarized as:

- *the sample holder*: the sample is positioned in the X-Ray beam by the *H-810 Miniature Hexapod* from *Physik Instrumente* (PI) (which datasheet can be found in Annex A). This instrument is also capable of rotating or tilting it for certain experiments. The maximum supported weight of must not exceed 5 kg. It has a range of movement of $\pm 20 \times \pm 20 \times \pm 6.5$ mm^3 and has maximum stability with full distension along its vertical axis. Thus, the height from the base of the AFM to the sample needs to be minimized. The hexapod has a base with 100 mm diameter.

- *the upstream shielding*: to prevent retro-diffraction and isolate the measurement from background noise, a lead foil with a pinhole is placed between the last optical focusing element and the sample. It is made to accomodate the different elements of the beamline. A rough sketch can be found in Figure 2.1. The main constrain is the working distance, from the pinhole to the sample along the beam, of $d_{\mathrm{x}}^{\mathrm{up}} = 10$ mm. This and the other dimensions of the foil are target specifications with some freedom allowed, within certain tolerances. After the construction of the AFM, and after an upgrade of the focusing instrumentation of ID13, a special lead foil will be custom-made to fit perfectly with both instruments, assuring optimal shielding and steady AFM performance at the same time.

- *the alignment apparatus*: an optical microscope is used to pre-align the sample and the nanosized X-Ray beam. When aligning, this microscope's objective is placed downstream of the sample at the projected beam height. The objective and the positioning of the optical microscope are build so that its focal point coincides with the one of the X-Rays, and the alignment can be done optically. After the alignment, the microscope is retracted and several detectors are approached. The main constraint is the optical microscope, as it is placed at $d_{\mathrm{x}}^{\mathrm{down}} = 10.55$ mm from the sample. The objective of the microscope has a radius of 12 mm. There are no constraints in the y direction.

- *the scattering cone*: In order to perform *Wide Angle X-Ray Scattering* (WAXS) experiments, which makes possible the investigation of subnanometer characteristics of the sample, one has to collect all of the

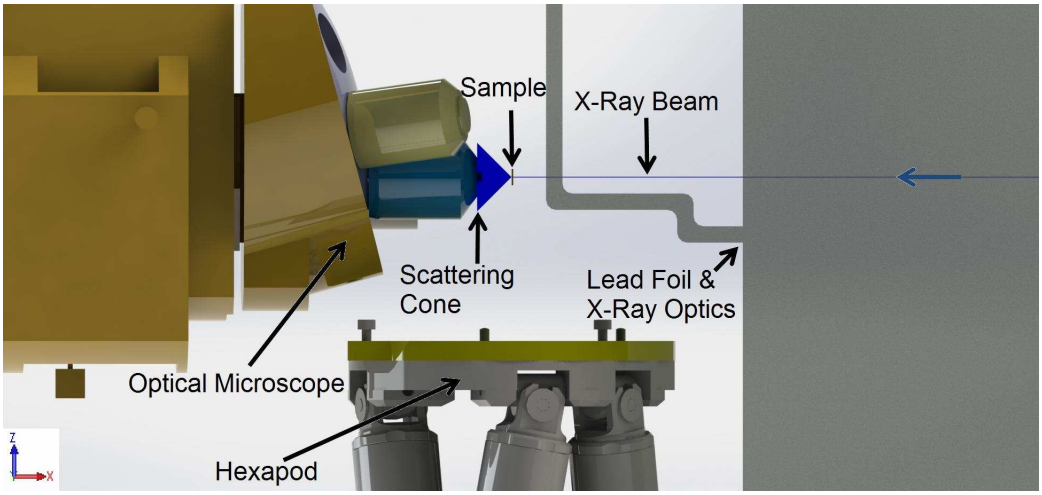

Figure 2.1: xz profile sketch of the experimental Setup of ID13. The main components that constrain the design of the AFM can be seen: the Optical Microscope is placed at $d_{\mathrm{x}}^{\mathrm{down}}$ from the sample, while the lead foil distances $d_{\mathrm{x}}^{\mathrm{up}}$ from it. The profile of the X-Ray Optics support can also be seen, as well as a representation of the cone which is to be left free in order to allow wide angle scattering measurements.

> photons scattered through a large cone angle from the sample. The AFM should be designed leaving free a cone with half-angle of 45° downstream of the sample, allowing scattering along these angles.

One of the very important applications of this kind of AFM is the possibility of localizing the nanometric beam exactly, within a macroscopic sample. The cantilever can be used as a detector of electrons emitted under X-Ray illumination [30]. Also the very small and precise movements associated with the AFM operation seem to be a perfect opportunity to include some of the optics of X-Ray instrumentation in the AFM structure and very close to the sample. For this reason, one of the important requests of ID13 was the inclusion of some on-board optics in the structure of the AFM. Namely, order separating apertures (OSAs). These are simply pinholes, with diameter of some hundreds of nanometers, and their placement permits the user to select the energy of the incident beam in an automatic way, and without much cost in time and redundant instrumentation. If made properly, the inclusion of this kind of apertures would be a key aspect of the instrument. It would configure one of the first instances where X-Ray optics could be placed so close to the sample and with such an extremely good resolution in its positioning.

If provided, these requests should make the HSX-AFM an instrument

capable of intervening in different experiments using X-Rays. Besides using the radiation as a simple exciting pump of the experiment, the design will also make possible X-Ray absorption spectroscopy experiments (for instance measuring the total electron yield) and also X-Ray diffraction experiments (like coherent diffraction).

The above requests alone make it clear that the construction of a simple AFM to be integrated on a beamline is complicated, without severely compromising some of the performance associated with the instrument itself. However, the gains in operation should well exceed these costs. It also demonstrates the novel character of the work done: the extremely hard environment for the placing of the AFM is perhaps the main reason this instrument was successfully built by an extremely limited number of groups in the scientific community, and going from a micro-focus to a nano-focus beamline makes all the spatial requirements even harder to be met.

2.2 What does it mean to go high speed?

This section presents a review of the main aspects necessary to be addressed in the construction of the HS-AFM, compiled from the work of the main authors that led the development of this technique [1, 48, 2].

There are different measurement modes in AFM. However, all of the high speed AFMs use amplitude modulation mode as the main work mode of the instrument. Contact mode is not well suited for the study of biological matter, due to the fact that damaging high friction forces intrinsic to this measurement mode are incompatible with soft samples. Meanwhile, despite recent advancements in using the frequency modulation mode for imaging biologic matter in liquids [50, 51], FM-AFM seems to be only suitable for relatively flat samples. AM-AFM provides low invasiveness and can image rough samples routinely [24]. This mode was then chosen to guide the construction of the HSX-AFM.

Considering a driven cantilever with elastic constant, k, damping ratio, γ, and mass, m, its natural oscillation frequency is $\omega_0 = \sqrt{k/m}$ and quality factor $Q = \omega_0 m/\gamma$. The quality factor of an oscillator is related to its relaxation time by $\tau_c = 2Q/\omega_0$. An amplitude setpoint is defined, which defines a certain tip-sample average interaction. When scanned over a region of the sample with a different height, or a different material, the interaction changes. The response of the cantilever to a step-like force happens after a response time given by τ_c. The change in the resonant curve of the oscillator is measured by a change in the oscillation amplitude of the cantilever detected via a lock-in amplifier. This instrument has a measuring time constant τ_{lock} which determines the time it integrates the oscillation amplitude. The output of the lock-in is compared with the reference signal and a PID controller outputs a signal after a time τ_{pid}. This signal is fed back to the controller of the sample movement, changing the distance between the tip and the sample. This mechanism takes some time τ_z that depends on the controller, but also on the mechanical assembly of the whole AFM. Finally, the sample is displaced laterally so the measurement takes place in another point. A schematic diagram can be observed in Figure 2.2.

The maximum imaging speed will depend, not only on the performance of each element mentioned above, but also on the image characteristics (how many points we have to measure) and the sample itself, that may be more or less difficult to measure. We can define the frequency of the loop, $f_{\text{loop}} = (\tau_c + \tau_{lock} + \tau_{pid} + \tau_z + ...)^{-1}$, and spatial frequency of the corrugation of the sample ν_{sample} and the line velocity in an image, V_{line}. To perform an image the feedback loop needs to be able to compensate every change in

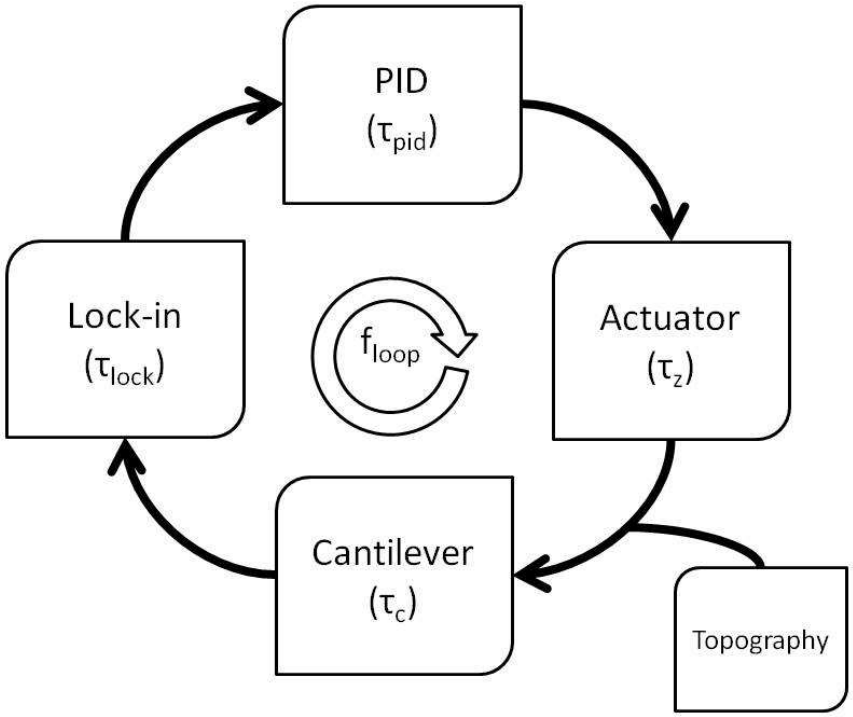

Figure 2.2: Diagram representing the feedback loop in amplitude modulation AFM. Each element in the loop has an associated time constant, which limits the maximum frequency attainable in measuring the topography at one single point in the sample, f_{loop}.

topography. Thus we have:

$$\nu_{\text{sample}} V_{line} \leq f_{\text{loop}} \tag{2.1}$$

Usually two images are performed simultaneously, measuring the same line while rastering the sample forwards or backwards (trace and retrace). This helps in the measurement procedure to verify the result imaged and to choose the control gains appropriately. For an image with dimensions $W \times W$ m^2, the time it takes to perform a line is then:

$$T_{\text{line}} = \frac{2W}{V_{\text{line}}} \tag{2.2}$$

Which means, for an image of N lines, the imaging frequency, R, will be given by:

$$R = \frac{1}{T_{\text{line}} N} = \frac{V_{\text{line}}}{2WN} \tag{2.3}$$

and the maximum image rate by

$$R_{\max} = \frac{f_{\text{loop}}}{2\nu_{\text{sample}} WN} \tag{2.4}$$

To achieve high scan speeds there are 4 elements that have to considered: the time constant of the cantilever, the optimization of the measurement and control electronics and the construction of a scanner capable of achieving the required image rate. In the following an analysis of these components will be made.

2.2.1 Cantilever

The cantilever is central in AFM and thus it is one of the main elements of improvement in the last 30 years. The expression, $\tau_c = 2Q/\omega_0$ makes obvious the effect of the different characteristics of the cantilever in the measurment. Also, it can be shown that the average force applied by the cantilever to the sample during an oscillation period can be approximated by:

$$F_{sample} = \frac{k\sqrt{(A_0^2 - A_s^2)}}{Q} \tag{2.5}$$

where A_0, A_s represent the free amplitude and amplitude setpoint [52]. From expression 2.5 it is seen that both the decrease of Q and the increase of k, produce an increase of the force exerted on the sample. The HS-AFM is primarily a microscope for soft and biological matter which means that the forces exerted on the sample, if too big, will necessarily cause modifications or even destruction of the studied samples. The decrease of the imaging time was for this reason made, without sacrificing non-invasiveness, by increasing the resonant frequency and reducing the elastic constant as much as possible, while the quality factor is chosen so as not to cause damages to the sample and still produce fast images. Using the expression for the natural frequency of the oscillator and noting that the effective mass m of the cantilever is about $0.24m_{\text{t}}$, being m_{t} the total mass of the cantilever, we can use expression 1.1 to write:

$$\omega_0 = \sqrt{\frac{k}{m}} \propto \sqrt{\frac{\frac{Ewt^3}{4l^3}}{\rho wtl}} \tag{2.6}$$

and thus,

$$\omega_0 \propto \frac{t}{2l^2}\sqrt{\frac{E}{\rho}} \tag{2.7}$$

where ρ is the density of the cantilever. We see that an interplay of the different dimensions of the cantilever can reduce the elastic constant and increase its resonant frequency at the same time. Based on this fact the groups of Hansma and Ando worked to reduce the size of the cantilevers.

Nowadays the cantilevers used to perform measurements at high speed are commercially available. The Olympus BL-AC10DS, with nominal elastic constant 0.1 N/m, nominal resonant frequency 1500 kHz, and nominal dimensions (Length × Width × Thickness) $9 \times 12 \times 0.13$ µm and the Olympus AC55TS, with nominal elastic constant 85 N/m, nominal resonant frequency 1600 kHz, and nominal dimensions $55 \times 31 \times 2.4$ µm are examples of cantilevers used for high speed imaging.

2.2.2 Scanner

In most HS-AFM scanners, there are at least three piezoactuators that control the position of the sample stage to obtain a fast series of images that can be superimposed to form a video. The piezoactuators provide a reliable and high-resolution movement without too much noise. The difficulty, however, in the construction of scanners for HS-AFM is that increasing the mechanical resonance frequencies of just the piezoactuators is not enough: a series of interferences, non-linearities and noise appear as soon as the piezoactuators vibrate beyond the resonance frequencies of the supporting structure. To drive the sample at high frequency one needs to adapt the entire structure of the microscope. In particular one should consider the effects of the mechanical resonanaces present in the structure, along each direction of movement.

There are several strategies that the designer can follow in the increase of the scanner speed. A basic decision has to do with the desirable scanning frequency. When the piezoactuators are run at the resonance frequency of the scanner, the movement of the sample will be sinusoidal. This will result in a distorted image, which will have to be treated afterward. Otherwise, to obtain a rectangular motion that does not need any aditional data treatment, the piezoactuators have to run at a frequency signficantly lower than the scanner resonance frequency. Thus, one strategy requires aditional data treatment (which means more computational power), and the other requires a scanner with much higher resonance frequencies than the ones targeted for imaging, to run the microscope at the same speed.

Another issue is the geometry of the scanner, as the movement in an AFM measurement can be always decomposed in three different types: a vertical

one, very fast, to compensate the topography changes point to point, a fast lateral one, that rasters a line forward and backward a certain number of times per image, and another lateral, but slower, displacement, that increments in the remaining direction to make a measurement along a new line. The three different piezoactuators need not to be necessarily equal in terms of frequency, range and dimensions.

There are at the moment two different examples of scanners successfully providing high speed, the one designed by Ando et al. [53, 1] and another designed by Hansma et al. [3]. Due to the importance of both works in the design of the HSX-AFM, a brief review of each will be made in the following.

The most prominent work in high speed Atomic Force Microscopy is, without a doubt, the one of Toshio Ando's group. They were the first to produce the HS-AFM and are currently exploring all the possibilities offered by their instrument. The most characteristic feature of the scanner of their HS-AFM is the non-symmetry: the x, y and z-direction piezoactuators have all different resonant frequencies and scan sizes. The slow actuator pushes a block, that carries the other two; the line scanner then is stuck between the z-stage and a counterbalancing weight. Finally, the z-actuator sits on the on top of the line scanner and supports the sample stage, while an identical dummy stage is mounted simmetrically with respect to the line stage. This actuation mechanism, especially for the z-scanner and for the line scanner, was designed so the center of mass of the system does not move during rastering, to avoid the large impulsive forces transmitted to the scanner frame. These may cause parasitic vibrations in the movement. In this simple way the forces are counteracted and vibrations are kept to a minimum. This scanner was adapted, with some modifications, to the previous Grazing-Incidence HSX-AFM. In Figure 2.3 it is possible to see a picture of Ando's model and one of the custom-made scanner built in SSL.

Another way of doing is the scanner developed by Paul Hansma's group. The strategy was based on a system of flexure hinges, the piezoactuators were placed in a structure made to have a high mechanical resonant frequency in the pre-determined directions. Drawings of this scanner can be found in Figure 2.4. There is symmetry in the scanning directions, while the vertical piezoactuator has a resonant frequency as high as possible. The lateral actuators are stuck between two pieces, one very rigid, and the other (flexible) made in such a way that it allows the movement in one direction and provides stiffness in the others. There are two piezoactuators for each lateral direction, to reduce the trampoline motion for very fast actuation: by having always a piezoactuator doing a "push", one would avoid the asymmetry between this movement and the "pull", characteristic behavior of piezoactuators, and in this way, reduce unwanted vibrations. The vertical actuator

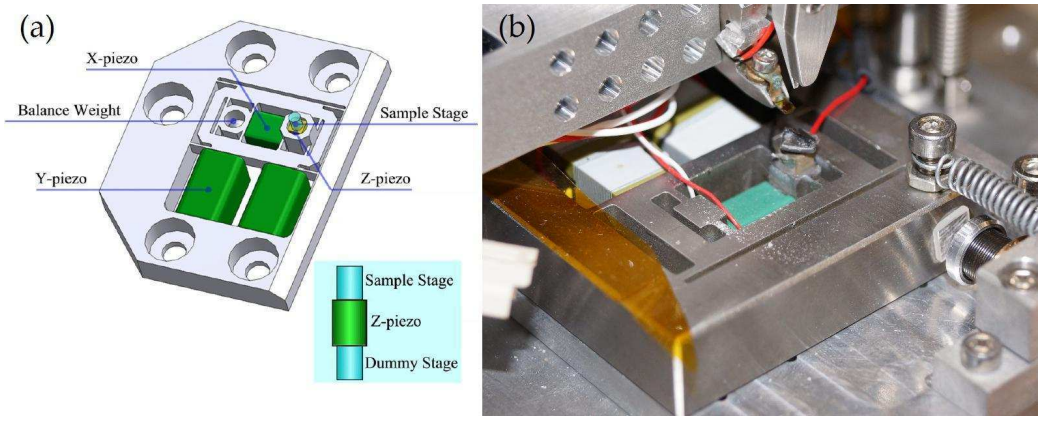

Figure 2.3: (a) high speed scanner for Ando's HS-AFM. Taken from [1]; (b) high speed scanner built in SSL for use with grazing-incidence X-Rays Experiments.

and the sample stage are placed in a central assembly, that is held by the flexible piece. Despite not having the dummy stage of the previous design, the scanner was tested for different degrees of acoustic noise, providing good results at high speed [3]. The whole AFM of Hansma's group was done to incorporate the different parts in a low-vibration encapsulation.

In the design of the HSX-AFM both scanners were considered. To finalize, we estimate here the target parameters for the scanner: if one desires a speed of 10 images per second, the slow direction needs an to oscillate at 10 Hz, implying a line frequency of $10 \times N$ Hz. For an image of 1000 lines this equals 10 kHz. To provide a square image the scanner it is required to have resonant frequencies in the order of 30 Hz and 30 kHz in the scanning directions. A vertical resonance of 100 kHz was defined as the minimum necessary to achieve, but this is ultimately limited by the fastest piezoactuator commercially available.

2.2.3 Electronics and Control

To provide the readout, generation and control of the signals in HS-AFM, special techniques had to be developed by the different authors. First, the measurement and signal generation have to be done with Analog-Digital Converters (ADCs) and Digital-Analog Converters (DACs) faster than the ones used for most commercial AFMs. For this, Hansma's group developed a fast data acquisition system especially for high speed AFMs, synchronizing the different scan signals with the converters [54]. Another important difference to regular AFMs is the control schemes applied to avoid several sources of

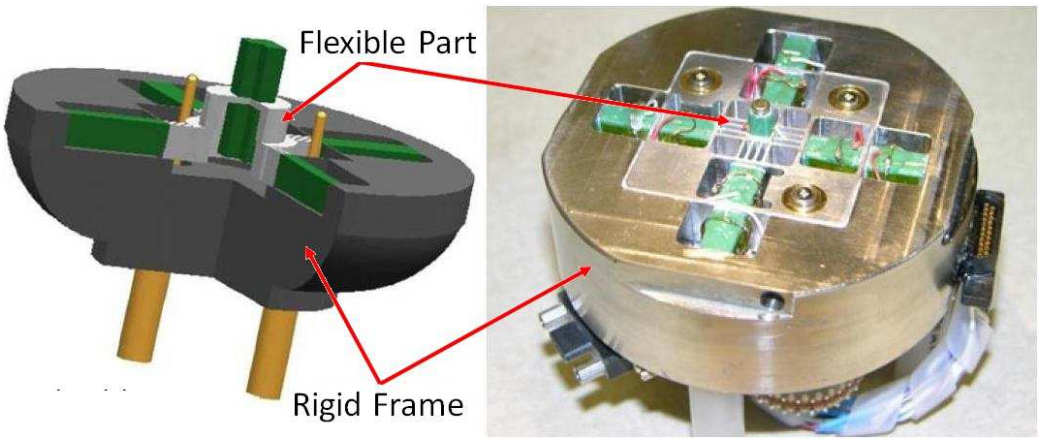

Figure 2.4: High speed scanner used in Hansma's HS-AFM, taken from [2] and [3].

noise in the measurements. Ando implemented an active Q-control on the z-scanner (where a signal proportional to the scanner speed is supplied to the piezoactuator in addition to the PID output) to reduce its quality factor (not the cantilever's) and thus permitting an actuation at a frequency 3 times lower than the resonance frequency of the scanner (370 kHz) without exiting this first resonance. Another problem that needed to be solved by this group was caused by the need to choose a setpoint very close to the free amplitude in a measurement of HS-AFM (to reduce the interaction with the sample, as it's seen in expression 2.5). Because of this, the error signal feeding the PID controller is usually extremely low when the tip detaches from the surface. Since this signal is very small, its integral will also be quite small, and thus the cantilever takes some time to encounter again the sample, a process that is called parachuting. This is a common occurrence for any AFM user, seeing some sort of "shadow", a dark region in the image, oriented along the motion of the cantilever well visible when the cantilever encounters particularly big particles in a flat substrate. This time had to be minimized, as it could easily extend to most of an HS-AFM line. Ando developed a dynamic PID which gains changed automatically when the error signal exceeded some set value, to maximize the integral gain when parachuting occurred. Finally, an extra feedback control was added to the system, to prevent the drift in the free oscillation amplitude due to an increased temperature of the system. The second harmonic of the cantilever is measured and its amplitude is controlled with a slow PID controller with a time constant bigger than the imaging period. It is assumed that the drift in the second harmonic will also manifest itself in the first harmonic mode, used for image, and in this way a feedback

control on this second mode keeps the free amplitude of the first one constant. In this way the value of the free amplitude is maintained for a long period of time, allowing for successive imaging of the same sample [55].

The development of the control and electronics schemes for the HSX-AFM was regarded as outside of the scope of this work for two main reasons: first the project is currently "financially limited" to the components currently available in the lab; secondly, it was known in advance that the existing electronics and control schemes allowed for an imaging framerate of up to 0.5 to 1.5 images/second, from tests with the previous grazing-incidence HS-AFM. As part of a long-term project of SSL for coupling AFM and X-Rays, we left the upgrade of the electronics for future times when both instruments were operational and functioning in their respective beamlines. However, they should not be disregarded in the construction of a high speed instrument. Like it was mentioned before, a severe improvement of this part of the instrument is necessary to achieve sub-second imaging. The current electronic module that is used for the HS-AFMs of SSL is the *Nanonis SPM Control System*, from *SPECS*.

2.3 The Design of the Instrument

This section details the different strategies followed in the design of the HSX-AFM. A review of the different components will be made. Then, the different possible displacements of microscope will be analyzed. The project of the HSX-AFM shown throughout this chapter was done using the 3D CAD software *SolidWorks®Premium 2013 Edition*, with the add-on *SolidWorks Simulations* for the simulations. It is the result of the work done by the author with important inputs from the staff of SSL and from the engineer Harris Alistair, who gave technical advice on feasibility and stability of the assembly. Some pictures of the model and its parts will be presented, giving a general overview and a simple description of them. The pictures were taken using the add-on *SolidWorks Photoview 360*. For completeness, and to not expanding this text too much, the 3D model is attached as a digital support to this work.

2.3.1 The Approach and a General View

For the design of the HSX-AFM a great number of requirements have to be met. However, they are hard to conciliate and sometimes even conflicting: for example, the stability in the measurement required for fast measurements directly contradicts ID13's requirement of a thin structure. For this reason, the several constraints had to be prioritized, following a design strategy that can be summarized as follows:

- Be sure of the functionality of the AFM: the main parts have to be designed and modeled;
- Follow, as much as possible, the requirements of ID13 **without compromising the previous point**, in order to have impact on its research for a long period of time;
- Achieve at least a frame rate of 1 Hz knowing, *a priori*, that the electronics would limit the image rate at about 0.5-1.5 images per second.
- Modularize the design to permit further improvements of each part: the AFM was divided in several components and if any of them had to be improved, the replacement can be made without changing the entire AFM;
- Attention to the cost: the cost of the AFM is supported by the ESRF, funded by European and extra-European taxpayers. Smart, efficient and cost-effective designs had to be implemented.

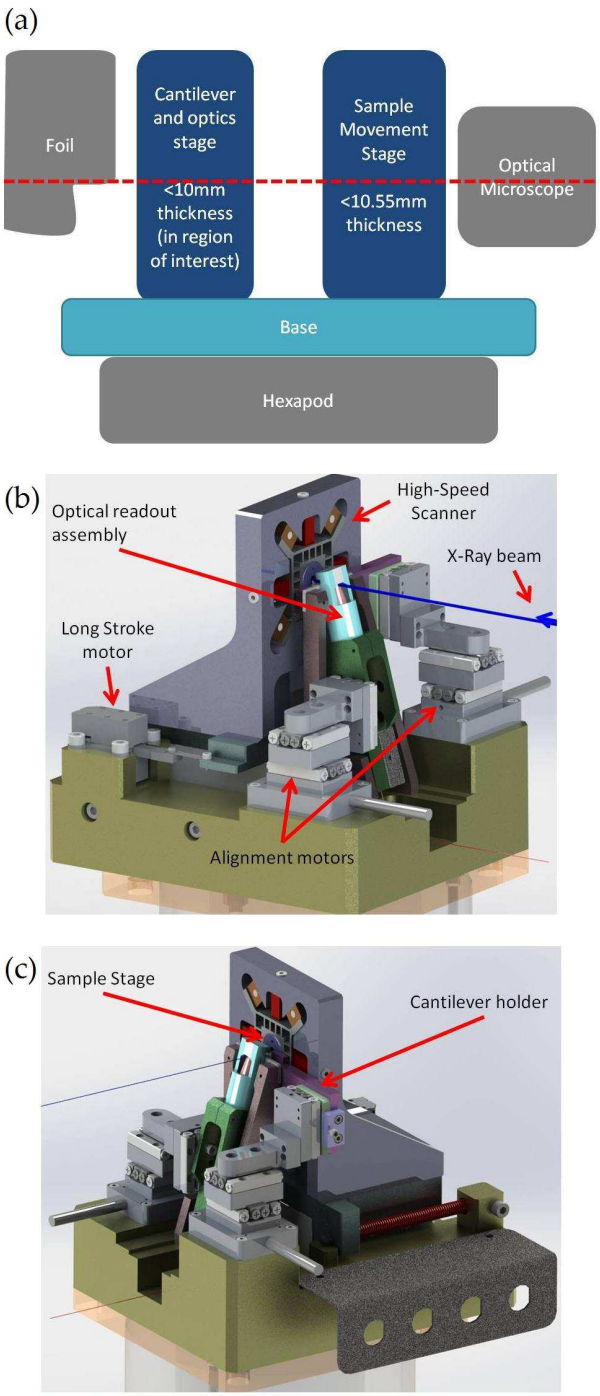

Figure 2.5: (a) design strategy of the HSX-AFM: a schematics of the approach and different parts; (b) final version of the model; (c) another perspective of the model; some of the main parts of the AFM are detailed.

Following this design strategy a basic approach was launched. Figure 2.5 (a) presents a sketch detailing the approach followed. The AFM was broken up in three different components: a sample holder and scanner stage, a force detection stage and a base that would support all the others and make the connection with the hexapod of ID13. The body of the stages had to be, along the direction of the X-Rays, thin enough to fit in the working space of about 20 mm. To compensate the inherent loss of stability, the structure of the parts had to be made rigid enough to eliminate unwanted vibrations.

An important mention should be made that, despite the natural environment of the experiments done with the microscope being liquid media, this was not fully considered yet in the design of the HSX-AFM. The reason is that, to avoid the interference of this media in the X-Rays scattering experiments, the amount of liquid on the sample would be so small that in normal conditions this solution would evaporate very fast. A humidity control assembly was planned to solve this issue. However, the project of this humidity chamber is scheduled for a future development of the HSX-AFM and is not in the scope of this thesis.

Figure 2.5 (b) and (c) show the final model of the instrument designed with details of the different parts. In the next subsections each of them will be analyzed separately.

2.3.2 The Scanner

The custom-made scanner was an adaptation from the scanner introduced by Hansma et al. in [3] and [2]. This approach was followed for 3 reasons: firstly, it provided, unlike other versions, a squared scan size without sacrificing scan rate; secondly, a symmetric scanner, like the one chosen, puts the AFM's center of mass in the axis of the structure. This would provide extra mechanical and thermal stability; thirdly, for scientific interest: exploring both scan designs (Ando's scanner had already been developed in the lab) allows a more complete knowledge of the field, and makes possible the identification of the strong features of each scanner. Figure 2.6 presents a general view of the scanner. It is comprised of four elements: the outside frame, the inside frame (both made from aluminum), the central structure holding the sample and the piezoactuators. These are tightly squeezed into the frame, by screws.

To perform the lateral scans (in plane with the sample), four piezoactuators P885.11 from PI were chosen. These have a nominal displacement of 6.5 µm and a resonant frequency of 135 kHz, well above the minimum desired scanner frequency. Annex A includes the datasheet of these piezoactuators. The inner structure is composed of a series of fins connecting the piezoactu-

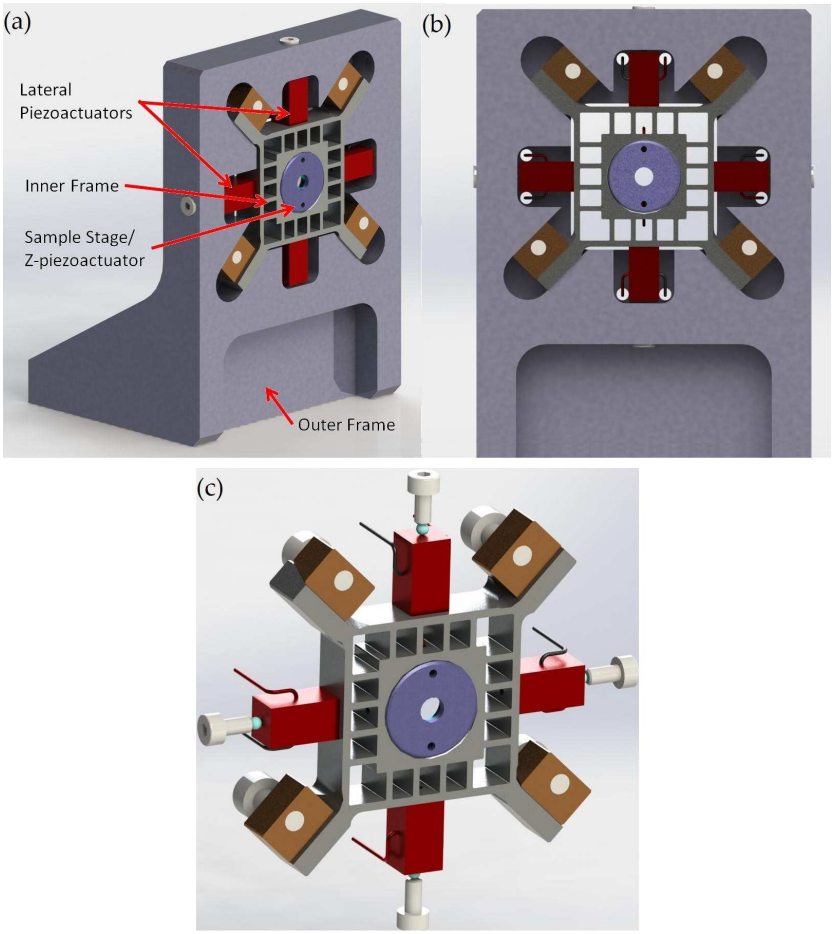

Figure 2.6: (a) custom-made, high speed scanner created for HSX-AFM; (b) front view of the scanner; (c) inner skeleton of the scanner. Some of the constituents of the scanner are detailed.

ators to the center of the piece. These fins provide rigidity in the direction of the piezoactuator to which they are connected, and also in the direction of the X-Rays, but offer flexibility in the remaining direction. In the center there is a hole in which the last piezoactuator will be mounted, along with the sample stage. The actuator chosen was the piezotube *PD080.30*, also from *PI*, with an axial resonance frequency of 500kHz (datasheet in Annex A). The actuator is mounted on the supporting structure and carries a sample holder (magnetic). Both the supporting structure and the actuator have a central hole, to allow the passage of the scattered X-Ray beam. The support has been designed with an opening in the shape of a cone with half-angle of 45°. To mount it, the sample is fixed on a magnetic support that is then

placed on top of the magnetic sample holder in the AFM. The dimensions of each part have been optimized to increase the scanning frequency.

However, the dimensions of the most suitable piezotubes did not allow for an opening angle of 45°. Since it was impossible to get a large enough angle and still have an interesting working speed, it was decided that the angle requirement would have to be relaxed. With a bit of tinkering with the dimensions of the piezoactuator it has been possible to achieve a possible scattering angle of 40°. In Figure 2.7 one can find the different pieces that compose the scanner.

To estimate the speed achievable by this scanner, an analysis of its resonant frequencies was made using the *SolidWorks Simulations* tool. The inner frame is the one that will dictate the behavior of the entire scanner, as it will be the one with the lowest resonant frequencies in the directions perpendicular to the beam, y and z. In the remaining direction, the deciding factor would be the piezoactuator and the sample holder that is placed on top of it and the screw-like assembly that holds it, since the aluminum inner frame is not excited in this direction. However, to ensure that there is no parasitic vertical motion when the sample is scanned, the vertical resonance frequency of the central piece must be higher than the others, so it is not excited by the scanning motion.

Making several improvements and minor changes to the piece to increase its frequencies lead to a version that exceeds the minimum specifications required. With the simulation software, the resonant frequency in the horizontal directions was found to be 18.4 kHz, and 20.8 kHz for the vertical one. With the right clamping, the vertical scanning frequency can be much higher. This would ensure an image rate of 6.1 Images/second is. Note that this studies were done not considering any masss attached to the scanner, which will have an impact in its resonance frequencies. However. in order to get better results, one would have to develop a central frame with an even more intricate pattern of fins, which would increase the cost, and would anyway not be exploitable by the current electronics. Figure 2.8 presents the results of the final study. A more complete report of the simulation done can be found in Annex B.

Finally, one should detail the electrical scheme (figure 2.9) for the different piezoactuators. To ensure the extension and compression of opposite piezoactuators during a scan motion, they have to be fed with opposite signals. As their actuation is not centered at 0 V, they will be fed with a voltage centered in the middle of their actuation range, 60 V. Each pair of piezoactuators requires 3 voltage references (120 V, the drive voltage and a ground).

The scanner follows all the constraints indicated by ID13. The design

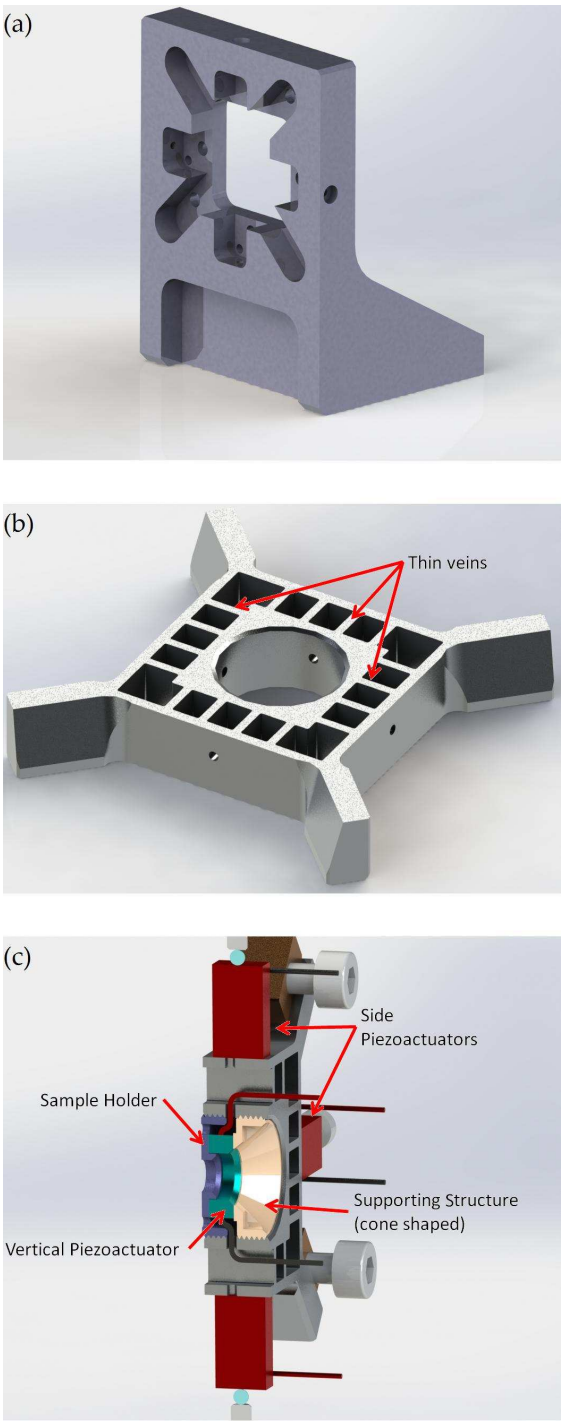

Figure 2.7: (a) scanner's outer frame; (b) scanner's inner frame; (c) details of sample holder/vertical-stage. Some of the constituents of the scanner are detailed.

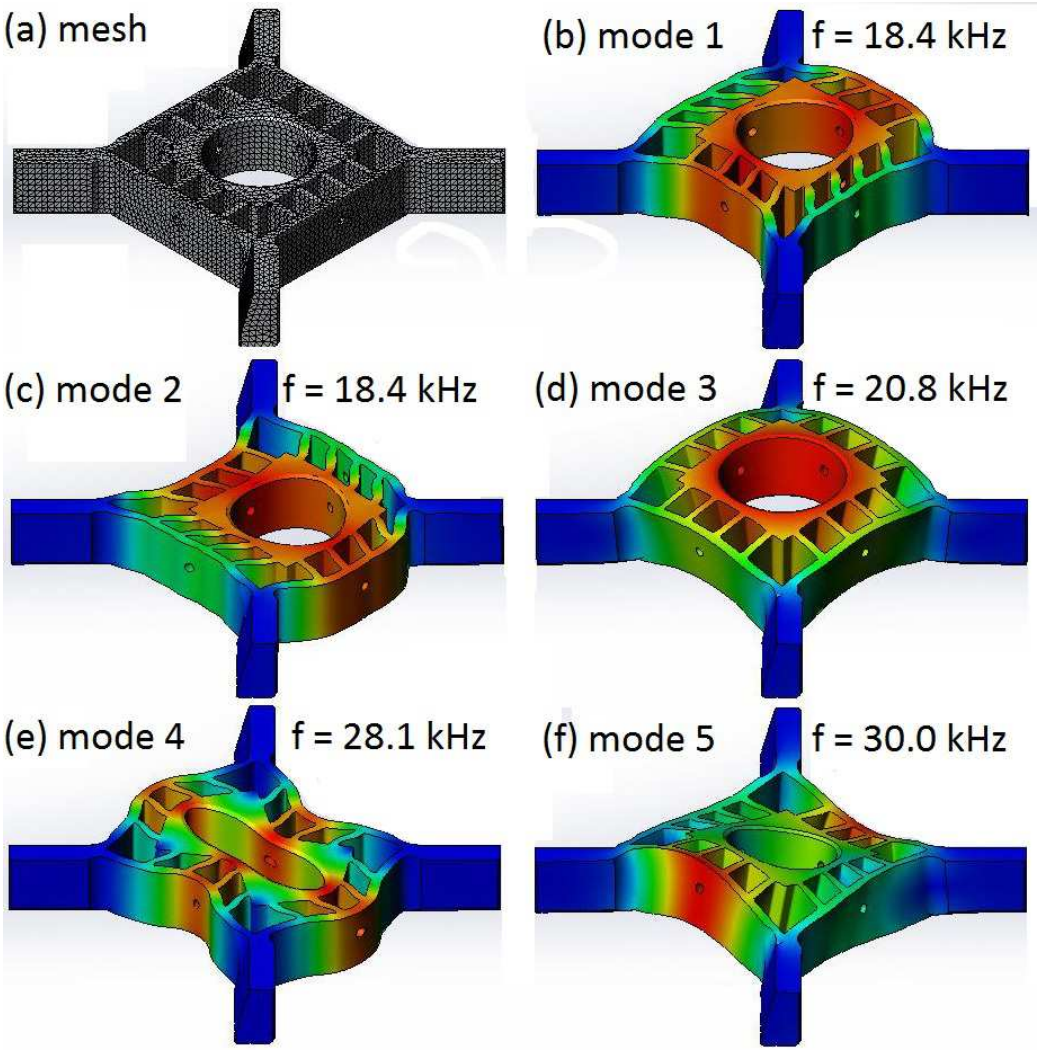

Figure 2.8: Frequency study performed for the inner frame of the scanner. (a) the solid mesh used to perform the simulation; (b)-(f) the first 5 modes of vibration, with the respective frequency of oscillation. To provide more accurate results, the fixtures and connections were done taking into account the ones in the assembly.

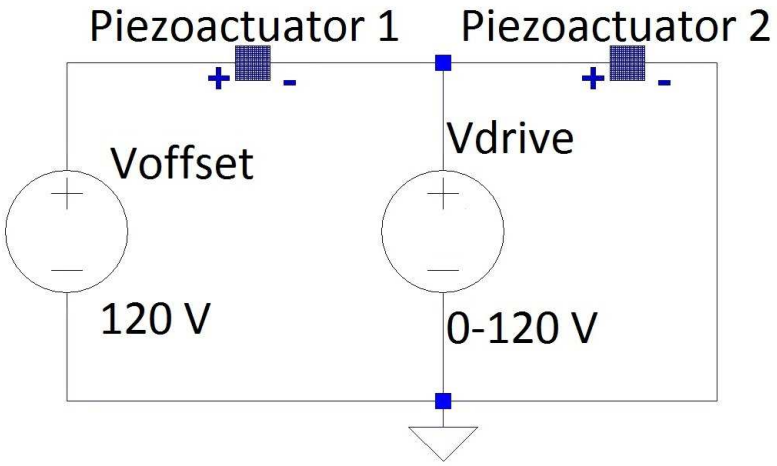

Figure 2.9: Schematics of the circuit implemented to drive each pair of piezoactuators controlling the scanning motion of the sample.

materials are the aluminum ENAW2017, bronze for the supporting structure of the x-piezoactuator, and magnetic steel F16PH for the sample holder. A positioner for the y and z piezoactuators, to ensure that they would be mounted as parallel to each other as possible, was also manufactured. Figure 2.10 shows how it is assembled on the main frame that connects to the hexapod of ID13.

2.3.3 The Detection Mechanism

The detection of the force in an AFM is made mapping the force between the last atoms of the tip and the sample into a deflection, by means of a cantilever beam, and from a signal of deflection to a voltage, readable and controllable by the user. This last step is usually done through an optical beam deflection scheme, that allows for a good force resolution and it is generally a user-friendly system without too much thermal drift [18]: the fact that the measurement is of an angle means that the signal read is much more stable than, for instance, a measurement of the position.

However, another possible scheme is offered by the application of a Fabry-Perot interferometer [56, 57]. In it, the light from a laser is split by a coupler into two branches. One of them is left unused and the other one is directed, through an optical fiber to the cantilever beam, perpendicularly to its back-side face. The light reflects back on it and a cavity is formed between the two perfectly parallel surfaces, cantilever backside and fiber end. The light is fed back through the fiber and couples again with the other branch. It is then

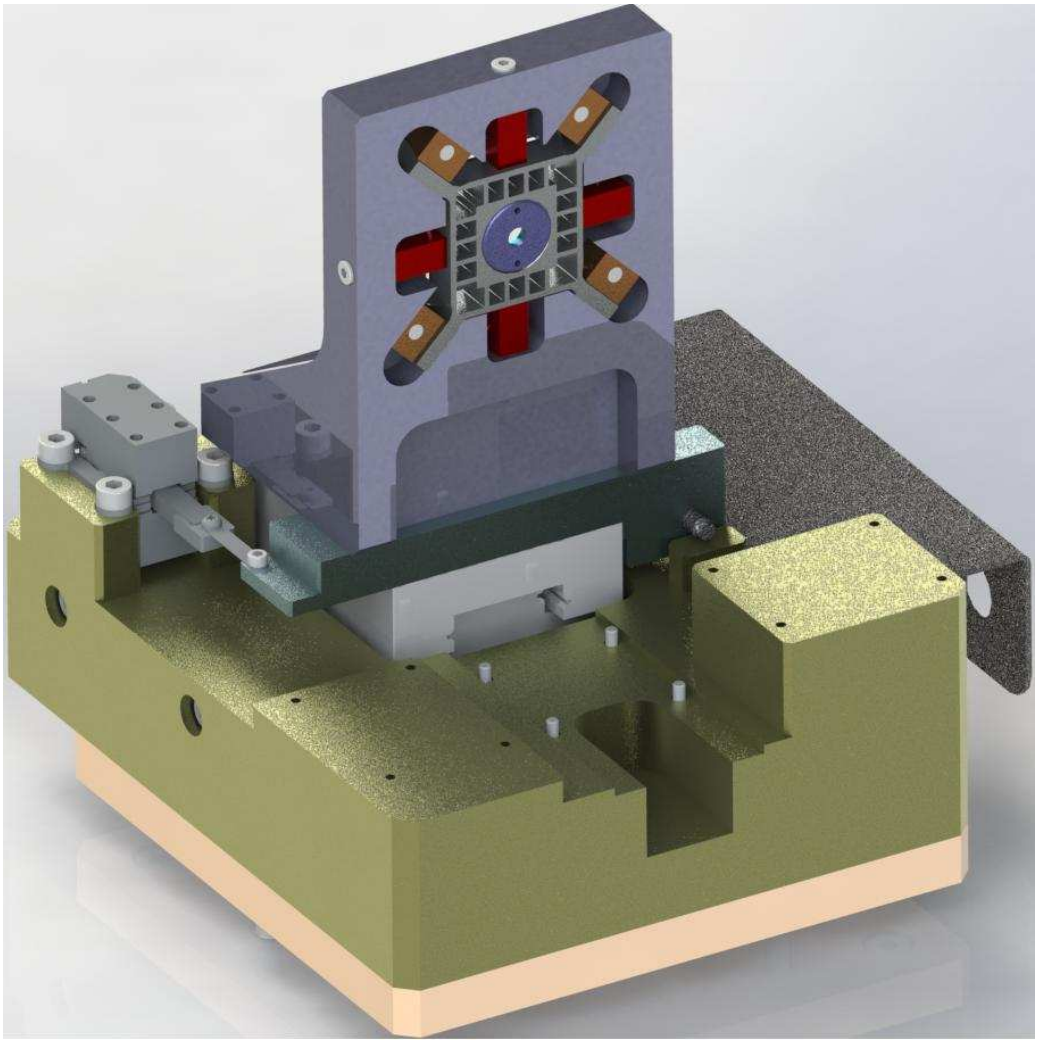

Figure 2.10: The scanner of the HSX-AFM. It's also seen the movable assembly that controls its positioning, the base and the connecting plate to the hexapod, that will be detailed in this report further ahead. On the right, in gray, part of the BNC connecting stage can be observed.

detected by a photodiode. The intensity measured by the photodetector can then be modeled as a two beam interference, ignoring any other reflections. Thus, the current of the photodiode will have the form of [11, 56, 57]:

$$I_{det}(d) = I_{av} + I_{sig} \sin\left(\frac{4\pi}{\lambda} d\right) \tag{2.8}$$

where d represents the distance between the fiber and the cantilever, I_{av} an average, distance-independent background signal and I_{sig} represents the oscillation resulting from the optical interference between the two beams. This distance can be optimized to achieve the best signal-to-noise ratio in a dynamic experiment, taking into consideration the change of the damping factor of the media in the presence of the large surface of the fiber [11]. This detection mechanism was chosen to be implemented on the HSX-AFM because of three reasons: the fact that there is one less component in the region of the cantilever provided a better flexibility in the design of the microscope; having developed the Force Feedback Microscope, it would be interesting for the lab to include this methodology easily to the new microscope in a second phase of the project, which would be more practical with an interferometry scheme; and finally, because of scientific interest: being previously involved in the construction of an optical-beam-deflection-based-AFM, the author was interested in enlarging his experience with this different method of detection, in which the personnel of SSL had already a considerable expertize. However, the goal of the design was, as said in the beginning, to build an instrument that could be easily improved after the first version, whether, for instance, to incorporate optical beam deflection or any other functional modification.

No matter the type of detection used, a big setback when downsizing the cantilever used, necessary to achieve high speed imaging, comes from the fact that the reflective area of the backside of the cantilever will also decrease, and with it the signal-to-noise ratio of the measurement. To increase the *signal* part of the equation, that is, the number of photons emitted, reflected by the cantilever, and detected by a photodetector, one has to ensure that the maximum possible quantity of light coming out of the laser illuminates the cantilever. One way to do it is to approach the laser source, a laser diode or an optical fiber, very close to the cantilever so that the divergence of the beam does not pose a significant problem. However, these have to be approximated typically to a few micrometers from the cantilever for the measurement system to be effective. Additionally, in the interferometry scheme, the illumination has to be done perpendicularly to the cantilever surface. The cantilever is usually inclined in respect to the sample by $15 - 20°$, to ensure that the tip touches it before the chip where the cantilever is held. This presents an additional alignment problem. This geometric configuration will,

if one looks closely, violate one of ID13's constraints: there is no way to place the fiber close (or far) from the cantilever without using the space occupied by the beamline experimental setup. Two consequences follow directly from this problem: 1) the fiber has to be placed far away from the sample, implying a focusing scheme; 2) the fiber cannot be placed perpendicularly to the cantilever, which implies an optical system to guide it in the right direction. A rough sketch is seen in Figure 2.11 (a). It is possible to see that the easiest solution is to place the optical system in the space left free by the lead foil of ID13, as the space between the sample and the lead foil will be extremely small.

Different authors have presented modified AFMs where the laser beam is focused on very small cantilevers suitable to high speed measurements, both in interferometry [58] and in optical beam deflection [59]. Inspired by this, and with the guidance of the optical engineer of the ESRF, Olivier Hignette, a system employing two different aspheric lenses was designed to be a part of the HSX-AFM. This optical system is fairly simple: light is emitted by the laser source, which is a *Laser diode beam source 51nanoFI* from *Schäfer+Kirchhoff*, with numerical aperture $N_{A1} = 0.11$. It is coupled to a single mode fiber, *SM600* from *Thorlabs*, which has mode field diameter of $D_1 = 4.3$ µm, and a nominal numerical aperture of 0.11. Both components datasheets can be found in Annex A. After, it passes in the coupler (FBS-660-X from *Schäfer+Kirchhoff*). The light is emitted by one of the fiber branches and is collimated by the first lens and then focused in the cantilever backside with a spot of $D_2 = 3$ µm, the width of a high speed cantilever. Taking $N_A = n\sin(\theta)$, the magnification, M, will be:

$$M = \frac{D_1}{D_2} = \frac{N_{A2}}{N_{A1}} \approx 1.43 \tag{2.9}$$

from simple geometrical considerations and the fact the instrument is in air. Thus $N_{A2} \approx 1.43 N_{A1} \approx 0.16$. We then consider that the two beams are focused by two lenses, which, again from simple geometry, have focal lengths, f_1, f_2 such as:

$$\frac{f_1}{f_2} = \frac{N_{A2}}{N_{A1}} = M \approx 1.43 \tag{2.10}$$

Figure 2.11 (b) presents a sketch of this optical focusing system. In order to get the best focusing in the cantilever one has to select the lenses to do it accordingly. Different lenses can be used in HS-AFM with different imaging characteristics, but for the HSX-AFM we chose aspherized achromat lenses. Aspheric lenses, as the name suggests, do not have spherical symme-

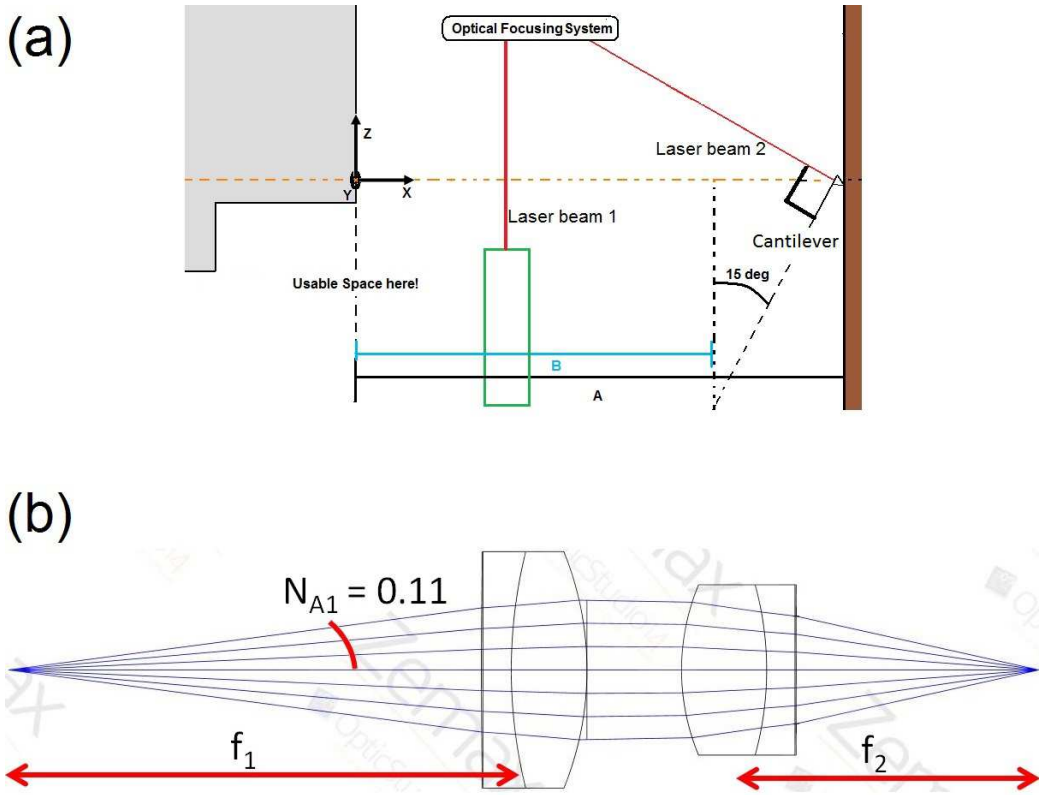

Figure 2.11: (a) The optical setup for focusing the laser beam on the cantilever backside. The geometry of the problem leads to a solution that utilizes the space bellow the lead foil that is unused. The X-Ray beam is represented by the dashed orange line, and the laser beam by the red line. On the right, in brown, the sample, and in black, a representation of the cantilever. The whole system needs to have, in the region of the beam, A, thickness in the order of 10-12 mm, but some of this space is not usable, A-B, due to the apparatus necessary to hold the cantilever in the right fashion. (b) scheme of the focusing system used in the HSX-AFM (simulation with the software *OpticStudio*®by *Zemax*). The light is collimated by the first lens and focused by the second. Their focal distances are chosen so the magnification of the system allows for a spot with the dimensions of the cantilever used.

try. Playing with the asphericity of the lens is then possible to solve most of the aberrations, that ultimately increase the spot size [60, 59].

The selected lenses were "off-the-shelf" *Aspherized Achromats* from *EdmundOptics*. Their size was chosen according to the required magnification and the space available in the assembly. Lens 1 was chosen to have an Effective Focal Length (EFL) of 25 mm and lens 2 was chosen with EFL=18 mm, giving a magnification of 1.39. Note that the two lenses come with different diameters which makes them hard to fit into the rest of the assembly. For this reason the diameter of the larger EFL lens was downsized (resorting to an external contractor) to the diameter of the smaller EFL lens, 9 mm. The datasheets and references can be also found in Annex A. To direct the light perpendicularly to the cantilever a mirror has to be installed. For a reason of practicality in handling and mounting, a *Right Angle Mirror* was chosen, also from *EdmundOptics*. The mirror chosen has a coating of aluminum. The length of the catethus in the right angle triangle, is 5 mm.

A good feature of this focusing system using aspheric doublet lenses is the large tolerance in terms of alignment between the different elements. The tolerances calculated were ± 1 mm for the longitudinal distance between optical fiber and the first lens, ± 0.5 mm for lateral alignment. These, together with the fact that these lenses come with an uncertainty of focal length and thickness of ± 0.2 mm makes possible to position them rigidly and definitely into the structure. The system requires the positioning of the optical fiber in the focus of the first lens and of the cantilever in the focus of the second. The two lenses should be distanced at "infinity" between each other. A piece was designed to hold the lenses in a tube with their diameter, and keep the distance between them fixed. The fiber is also mechanically held, and the mirror is glued. The whole system is thus mechanically pre-aligned before any measurement is done.

However, even with perfect pre-alignment of the optical components, because of the large tolerances and the present uncertainties, a motorized system has to be used to place the focus of the optical system exactly in the cantilever backside. This system will be explained in the subsection 2.3.5. Figure 2.12 shows different details of the assembly designed.

An interesting feature of this optical scheme is that, while a small misalignment (estimated by Hoogenboom [58] to be 11° in his specific alignment system) of the cantilever backside and the incoming laser beam would make impossible coupling the reflected beam into the optical fiber, and thus the interferometric measurement, it will despite this make it possible the measurement of the beam deflection, as long as one includes a photodetector somewhere in the assembly. The change of the measurement scheme can then be done easily.

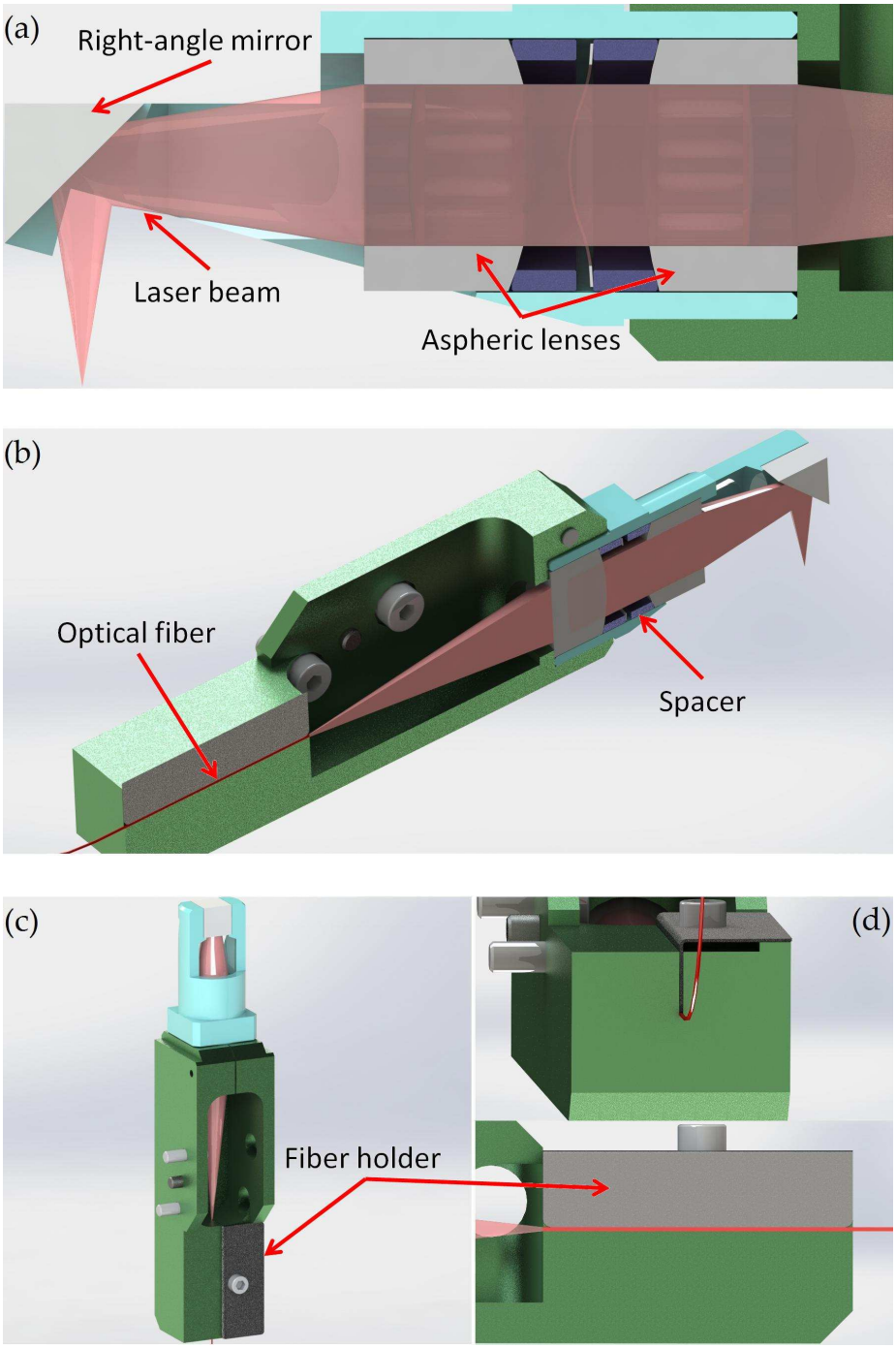

Figure 2.12: Optical assembly designed for the HSX-AFM: (a) cross section of the lenses holding assembly, together with the right-angle mirror; (b) section view of the whole piece; (c) complete piece; (d) details of the fiber holder.

Finally, a structure was designed to position an order separating aperture close to the sample. Following the requests of ID13, the OSA should be placed at a maximum distance of 7 mm from the sample. The aperture should be a disk of 2 mm radius with 1.2 mm axial thickness. Such dimensions, however would block (at least partially) the laser beam to the cantilever. A compromise has been made by reducing *a posteriori* the size of the OSA, literally cutting a part of it, so it would fit in the AFM assembly. Figure 2.13 (a) and (b) show the AFM assembly and the OSA. The whole structure is presented in Figure 2.14 (a)-(d). As evident from the insert (b) of the figure, the optical assembly would interfere with the proposed lead foil, 10 mm apart from the sample. However, there is still some space that can be used to custom-make a new lead foil. This solution was accepted by the scientists of ID13 since is cheaper and easier than redesigning the AFM. The assembly will have 73.6 mm of height, 26.5 mm of width and 10.6 mm of thickness in the region of the beam. The materials chosen are aluminum ENAW2017 for the whole structure and INOX for the fiber holder. Figure 2.14 (d) shows the structure on top of the base of the AFM.

2.3.4 The Cantilever Holder

In the design of the cantilever holder several aspects need to be considered. First, and perhaps more important, it has to be mechanically very stable. For this reason it is usually constituted by a compact piece made of hard materials; then, it has to provide an easy way to remove and reposition the cantilever without hassle for the user; it should position the cantilever to make an angle of 15° with the sample; it should provide a way to excite the cantilever (usually, and in the present case, this is done acoustically). In the assembly of the HSX-AFM some other requirements had to be addressed: the cantilever holder should be thin enough to fit in the very small space

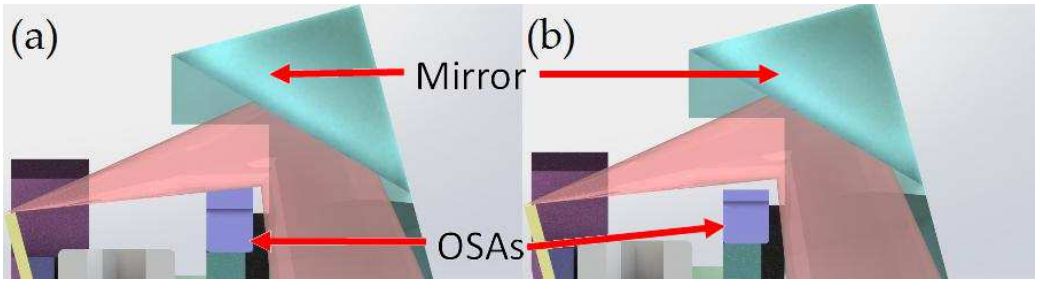

Figure 2.13: Set of optical system and OSA for (a) original-sized OSA and (b) machined-down one.

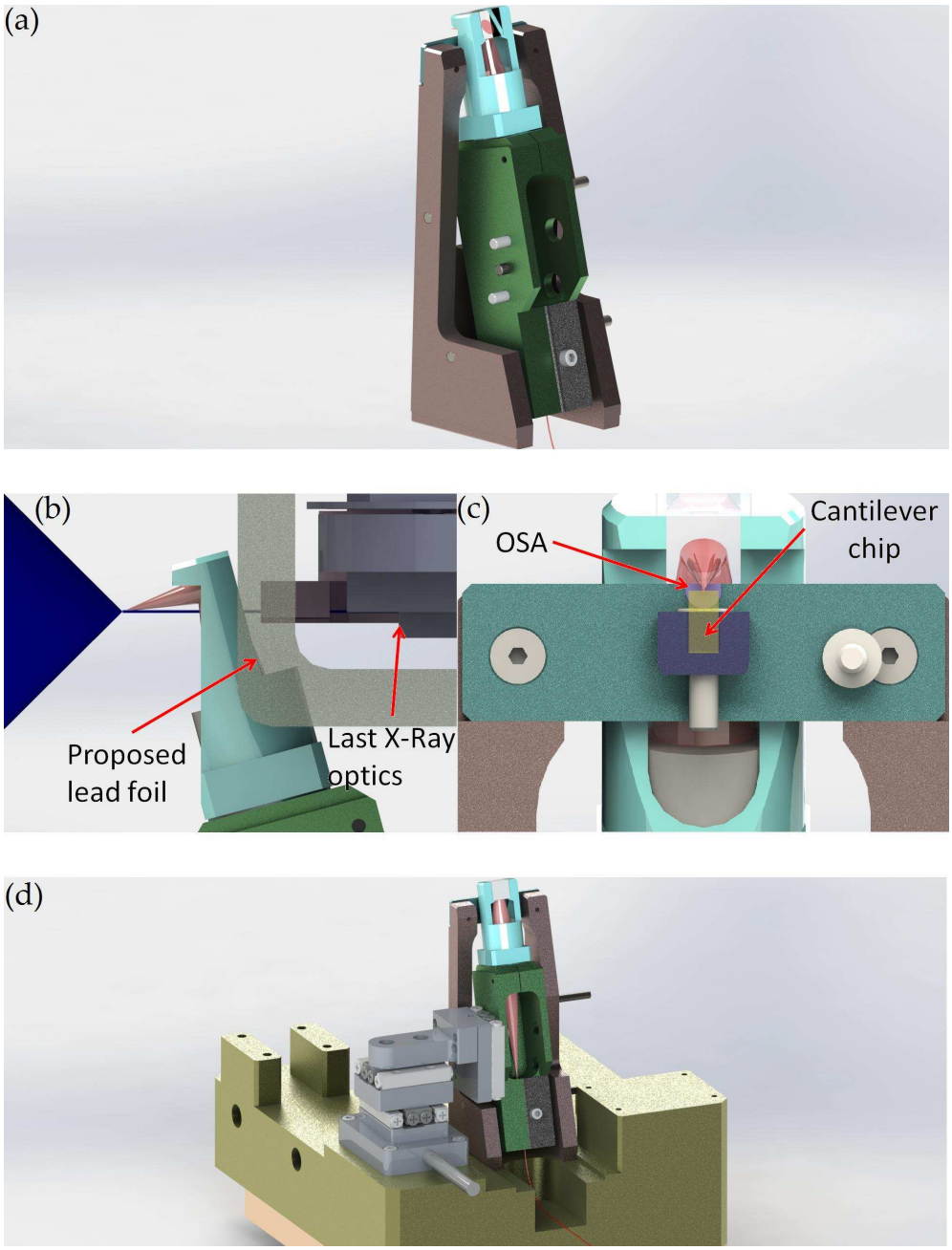

Figure 2.14: Optical assembly of the HSX-AFM: (a) the complete assembly; (b) side view with the detail of the experimental setup of ID13; (c) detail of OSA aligned with the laser beam and cantilever; (d) the whole structure on top of the AFM base, together with the motorized stage that will position it.

between the scanner and the optical readout assembly; the holder should be easily removable, since the amplitude of movements of the scanner (which we will see in the section 2.3.5) could not be very large.

The component has been designed following the concept of cantilever holders of some commercial and custom-made AFMs present in SSL. It consists of a stiff body, thick in the region far from the cantilever which connects to a motorized assembly, that elongates into the center of the microscope where the cantilever is held. To position the cantilever one just has to slide it into a slot machined with the right inclination, and tight it down with a small screw. This components gives the possibility of reading the electric current from the cantilever, which is important when using the cantilever as the X-Ray beam probe [30]. To excite the cantilever a piezoactuator is fit tightly in the holder, somewhat away from the cantilever chip. This was done to prevent the increase of thickness near the cantilever region, keeping however a good excitation of the cantilever through mechanical vibrations of the piece at the right frequency. The piezoactuator chosen was the *PL022.30* from *PI* (datasheet in Annex A). The whole holder can be positioned with a motorized assembly detailed in section 2.3.5. Using the full potentialities of the nanometric movements in an Atomic Force Microscope, a second order separating aperture is glued in the cantilever holder, away from the cantilever region. With this, it should be possible to position the beam in the sample exactly, while not performing AFM, by approaching the OSA as close as needed to the sample. To remove the cantilever holder the whole piece slides off to the side without having to displace too much the cantilever. To firmly keep the cantilever in place and allow for easy removal, a set of magnets assure the connection between the holder the rest of the AFM. This will be useful when performing several measurements requiring cantilever changes, allowing to land in the same area of the sample. With the exception of the magnetic parts, all of the pieces are in aluminum (ENAW-2017). Figure 2.15 presents several views and details of the cantilever holder.

2.3.5 Movement in the HSX-AFM

Besides the design of the different components of the AFM, attention must be given to their different displacements. An AFM is a complex system where a good alignment of the parts is crucial for the success of a measurement. This is even more true when placing this AFM in the beamline. Several different displacements have been identified and different strategies have been adopted to address each one. In the following, each of them will be detailed:

- Fast scanning of sample: this was already detailed in section 2.3.2. The

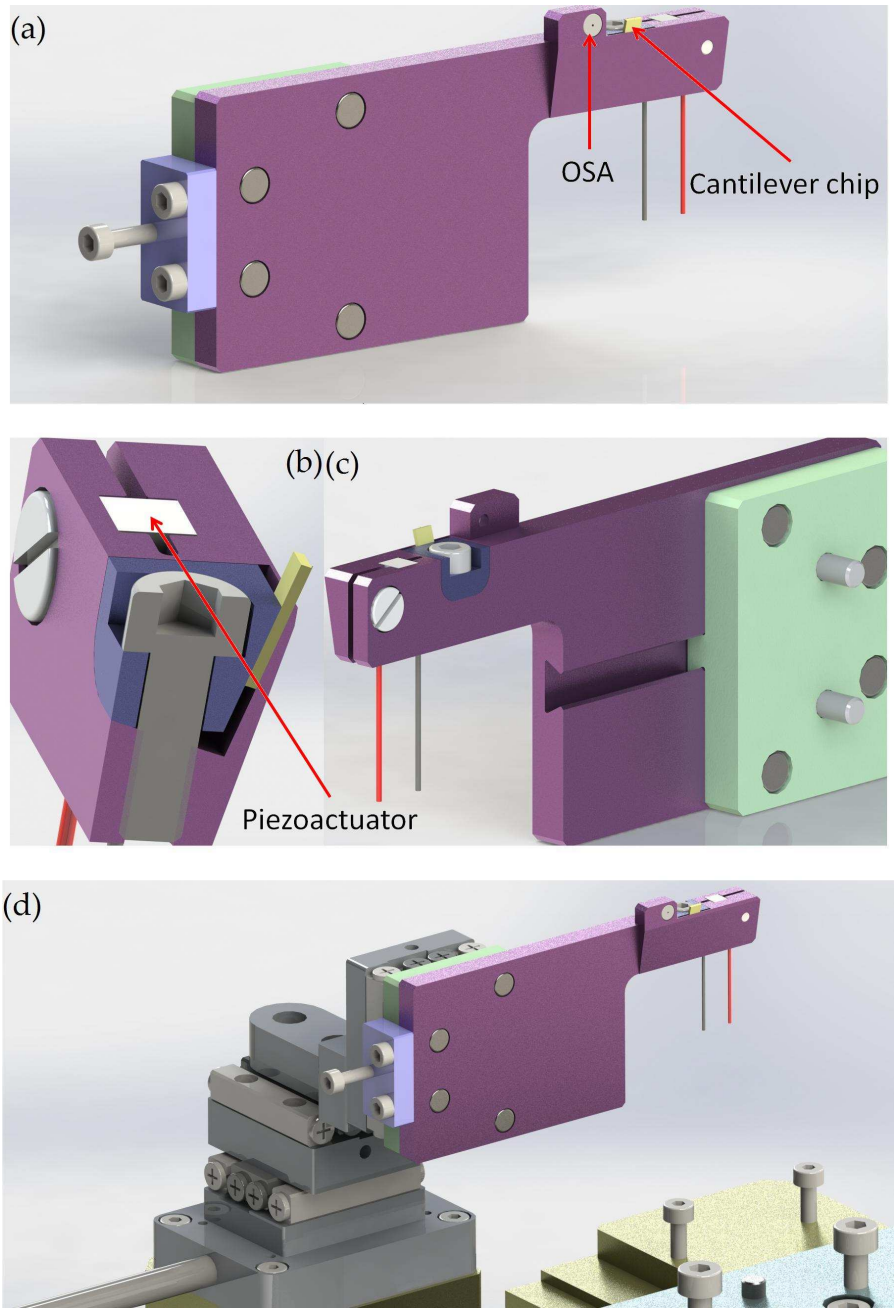

Figure 2.15: Cantilever holder designed for the HSX-AFM: (a) front view, where we can see the cantilever chip, the OSA and the screw mechanism for removing the holder from the assembly; (b) side cut with the cantilever positioning system; (c) backside, where we can see the sliding mechanism; (d) the whole assembly with the motorized stage. Some of the constituents are detailed.

maximum scan size is $6.5 \times 6.5 \times 2$ µm. The resolution of the movement can achieve the picometer.

- Long displacement of the sample in the yz plane: to be able to analyze routinely different areas of a sample it is necessary to provide longer displacements than the one mentioned above. A simple methodology was used: the stick and slip actuation. This type of actuation is based on the friction between two surfaces. An object, in this case the sample, sits on top of a larger surface, the sample holder. Normally in an AFM when the sample holder moves slowly enough, the object moves with it. However, a very fast "jerk" of the sample base overcomes the friction and sample slides a considerable distance before it stops. This is used to displace it in small steps.

  The size of the step is dependent on the type of force applied and the two surfaces and be optimized to be reproducible. A preliminary test of this motion was done in SSL using another custom-made scanner, providing strokes of 100 µm-1 mm. An important detail is the electrical circuitry necessary to extend fast enough the piezoactuators. With this objective, a special switch amplifier is being developed in the lab to drive this stick and slip movement. Technical details of this fast switch can be found in Annex C. This amplifier was not developed in time for the end of the project and so its calibration and test is outside of the scope of this thesis.

- Long displacement of the sample in x: to approach and retract the cantilever from the sample, in order to change cantilever or sample, a long displacement of few millimeters (at least) is needed and a reliable stage is then necessary. In this type of motion one looks for a resolution better than the maximum displacement of the vertical piezoactuator (2 µm), a maximum stroke high enough to remove the sample easily (for this microscope in the range of 1-20 mm), and, perhaps more importantly, stability: during the measurement the sample can only be displaced by the scanner and not by any other motor.

  A somewhat complex assembly was designed to achieve the purpose. The whole scanner will be displaced with a motor: the *PiezoLEGS* LT2010A from *PiezoMotor*. This is a motorized assembly that combines the movement of different piezoactuators functioning in shear mode (expanding to directions perpendicular to their axis) as well as in the "normal" way, to move a bar that is attached to these piezoactuators. They function like little legs protuding from this bar, hence the name. There is always one or more piezoactuator in contact with the

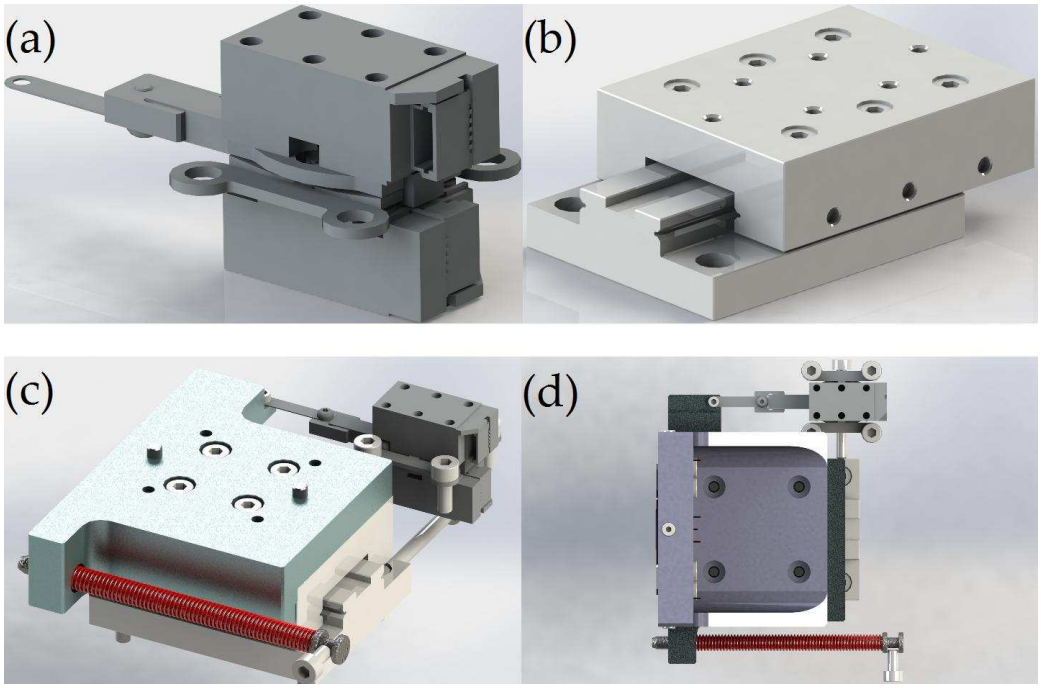

Figure 2.16: Scanner movement assembly: (a) PiezoLegs motor; (b) Sliding plate; (c) the base of the scanner with the motor, the plate and the pre-loaded spring; (d) top view, with the scanner on top of the movement stage.

bar, and which makes the blocking force is much higher than in most of the high resolution motors (in the case of the motor chosen 22N). The datasheet can be found in Annex A. To avoid sideways movements the scanner is placed in a structure that is attached to a sliding guided plate, *NKL2-50-RF* by *Axmo* (reference in Annex A). Pushing one side of this plate is the motor, and on the other side is a pre-loaded spring that avoids also any backlash in the movement or bending. The assembly provides a 10 mm range of displacement. Despite the small space to change the sample, a larger stroke motor would have implied a larger assembly, more costly and heavy, and would not improve too much the working space, which was considered then high enough. The resolution in displacement is in the order of the nanometer. The designed scanner base material was chosen to by aluminum (ENAW-2017). In Figure 2.16, it is possible to see this assembly guiding the scanner.

- The alignment of cantilever, laser beam and X-Ray beam: the cantilever and the laser focal point need to coincide with the X-Ray axis in the same point. As such, two different movement stages are needed.

The cantilever is positioned placed in the X-Ray beam by a modified assembly of a 3d positioning stage consisting of three *SLC-1720* positioners by *Smaract*. In this stage the vertical positioner is inverted from the normal configuration, to reduce the size of the cantilever holder, increasing its stability. To position the laser spot in the cantilever backside another *Smaract* assembly is used. The 3d manipulators provide a working space of $12 \times 12 \times 12$ mm^3, and a sub-nm resolution. Drawings of the motor and both assemblies can be found in Annex A.

- The alignment of the whole assembly with the X-Rays: done by the hexapod of ID13, already detailed. It has a range of ± 20 mm in y and z, with a minimum step of 1 µm, and ± 6 mm in the x direction, with the step size of 0.5 µm.

These different displacements have to be well coordinated to make an AFM measurement. In Chapter 5 the alignment procedures thought for this microscope will be detailed.

2.3.6 Some other parts and the Final Assembly

Finally, there is the need to carefully position all of the elements with respect to each other, and with respect to ID13's hexapod. Two different pieces were created, both in aluminum (ENAW-2017). One serves as a support for all of the pieces, and the other makes the connection with the hexapod. No special consideration was needed for these, besides trying to maximize the stability minimizing weight and cost. The two pieces can be seen in Figure 2.17

Upon mounting, the instrument has a design weight of 1.83 kg. It will measure 114.0×94.0 mm^2 on the base, and the height of the instrument will be 127.8 mm. From the base to the sample height it will measure 100 mm. The total thickness, in absence of any sample and with the cantilever "in contact" will be 21.25 mm. All of the parts have been contracted out to reduce delivery time. Figure 2.18 shows different views of the final assembly.

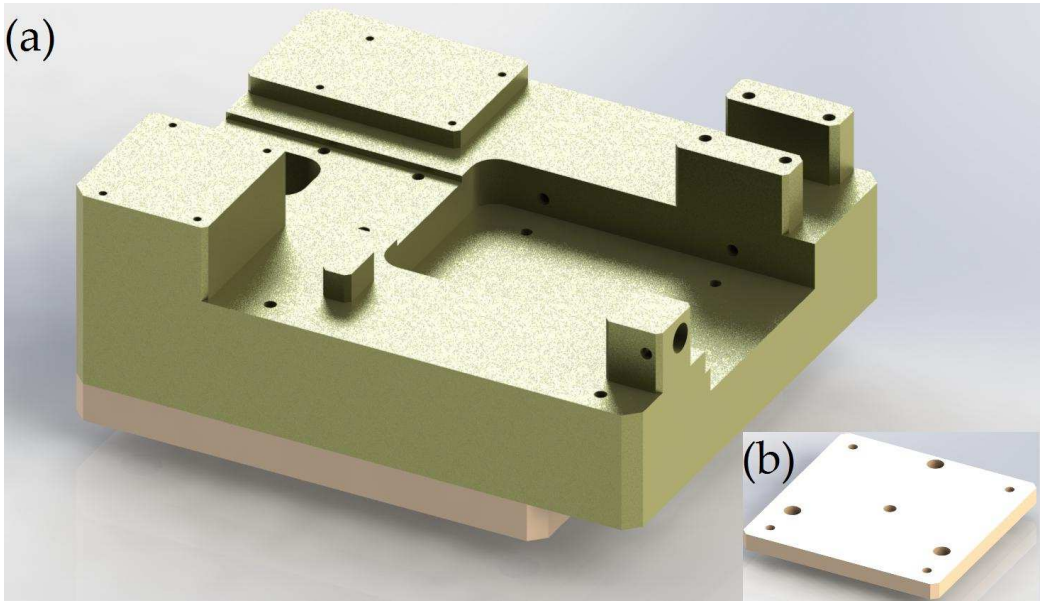

Figure 2.17: Base of the HSX-AFM (a) the two pieces interconnecting the HS-AFM and the hexapod; (b) the bottom plate.

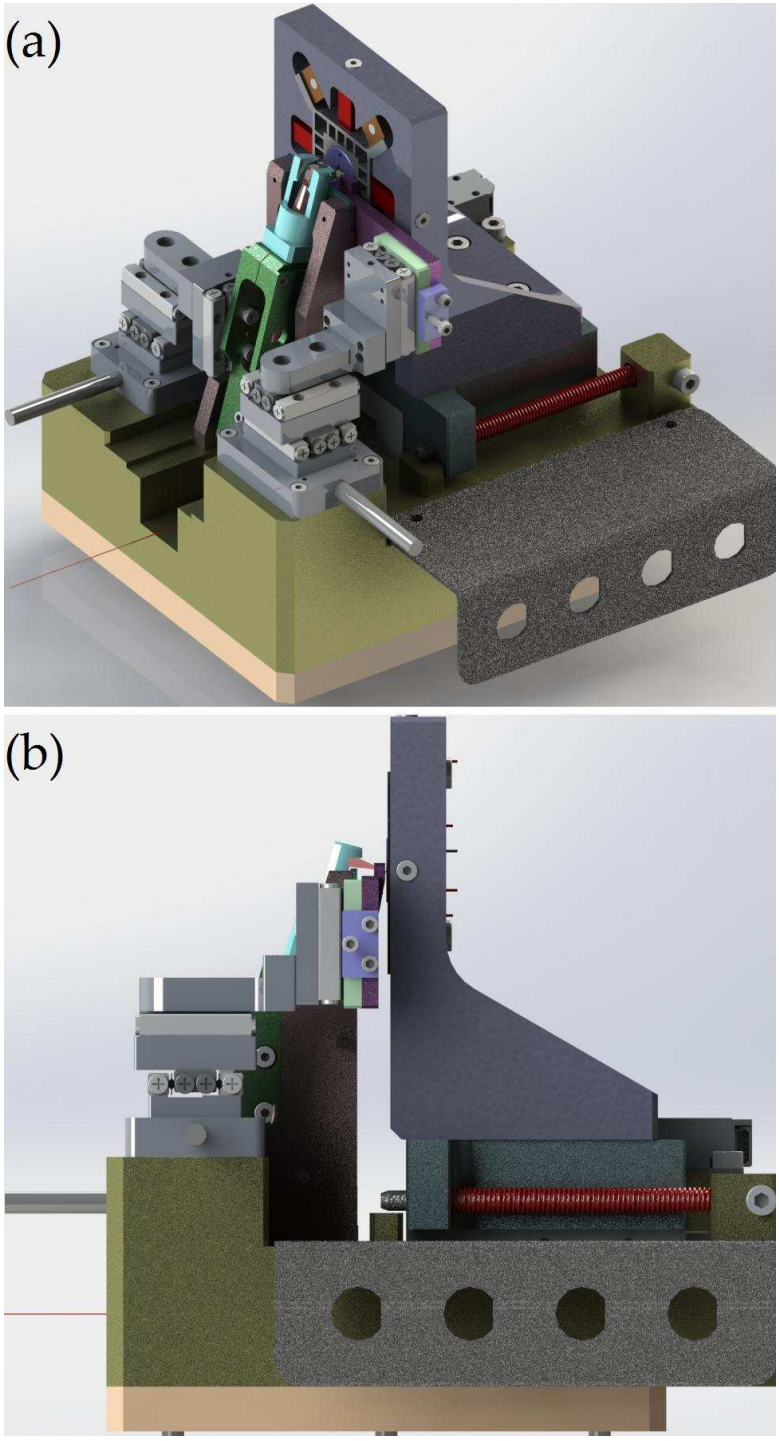

Figure 2.18: The model of the HSX-AFM: (a) isometric view and (b) side view.

Chapter 3

The Construction of the HSX-AFM and first tests

When constructing an atomic force microscope several parameters need to be optimized, such as the positioning and the pre-loading of the different piezoactuators essential to achieve fast and reproducible movement of the sample, the position of the lenses, mirror and fiber to achieve the best signal-to-noise ratio and the smallest laser spot size on the cantilever, the angle between the laser beam and the cantilever, and many more. To give an idea of the processes involved in building an AFM, a chronological description of the assembly and calibration of the HSX-AFM can be followed in this chapter. All the measurements shown in this chapter have been performed in air.

3.1 Building an AFM and the pursuit of the first image

Several chores have to be performed in the construction of the microscope: screwing the parts together, soldering electrical wires to the piezoactuators and designing an easy-to-plug electrical scheme, connecting them to the electronics module. The installation of the optical components follows. The mirror is carefully glued onto its support with UV epoxy bonding. The optical fiber is cleaved using a simple procedure that successively strips the core part of the fiber of its outer components to ensure a perfect planar surfacem, parallel to the surface of the cantilever. The other end of the fiber is connected to the coupler, and its other three branches output to the laser, to a photodetector and the remaining one is left free. The output of the photodetector is connected to a transimpedance amplifier *FEMTO DLPCA-200*

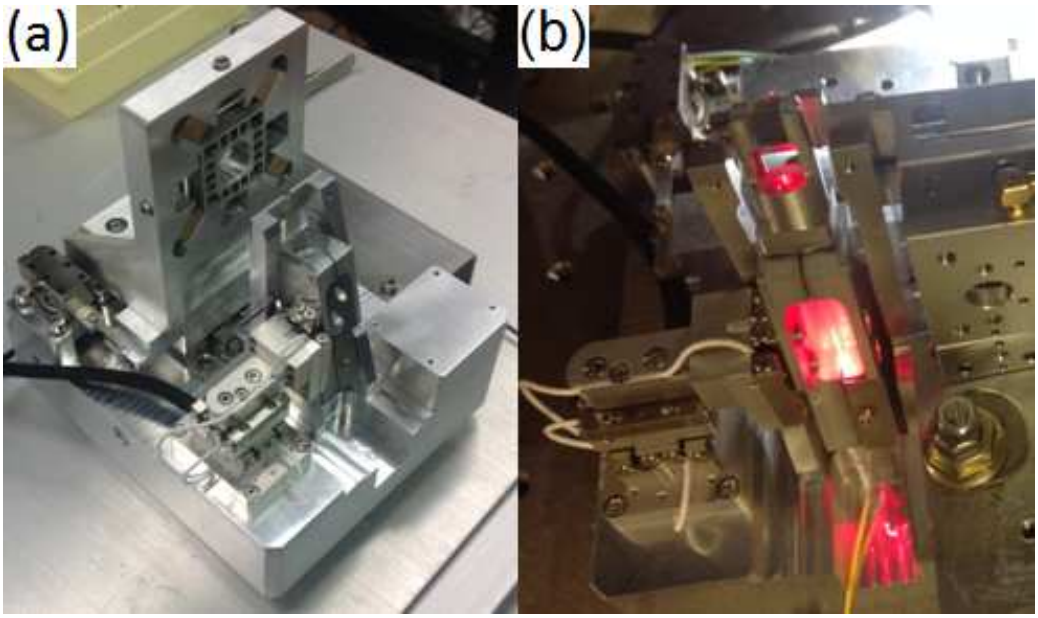

Figure 3.1: The first steps of the assembly of the AFM: (a) mounting the scanner; (b) turning on the laser beam and a first attempt to focusing.

and the resulting voltage signal is fed to the electronics module. The long-approach motor is plugged to a 12 V stabilized voltage source. The input of the motor is a voltage source, ranging from -12 V to 12 V, that controls the speed and direction of the movement. After all the motors are screwed to the AFM base, the user can control the movements of the optics, cantilever and scanner with the graphic user interface provided. In Figure 3.1 pictures with the different stages of building and components of AFM are shown.

An important problem in the construction of the HSX-AFM came from the fact that the delivery of the modified Smaract assembly responsible for the positioning of the cantilever took much longer than what was anticipated. Because of this, the mounting and operation of the AFM had to be done using a different motor set, already present in the lab. It consisted of three *MS 30* translation stages from *Mechonics*. Their performance is similar to the one of the original motors but they suffer from a big disadvantage: since the rest of the assembly was not designed to accommodate these motors, it lacks the correct screw holes to connect the motors to the AFM base and the cantilever holder to the motors. This was "solved" by mechanically clamping the different parts, a solution that was obviously far from ideal and, as it will be seen, affected greatly the measurements obtained with the instrument.

The adaptation of the motors has two main effects on the microscope. The

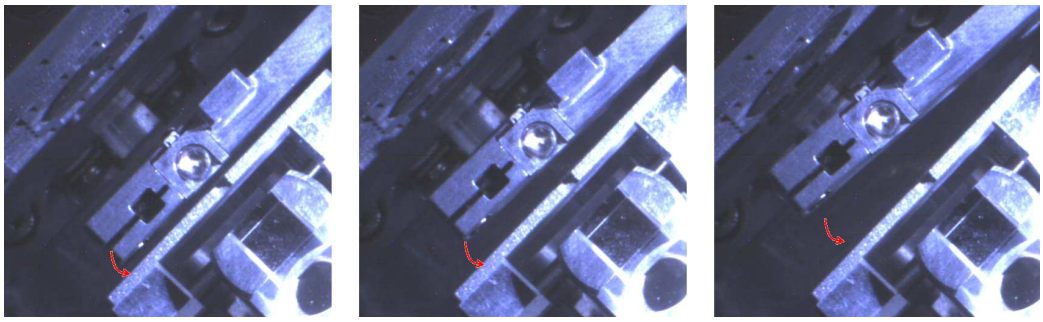

Figure 3.2: An example of the misalignment caused by the adaptation of another motorized assembly. To increase the signal-to-noise ratio and perform better images these sources of error must be eliminated.

first one, of easier solution, is that it originates a misalignment between the beam and the cantilever that was previously minimized by the constriction of the motors to the right orientation. As it is seen in Figures 2.5 (c), 2.15 (d) and 2.18 (b), the cantilever holder has to be held with a precise orientation such that its lateral faces are parallel to the sample holder. If not, the reflected laser beam will not re-enter the fiber and no interference can be measured. Figure 3.2 exemplifies this situation. To correct this, a system of screws and holders was built to constrict the orientation and position of the motors. Tinkering a bit more with the cantilever holder provides an alignment that is, at least, sufficient for regular measurements. The second effect comes from the drift: the cantilever holder is now held by glue and scotch tape, instead of screws. This causes permanent drift that has an effect on the stability and signal-to-noise ratio of the instrument. It is difficult to keep measuring on the same position of the Fabry-Perot cavity, since in most of the time the cantilever is moving in all three directions of space. The sensitivity will depend on the alignment of the cavity and so the ability to perform measurements at high speed and with biological samples, since these require a high signal-to-noise ratio.

In the first tests of the microscope an easier configuration than the one demanded by ID13 was tested. It consisted in placing the optical fiber not at the focus of the aspheric lenses, but some millimeters closer to the first lens. The effect is that the spot of the optical system will also move some millimeters farther away, which would facilitate the alignment with the adapted motors. Progressively this was corrected until the right configuration was achieved. In Figure 3.3 this procedure is shown.

To align correctly the laser with the cantilever end, a somewhat complex operation has to be performed. The cantilever can be moved in x, y and z.

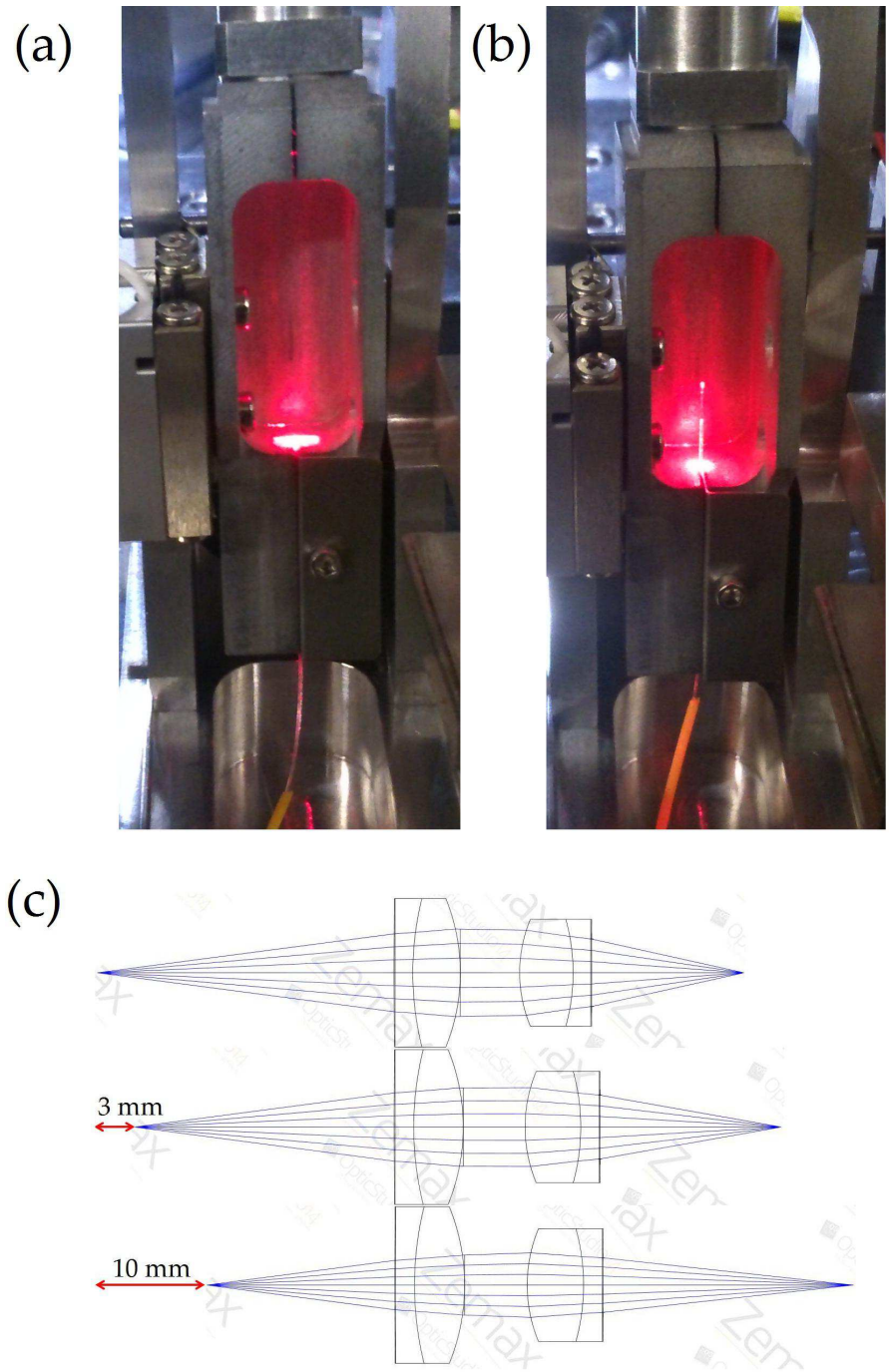

Figure 3.3: Offset of the fiber position, and its effect on the focus position: (a) original position of the fiber; (b) the position of the fiber for the several measurements performed; (c) effect of the offset in the focal position (simulation with the software *OpticStudio*®by *Zemax*).

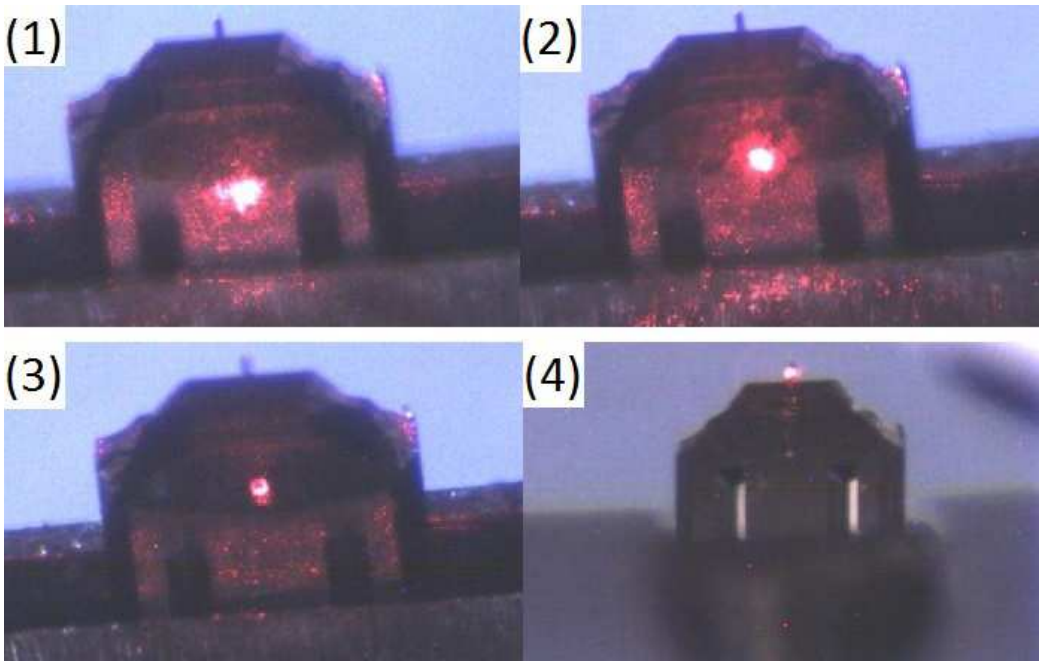

Figure 3.4: Several pictures detailing the different steps of the alignment procedure: 1 - the laser spot is placed on the cantilever chip; 2-3 the position with minimal spot size is found by moving the cantilever in x; 4 the cantilever is finally positioned on the focal point of the system.

However, the laser beam propagation direction is not along any of those (see Figure 2.11 (a)), which means that a movement along x changes the visible spot size on the cantilever beam and also the longitudinal position of the spot, along the cantilever. Thus, the alignment procedure starts by placing the laser spot on the cantilever chip, to allow for better visualization. Moving the cantilever (or the optics) in x one finds the position where this spot is minimum. Afterwards, the spot is placed on top of the cantilever and is fine tuned in all three directions. The cavity can be carefully adjusted and the x position of the optical system is then controlled using a proportional-integral controller. This controller keeps the DC signal of the photodetector constant throughout the experiment. Figure 3.4 shows the alignment procedure.

Figure 3.5 presents the first interference fringes and Figure 3.6 (a) presents the first resonance curve obtained with the HSX-AFM. The cantilever used was the CSC17 from Asylum suitable for contact mode, with nominal stiffness $k = 0.18$ N/m and resonance frequency 13 kHz. This was part of the strategy to start with cantilevers more easy to detect, as they are larger and longer, and then converge to the extremely small cantilevers necessary for

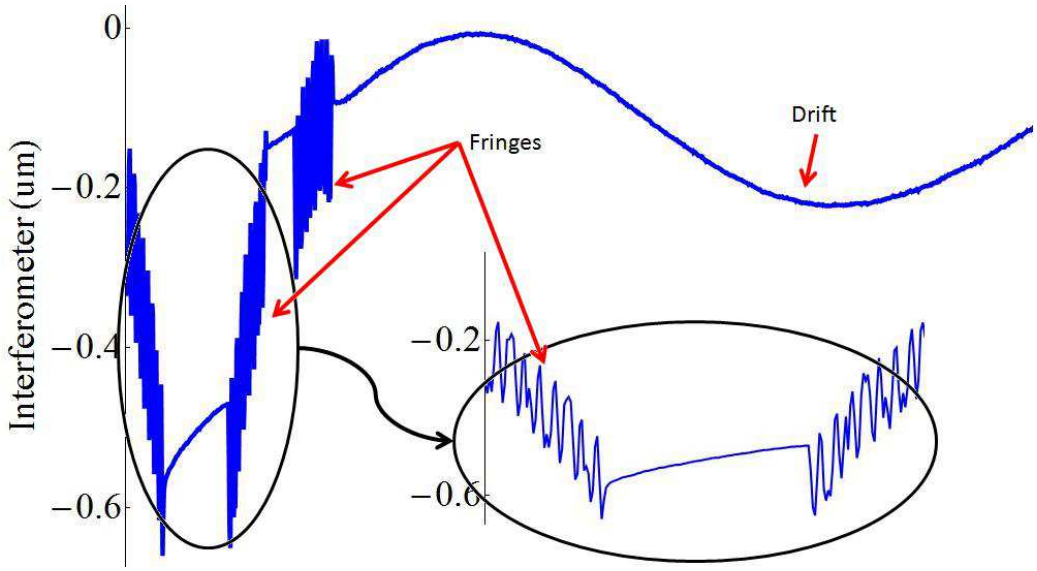

Figure 3.5: The first fringes obtained with the instrument: the cantilever is displaced by steps of 3 µm in x and afterwards is left to rest. The signal aquired by the photodector can be seen. After the observation of the fringes, a fast oscillation signal, a much slower periodic signal can be observed, indicating that the the distance between fiber and cantilever is slowly varying.

fast measurements of biologic samples.

The effect of the defectuous mounting of the cantilever can be seen on Figure 3.5: the fringes are followed by another oscillation, with a much longer period. This indicates that there is significant drift. The cantilever or the optical focusing system, even though these are more tightly fixed) is moving across space and the consequence is that the signal changes over time in a noticeable and periodic way. This causes problems to an AFM measurement, especially in contact mode. The sensitivity of the measurement depends on the position within the cavity: it will be maximum when expression 2.8 gives $I_{\text{det}}(d) = I_{\text{av}}$. The long oscillation during a measurement will change the calibration of the system and thus the value fed to the controller will no longer be correct. Furthermore, this drift is much higher due to the chosen detection scheme: an AFM employing optical beam deflection will measure the angle of the cantilever end, which will be much less prone to drift than the position measured by interferometry. Despite this fact, provided that the drift is minimized, it is possible to control the position of the cantilever to minimize this oscillation. Also, as it can be seen from figure 3.6 (a), the detection of amplitude and phase was made poorly, make a successful measurement difficult to obtain.

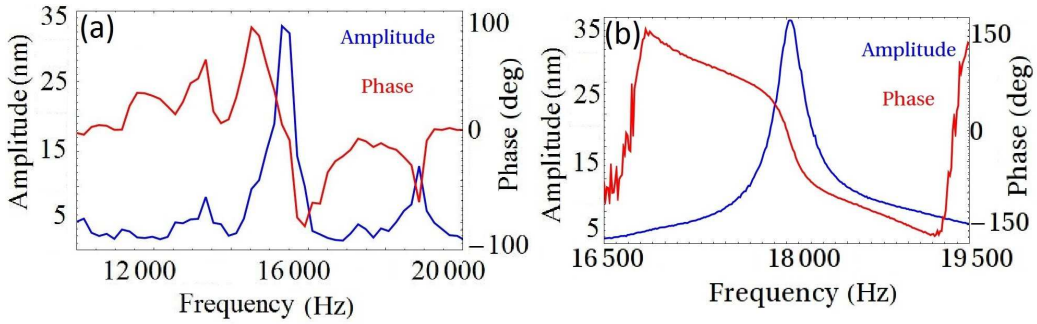

Figure 3.6: Amplitude and phase dependency of the cantilever frequency of excitation: (a) the first resonance curve obtained with the HSX-AFM; (b) the same experiment performed after a series of upgrades in the instrument.

At first the HSX-AFM did not provide the expected results. Figure 3.7 (a) presents an image of a calibration grating. This grating is composed of several squared holes with 5 µm side and 150 nm deep, separated by a distance of 10 µm between each hole.
The images of topography and phase do not provide any results that can be identifiable with the sample described. However, the last plot presents result of an experiment that clarifies the problem of the AFM in this point: the tip is first put in contact with the sample; after, with the interferometer controller off, the sample is displaced in the direction of the cantilever by the full range of the scanner. The tip will move together with the scanner and by observing the change in the photodetector signal it will be possible to retrieve the displacement of the scanner. The number of oscillation periods observed will give the displacement of the cantilever and, thus, of the sample and scanner. According to Expression 2.8 an oscillation period corresponds to $d = \frac{1}{2}\lambda = 329$ nm. In this plot we can observe only half an oscillation for the whole range of movement of the scanner, meaning that the tip only moved about 150 nm, instead of the displacement of 2 µm predicted. It was clearly a result not suitable for most experiments and samples and it would make impossible the measurement of the topography of the calibration grating. To improve the capabilities of the scanner, the central piezoactuator mounting stage has to be analyzed and optimized.

Several experiments like this were performed with different placements of the sample holder. The results suggested that the impact of screwing the assembly tighter produced a big change in the scan size. The placement of a sample holder also slightly affects it. Additionally, the size of the magnetic sample holder sheet also seemed to affect the scan size. Meanwhile, the macroscopic position of the cantilever within the scanner (centered vs.

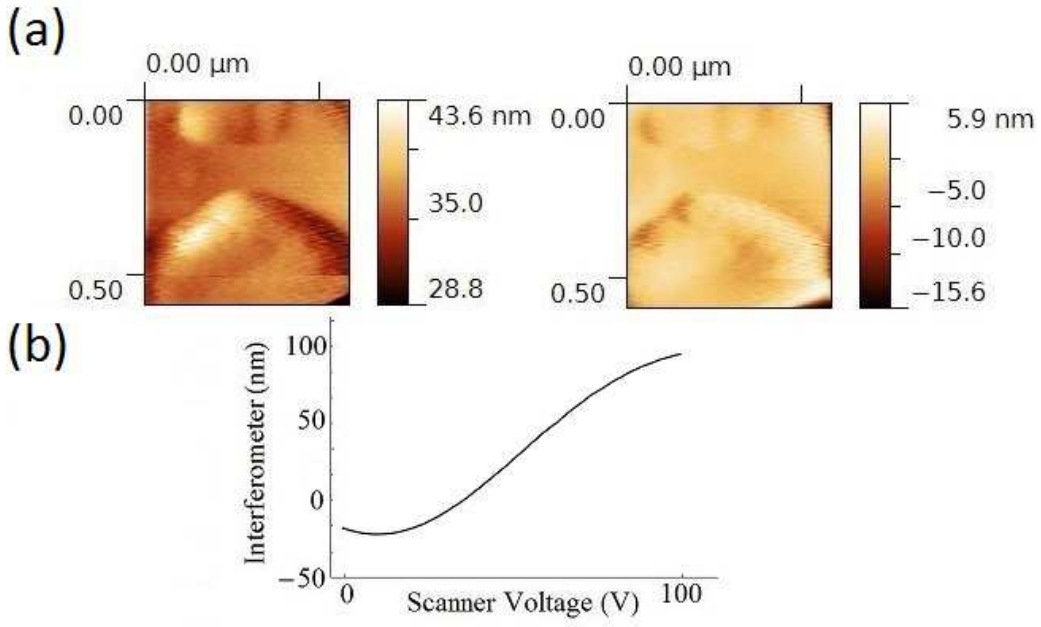

Figure 3.7: (a) Results of the contact mode experiment performed on the calibration grating with the HSX-AFM. Left: measured topography; Right: measured interferometer (error) signal. (b) measurement of the interferometer signal by pushing the cantilever with the sample.

displaced to the side) does not provide any change.

Further improvement of the microscope allowed also for detecting better resonance curves, as it can be seen in figure 3.6 (b). The AFM was now ready to be tested with a biologic sample. Figure 3.8 presents the measurement of single-strand plasmatic DNA, retrieved from an E.Coli bacteria, deposited on a mica sheet. These should present themselves as small wire-like structures, of 2 nm height, over the mica sheet. The cantilever used was the tapping mode MIKROMASCH HQ:NSC15/AL BS with a nominal resonance frequency of 325 kHz and a stiffness of 40 N/m.

The images, although lacking great quality, show the strands of DNA bound to the mica sheet. Furthermore, the default scanner calibration, at the time, provides the correct measurement of the height of DNA. It is possible to estimate that the maximum scan height at the time of the measurement was about 1.5-2 nm. This configures the first true measurement of biologic matter achieved with the HSX-AFM. There was still, however, room for improvement. The line scan makes it obvious that the amount of noise is too great to distinguish clearly any features of the sample provided.

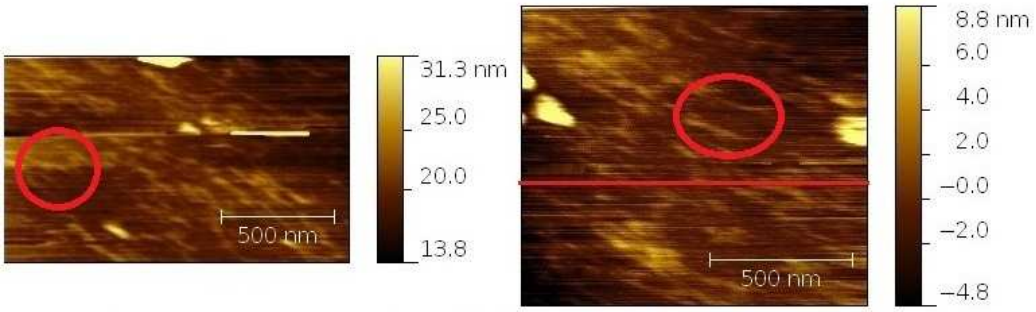

Figure 3.8: Single-strand DNA imaged with the HSX-AFM, topography measurements.

3.2 Perfecting the AFM for Biology and the road to high speed

In order to perform measurements at high speed of biological matter, the microscope has to be completely optimized to improve the signal-to-noise ratio. Apart from a better cantilever holder assembly, consisting of a more reliable interconnection between the AFM body and the *Mechonics* motors, a special attention was given to the position of the fiber: the maximum quantity of light has to be reflected on the cantilever, and back from the fiber to the lever, to improve the quality of the measurement. This can be done by gradually approaching the fiber position in the direction of its original placement. It was, however, verified that at about 1 cm from the pre-determined position the minimum in the spot size was achieved. The improvement in the measurement scheme was verified by imaging the same sample once more. Figure 3.9 presents the results. The images are now much sharper and the DNA much easier to be seen. The line profile makes it much clearer the presence of DNA than before, and its measured height is around 2 nm.

To test the capabilities of the instrument, the Olympus AC55, with resonance frequency 2.2 MHz and nominal spring constant 80 N/m was mounted. After careful alignment, all the measurement quantities were properly acquired. To note is the fact that this cantilever is already small enough such that it is not detectable with most of commercial AFMs, not equipped with small spot capabilities. To establish the capacities of the AFM, the cantilever was tested with the next sample, a new calibration grating. This time, the grating was composed of several "lines", 100 nm deep, arranged in a period of 3 µm. With the intention of properly calibrating the scanner, the sample was analyzed with both a commercial AFM, the *Asylum MFP-3D*, and the

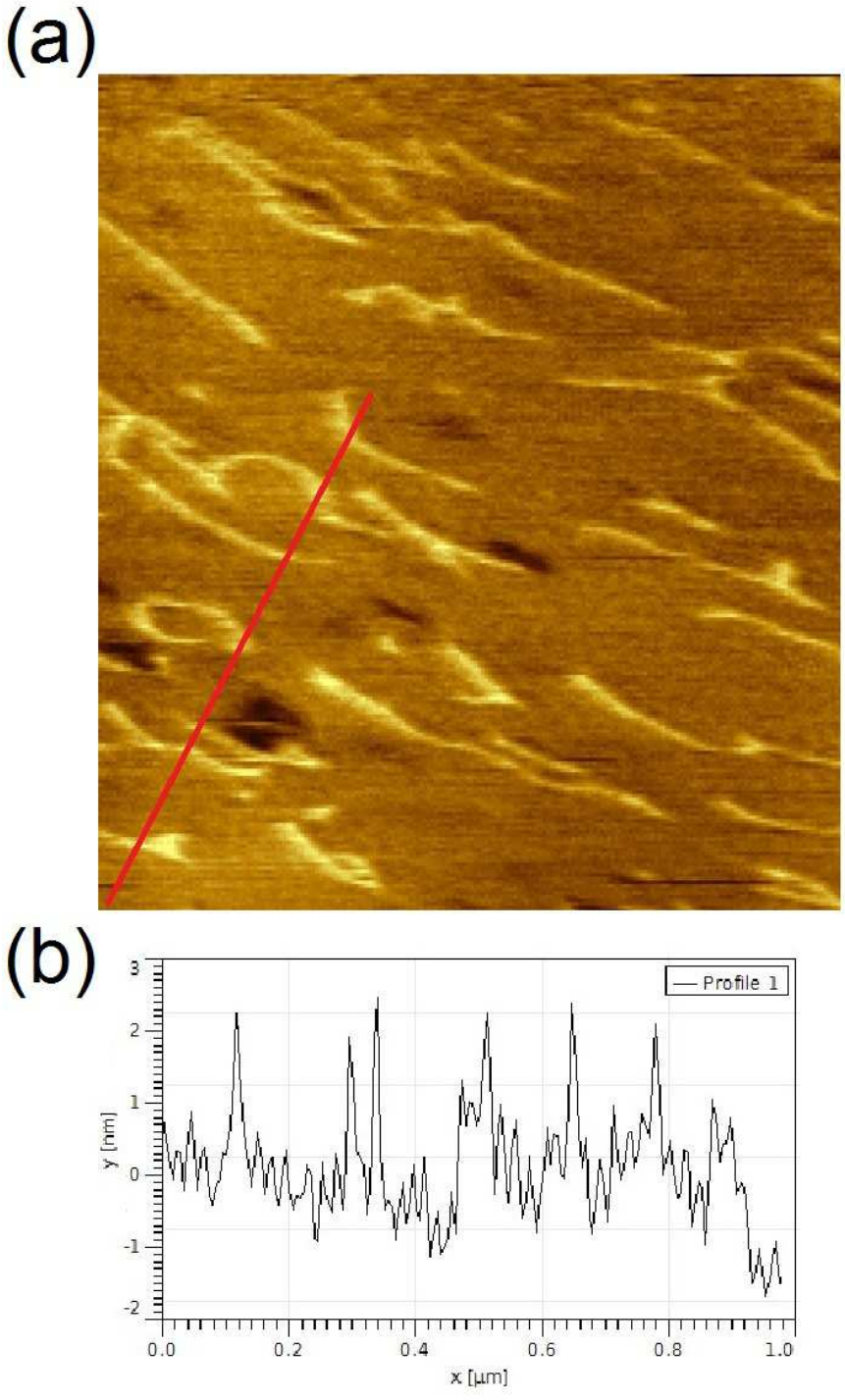

Figure 3.9: Single-strand DNA imaged with the improved HSX-AFM: (a) Topography measurement; (b) Line scan of the indicated region in (a).

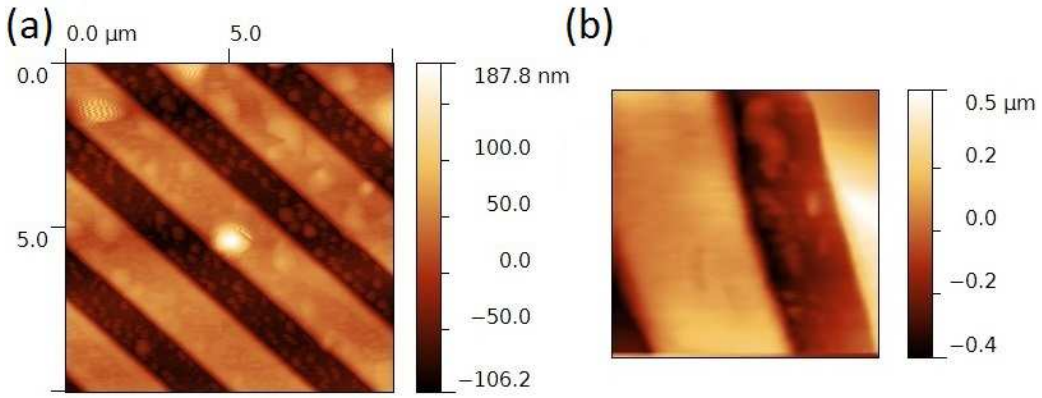

Figure 3.10: Topography images of a calibration grating: (a) measurement done with commercial AFM Asylum MFP-3D; (b) measurement done with the HSX-AFM.

HSX-AFM. Figure 3.10 presents the results.

The analysis of the images provides three important hints. Firstly, the scan range could now be calibrated properly: after comparing the two images the maximum scanning area was established as 3.5 µm × 3.5 µm. Secondly, the images also allow for a more precise calibration of the allowed scan height: the maximum vertical displacement was found to be 800 nm. This is a significantly shorter displacement than the one found previously, proving again that this characteristic of the scanner is highly dependent on factors such as the screwing force and the position of the piezoactuator and the type of sample holder. Thirdly, inspecting the image carefully, it is possible to see the effect of sample drifting in it. This drift (of the sample or the cantilever holder) is prejudicial to the measurement and causes the lines to be blurred. It would have to be solved. However, the drift also provided an opportunity to inspect the speed of measurement performed with the HSX-AFM. Increasing the scan speed would allow the following of this movement, frame by frame. Figure 3.11 presents the results.

The figure clearly shows the advantage of performing, in this case, the measurement at high speed. Between each image about 30 seconds passed. In a normal AFM measurement the scan speed is usually above the minute mark. Without high speed capabilities the HSX-AFM would not be able to perform (at this point) a measurement of this sample.

The final challenge, in terms of the object of measurement, is the detection of the smallest cantilever commercially available, the already mentioned Olympus AC55, used to perform measurements at high speed of soft matter. Its extremely small dimensions make the requirements for the spot size un-

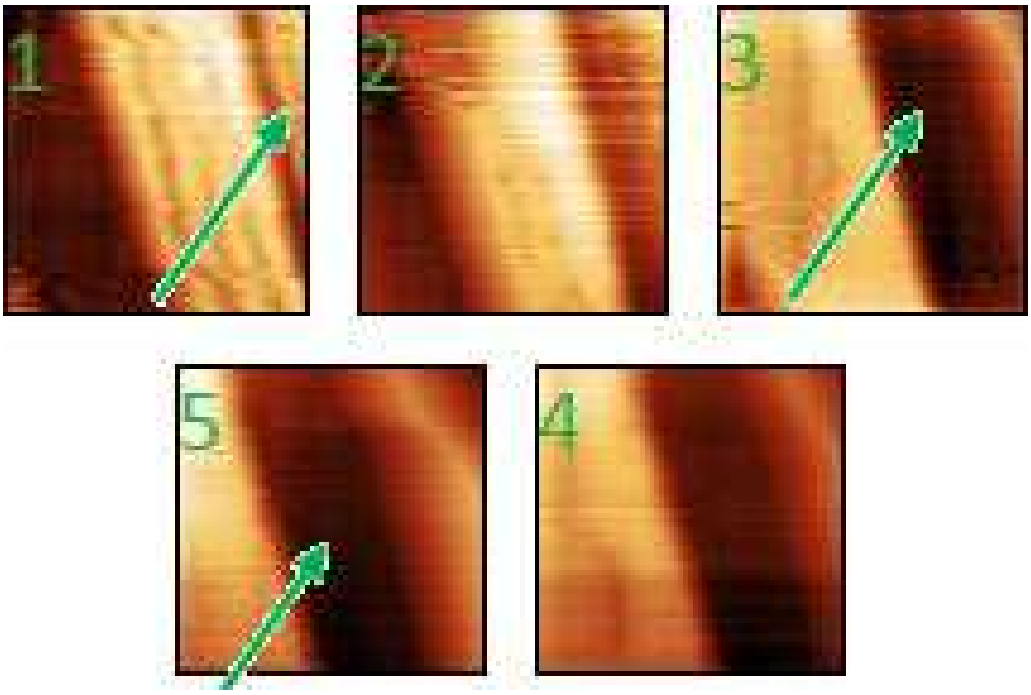

Figure 3.11: Sequence of images captured by the HSX-AFM: each frame was acquired in 2.9 seconds. The ones shown here correspond to intervals of 30 seconds each. In them, it is possible to observe the lines of the calibration grating drifting from right to left, as indicated by the green arrows.

surpassable. After the complex process of alignment of a cantilever so small, it was possible to detect the first fringes and resonance. These configure a clear achievement in regards to the objective of the project.

The detection of the small cantilever was tested making a measurement of another biologic sample. It was composed of phospholipids POPC deposited in a mica sheet. When deposited, these lipids can bind their hydrophilic part to the mica. In air, the lipids form a monolayer over the mica and so in an AFM image one should look for a sudden drop of 1-5 nm in the topography, where the lipids have not bound (or the opposite, depending on the quality of sample preparation) [61, 62]. Figure 3.12 presents the results.

In this figure it is possible to distinguish clearly the places where there is mica and where are the lipidic monolayers. The line scan indicates steps of about 2-3 nm, according to what was expected. Meanwhile, the phase image indicates that these regions are in fact two different materials (we could have, otherwise, a bilayer of lipids with some regions where there was only a monolayer). Our AFM is thus capable of performing high-resolution images

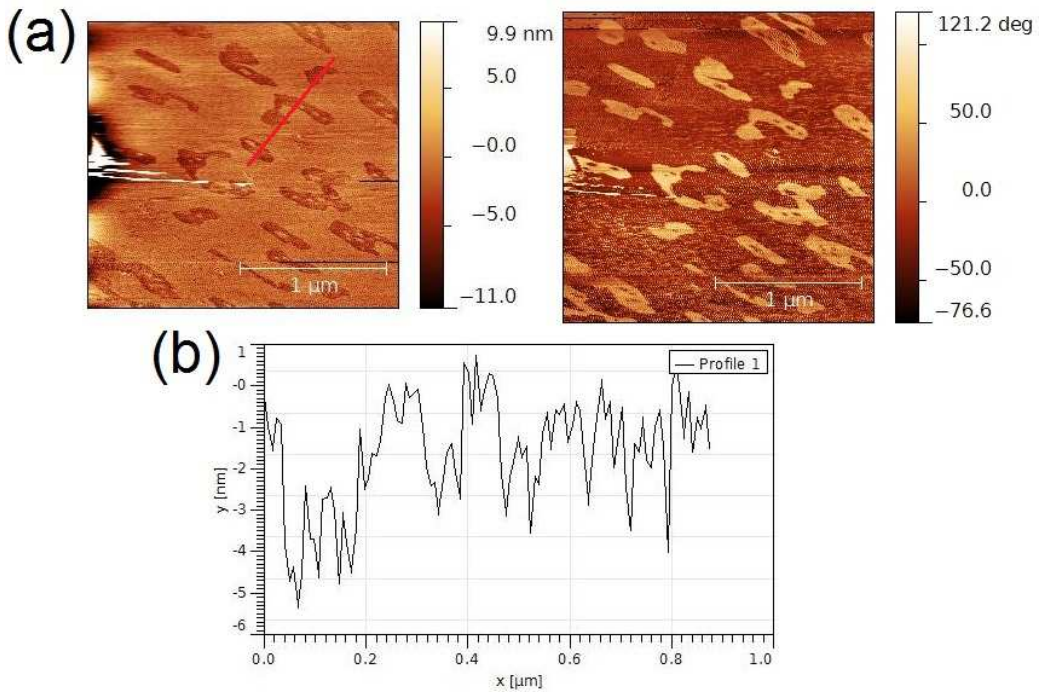

Figure 3.12: Lipidic monolayers imaged with the HSX-AFM: (a) on the left the measurement of the topography and on the right the phase; (b) line scan of the region indicated in (a) where the holes (mica) can be seen.

with extremely small cantilevers. The only off-beamline characteristic that is now needed to inspect is the maximum achievable speed. To investigate it, the same sample was analyzed. Figure 3.13 shows some of the frames acquired.

The scan speed was increased until the maximum achievable. The same two holes appear in successive images (red circles), showing it is possible to observe the lipidic monolayers until a scan speed of 0.6 Images/second! The limit found was, as predicted, the electronics: it was not possible to increase the speed of the imaging, and even to obtain the last one several manipulations of the software had to be done. This means that, in terms of speed, the HSX-AFM should be considered electronics-limited, being this the point to address to acquire faster frames. However, it is possible to observe that the images are affected by a great deal of noise (green circles). This causes the signal-to-noise ratio to not be high enough, and thus the maximum controller gains to be lower, to avoid instability. The result is the low contrast of the images acquired at high speed. Despite the limit of the electronics being present, it is important to discover the cause of the noise

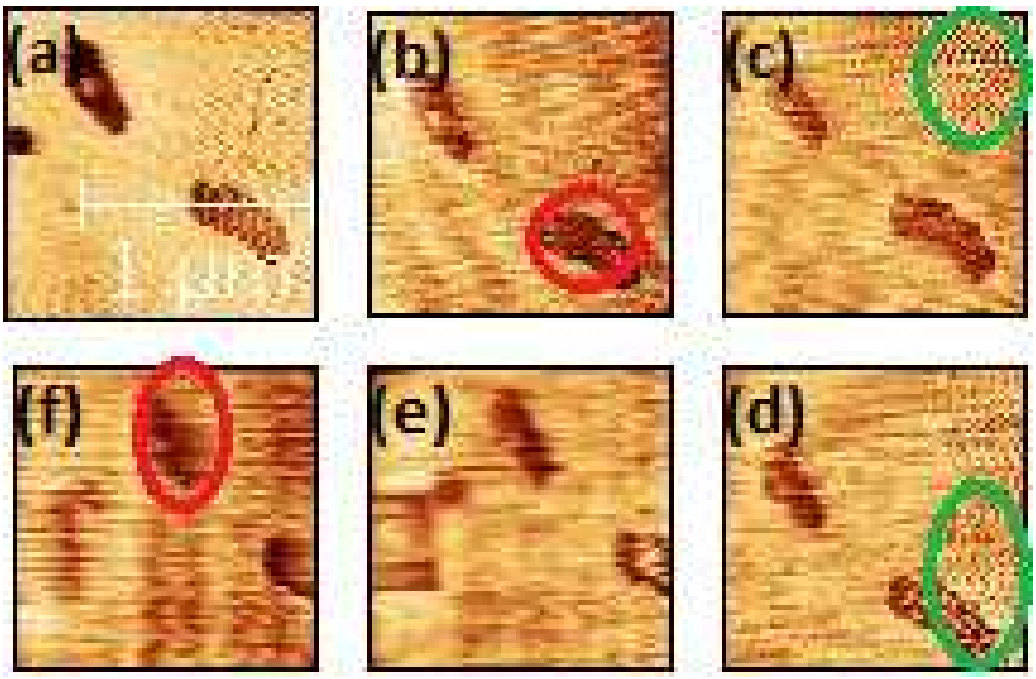

Figure 3.13: Several frames of POPC monolayers acquired at high speed with the HSX-AFM. The scan speed of each frame was (a) 37s, (b) 10.5s, (c) 8.5s, (d) 4.7s, (e) 2.5s and (f) 1.7s. In them are possible to see the holes in the POPC monolayer (indicated by red circles) and some noise (green circles) that appeared in the measurements.

in order to improve significantly the performance of the AFM. Also verified in this experiment is that the vertical and lateral scanners suffered from a loss of performance in their maximum displacement. The improvement of the scan size is important to ensure a more user-friendly microscope.

Despite these setbacks, the HSX-AFM is now ready to perform investigations at a moderately high speed of soft matter. To make this case, this chapter is ended with the results of an investigation over a sample provided by ID13. The sample chosen consisted of chitin, retrieved from specimens of Lamellibrachia, deposited on a sheet of glass. The same sample was analyzed with a commercial AFM and with the HSX-AFM, both experiments being performed with the mentioned tapping mode cantilever, with resonance frequency 325 kHz and stiffness of 40 N/m. Figure 3.14 presents both results.

The image of the commercial AFM reveals several structures, with different shapes (but mostly round). These have an average side of 1-1.5 µm and 1-1.5 nm height. These structures have almost all of them some holes, of about 1 nm deep. Meanwhile, in the image of the HSX-AFM one can also see

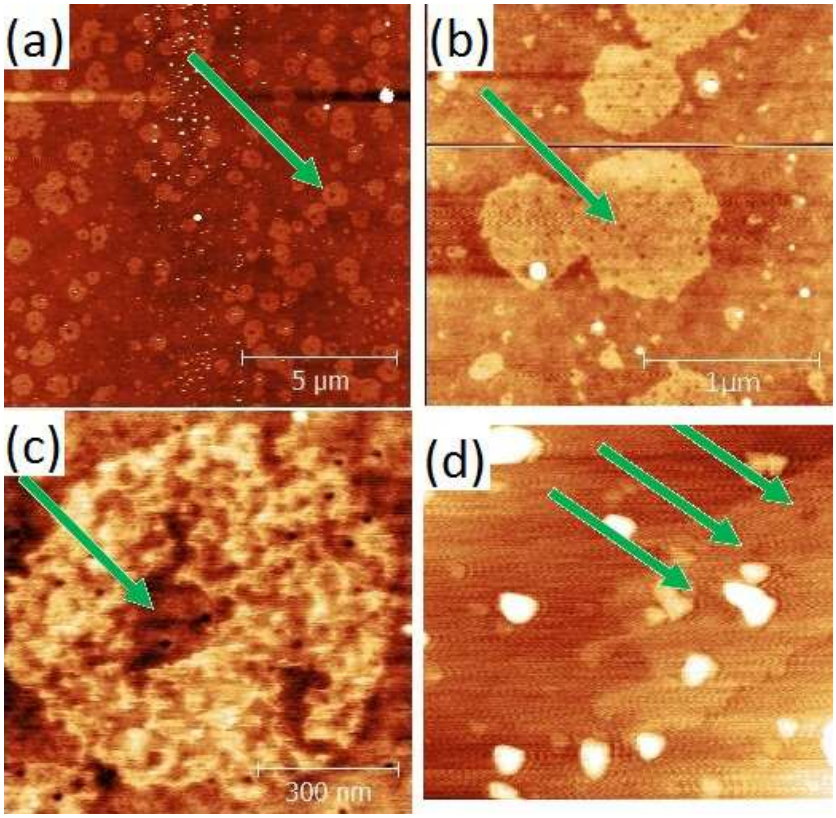

Figure 3.14: Topography measurements of Lamellibrachia chitin: (a)-(c) images from a commercial AFM. Different scan sizes are presented;(d)image of the HSX-AFM.The same structures of 2-4 nm height, with holes of the same size, can be seen.

a structure of about 2-4 nm height. It has also holes of the same size within it. However these structures when found did not present the circle shape. This, and the fact that the height measured is slightly higher than what was measured with the commercial AFM is probably due to the fact that the scanner performance had changed during the measurement. For instance, the irregular shape could mean that the scanner was moving in one direction more than the other. However, even with this calibration this experiment shows that the HSX-AFM is capable of ex-situ analysis of soft matter.

Chapter 4

"And now, for something completely different..."

4.1 "Giant resonance tuning of micro and nanomechanical oscillator"

Force Feedback Microscopy (FFM) is a technique developed in SSL by Rodrigues et. al [10]. It expands the functioning of atomic force microscopy with a simple mechanism. In FFM, the position is kept constant by a feedback loop that imposes a counteracting force on the cantilever, compensating the interaction force between sample and tip. In this way one can obtain a direct measurement of the interaction force, monitoring the force applied by the feedback loop, while measuring, through the AM-AFM mode observables of amplitude and phase, the gradient and dissipation of the interaction.

Another important feature of FFM is that this mechanism makes possible the use of extremely soft cantilevers, in the low oscillation regime, by avoiding the so-called jump to contact mechanism. This phenomenon happens for conventional AFMs, whenever the force gradient felt by the tip is bigger than the cantilever spring constant. In this case, remembering from Chapter 1, the effective spring constant of the system $k_{\text{eff}} = k - (dF_{ts}/dx)_{z_0}$ is negative. A positive feedback is established in the system, since an fluctuation of the tip towards the sample originates an even bigger force, that causes a further displacement, etc. Effectively, the cantilever snaps to the surface whenever it is approached beyond a certain point (where the gradients match). In order to image or make force-distance experiments AFM users are left with two possibilities: increasing the spring constant of the cantilever used, that is prejudicial to the resolution of the force measurement can damage soft samples, or increase the oscillation amplitude, meaning that the interaction

parameters will now be manifested in higher order modes. Additionally, to achieve the same resolution with stiffer cantilevers it is necessary to work at one of the the frequencies associated with the bending modes of the cantilever. FFM makes these approaches unnecessary, since the counteracting force applied is changing also the effective spring constant. The feedback loop in this system, carried out by a PID amplifier, changes equation 1.8 into:

$$m\ddot{x} + \gamma\dot{x} + kx = F_0\cos(\omega t) + F_{\mathrm{ts}}(z_0) + \left(\frac{dF_{\mathrm{ts}}}{dz}\right)_{z_0} x - \left(g_{\mathrm{P}}x + g_{\mathrm{I}}\int x\,\mathrm{d}t + g_{\mathrm{D}}\dot{x}\right) \tag{4.1}$$

with g_{P}, g_{I} and g_{D} the constants of the proportional-integral-differencial feedback controller. In effect, the effective spring constant is now $k_{\mathrm{eff}} = k - (dF_{\mathrm{ts}}/dx)_{z_0} + g_{\mathrm{P}}$ and the jump to contact can be completely avoided as long as the proportional gain is made high enough.

The FFM capabilities have been demonstrated in a large number of works, establishing its theoretical base [63] and possible applications [27, 64]. Recently, the author of this work has participated in an effort that adapted the methodology to the beam deflection measurement scheme, demonstrating that it can be applied to any conventional AFM, provided a special cantilever holder is developed [65].

There is still, however, one other FFM capability not yet explored. Solving expression 4.1 with the cantilever far away from the sample (meaning the interaction force is negligible) the same dependences of amplitude and phase with frequency that were detailed for the harmonic oscillator are obtained, accounting for the effective spring constant and damping ratio. In this case we get the new resonance frequency (ω_C) and quality factor (Q_C) of the oscillator:

$$\omega_C = \omega_0\sqrt{\frac{k_{\mathrm{eff}}}{k} - \left(\frac{\gamma_{\mathrm{eff}}\omega_0}{2k} - \frac{g_{\mathrm{I}}/\omega_0}{2k_{\mathrm{eff}}}\right)} \tag{4.2}$$

and,

$$Q_C = \frac{k_{\mathrm{eff}}}{(\gamma_{\mathrm{eff}})\omega_c} \tag{4.3}$$

where ω_0 represents the natural resonance frequency, $k_{\mathrm{eff}} = k + g_{\mathrm{P}}$ and $\gamma_{\mathrm{eff}} = \gamma + g_{\mathrm{D}}$. The FFM mechanism provides a simple way to change the dynamic parameters of an oscillator, at least within the range where the feedback loop is stable.

Meanwhile, as part of the trend in the miniaturization of technology, Micro and Nano mechanical systems (MMSs and NMSs) are being currently explored to diverse applications. For instance in mass sensing of biologically interesting species [66], detection of biological activities [67] or high-frequency displacements transducers [68]. These systems are usually mechanical oscillators (MMOs and NMOs), with their dynamic parameters tailored to the specific application. Recently more attention is being addressed towards their remote tuning. Tunable resonators are being developed to harvest vibration energy to power portable devices [69] or to control Radio-Frequency mechanical filters.

This tuning can be done in several ways. For instance, the use of an external electrostatic force gradient [70] or the thermal tune of the phase transition in specific materials [71] have been used to tune the resonance frequency. However, in most of the solutions found to perform this tuning, the change in resonance frequency or quality factor reported is quite low, ranging usually ±2-10% of the original resonance frequency of the oscillator, only exceeding those values (but only up to ±20%) for low frequency oscillators. Also, in the case of the static actuation, it can only be made only in one direction (to smaller values of frequency, with respect to ω_0). Meanwhile, the increase or decrease of the quality factor of the cantilever has been on the focus of AFM research for some time.

To test the potential of the FFM mechanism to tune the dynamic behavior of an oscillator, three different cantilevers were chosen. They were selected according to their potential applications: the *Olympus BL-AC40TS* with a nominal resonance frequency of 80 kHz (*cantilever 1*), the *Bruker MLCT - D* with nominal resonance frequency of 15 kHz (*cantilever 2*) and the *Olympus BL-AC10DS*, nominal resonance frequency of 1.3 MHz (*cantilever 3*). The wide frequency range of these oscillators can help to establish well the FFM actuation.

We focus first on cantilevers *1* and *2*. A custom-made FFM was used to tune the oscillators. In this FFM the detection of the cantilever is made through interferometry. An optical fiber is approached very close to the cantilever backside, to a distance z_0, and the light of the laser reflects back on it and couples back to the fiber. A capacitive actuation was chosen to apply the feedback force. To do it, the free end of the fiber was coated with 30 nm of gold, and a voltage was applied between the fiber and the cantilever. The PID counteracting loop was integrated in a FPGA, and an additional sinusoidal excitation was fed to the system. Figure 4.1 shows the operational scheme here detailed.

In this capacitive actuation, the control force is decomposed in an offset value, V_0, that is summed to the voltage fed by the FPGA, V_{PID}. We can

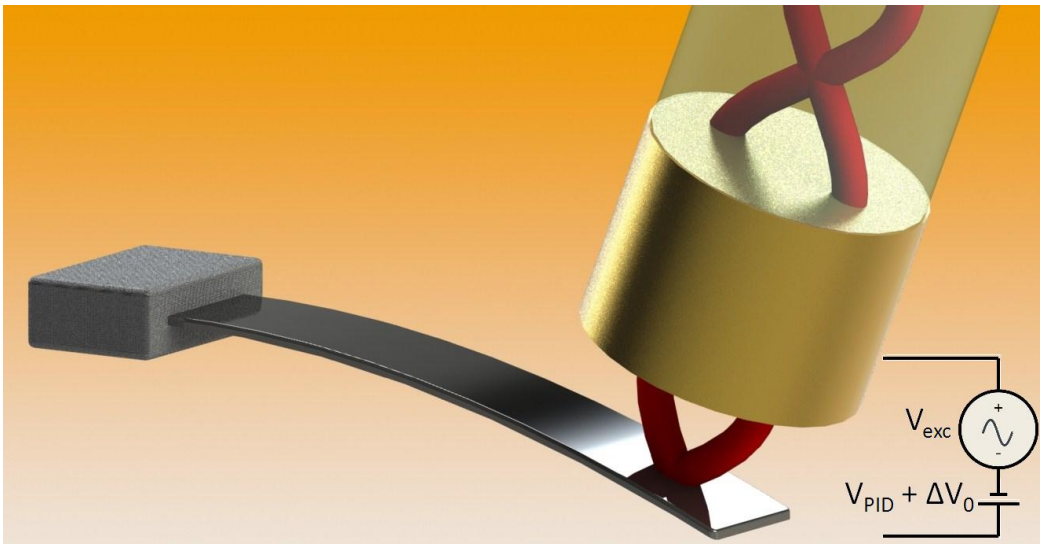

Figure 4.1: Operational scheme of the interferometry force feedback methodology. The fiber is coated with 30 nm of gold, and a capacitive force is applied.

write the force as:

$$F_{\text{control}} = -\frac{1}{2}\frac{\partial C(V_0 + V_{\text{PID}})^2}{\partial z} \tag{4.4}$$

where C is the capacitance and $z = z_f + x(t)$. z_f is the average distance from the fiber to the cantilever (some micrometers), so we can assume that $x(t) << z_f$. Also considering that $V_{\text{PID}} << V_0$ and $C = \epsilon_0 S/z$, this equation leads, in a first order approximation, to:

$$F_{\text{control}} \approx \epsilon_0 S \frac{V_0^2 + 2V_0 V_{\text{PID}}}{2z_f^2} \tag{4.5}$$

giving a linear dependence with the PID voltage. V_0 was set to 5 V in this experiment.

To observe the capabilities of the FFM several frequency swifts were performed for different parameters of the proportional and differential gains, exploring the full actuation of the FPGA, while keeping the feedback loop stable. The integral gain was kept to a minimum, and not changed for all experiments. Figure 4.2 presents the results of this study, for both cantilevers.

Relevant shifts were observed for both the cantilevers. For the low frequency cantilever (2) we obtained a gigantic shift of $\pm 75\%$ ω_0 and the quality factor can be freely tuned in the range of 0.17 Q_0 to 7.7 Q_0. Furthermore, the

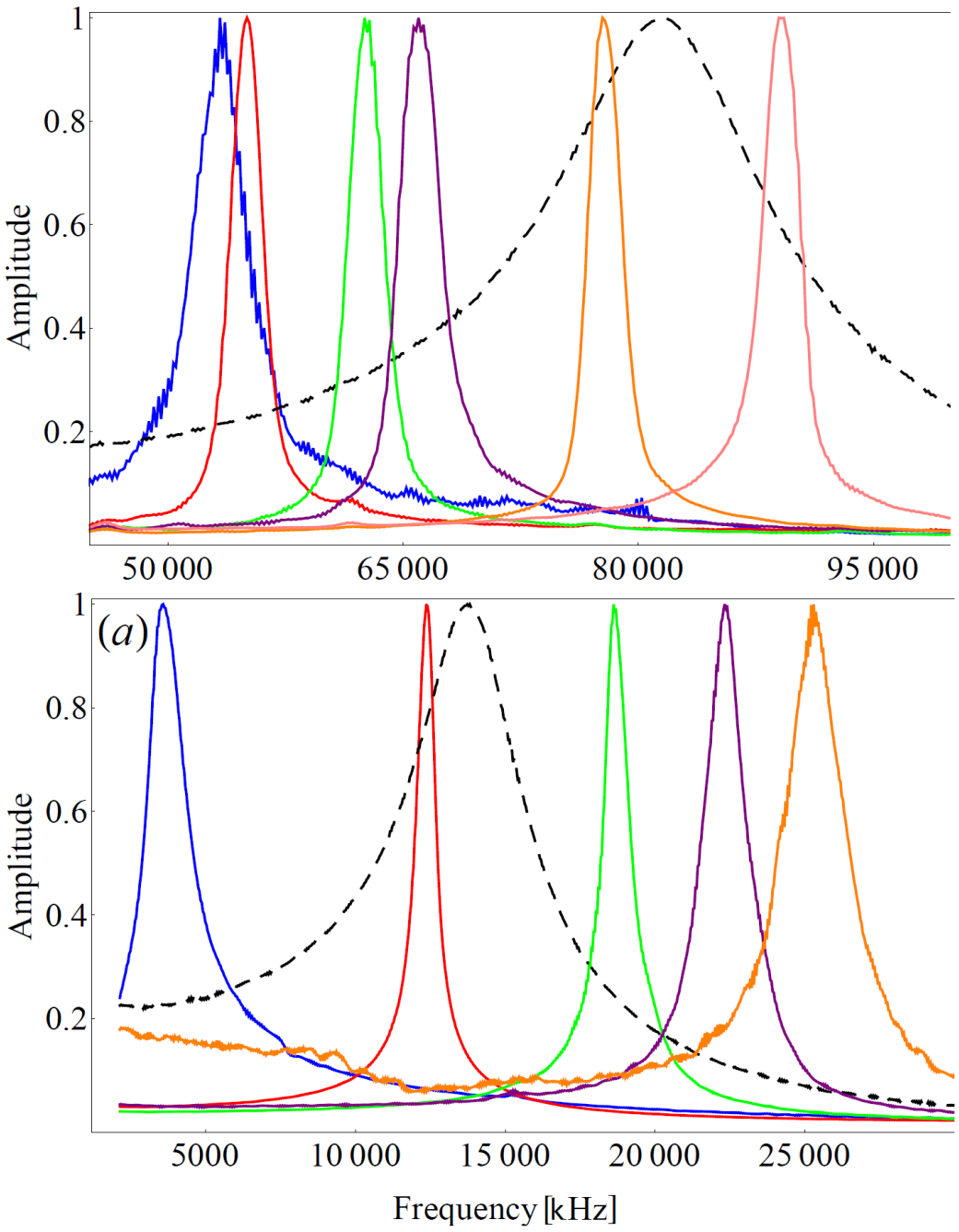

Figure 4.2: Tuning of the dynamic parameters of oscillators: normalized frequency response of the MMOs for an ensemble of control gains. On top, the tuning of the high-frequency oscillator; on the bottom the tuning of the low-frequency one. Dashed in black are the resonance curves of the uncontrolled oscillators.

quality factor tuning is decoupled from the frequency one. For the remaining cantilever (*1*) the shift was smaller, but still exceeding reported results. We observe 0.66 to 1.18 ω_0 (a 51% ω_0 interval, but not symmetric) and 0.75 to 10.37 Q_0.

The exceptional results provided by this methodology establish a base for further analysis of the of the PID counteracting loop in the behavior of the oscillators. For this, a study of the PID tuning was performed on cantilever 1. At first, to prove that the effect seen before was not due to the static gradient due to V_0, this voltage was swept, with the PID control turned off, around 5 V. Meanwhile, the frequency shift was monitored with a Phase Locked Loop. Figure 4.3 (a) presents the results of this experiment. As one can see, the value of the maximum frequency shift does not compare with the ones obtained previously. This means that the effect observed then was due solely to the effect of the PID control of the oscillation.

After, to analyze the validity of the model proposed, a systematic study of variation of the dynamic parameters with the proportional and differential gains was performed. In this study the value of g_P was swept from -0.023 N/m to 0.023 N/m. The differential gains were changed within the range of the FPGA actuation. For each pair of g_P and g_D the frequency response was acquired. The results can be seen in figure 4.3 (b) and (c)(coloured points).

To test the validity of the model an indirect method was used. The value of the differential gain could not be changed independently from the proportional gain chosen by the user. Additionally, the FPGA actuation proved to be itself non-linear with higher differential gains. Because of this, equation 4.3 was fitted to the quality factor dependence of the proportional gain allowing the estimation of the actual differential gains. These were used to plot the resonance frequency dependence with the proportional gain (equation 4.2) and establish the validity of the model by comparison with the data acquired.

Since the model equations are not valid for the high damping regime [63] only the data for $g_D < 0$ was fit. The differential gains used were: $-4.9 \times 10^{-6} g_P$ Ns/m to $-1.0 \times 10^{-5} g_P$ Ns/m. The estimations done for both model equations can be observed together as solid lines in figure 4.3 (b) and (c).

Generally, and given the non-linearities present, the data agrees well with the model. A deviation from the model is seen for increasingly negative values of g_P. This happens as predicted: for these values, the differential gain becomes larger and the regime of low damping no longer occurs. Therefore the model equations are no longer valid then.

Having established the model of actuation, the limits of this methodology were tested on a smaller, high frequency, NMO, cantilever *3*. The same

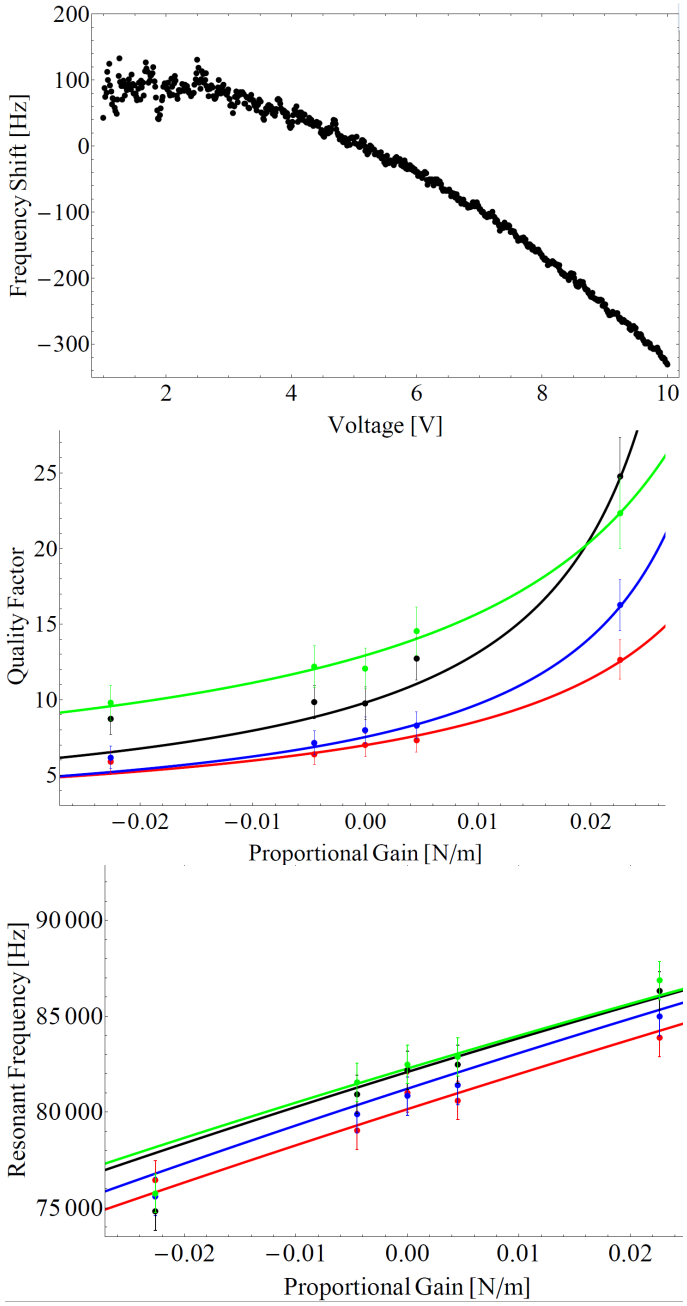

Figure 4.3: (a) Dependence of the frequency shift with the static voltage V_0 applied on the cantilever; (b) and (c) present the change of the resonant frequency and quality factor with the proportional gain. Measured (dots) and model (lines) data are presented. Different curves represent different values of g_D: $-4.9 \times 10^{-6} g_P$ Ns/m (green), $-8.7 \times 10^{-6} g_P$ Ns/m (black), $-1.0 \times 10^{-5} g_P$ Ns/m (blue), $-1.1 \times 10^{-5} g_P$ Ns/m (red).

type of capacitive actuation was employed. However, this cantilever has a significant smaller area than the ones used before. To compensate this, the offset voltage V_0 was set to 60 V. A special custom-made high frequency PD controller was developed and used to control the cantilever. The same experiment of frequency sweeps for different sets of gains was performed. The change of the resonant frequency with V_0 was also measured, to decouple the PID tuning from the static actuation. Figure 4.4 presents these results.

Again, a much larger frequency shift is observed with PID control than with the static voltage. Furthermore, it was observed a shift of 25% ω_0. However, this shift is not centered in ω_0. The reason for this is that the custom-made PID could only developed with a bandwidth of 1 MHz. The tuning to higher frequencies was for this reason much harder than for lower ones, explaining the asymmetry.

Table 4.1 summarizes the results obtained for all the oscillators tested.

Cantilever	1	2	3
k (Nominal, N/m)	0.09	0.01	0.1
ω_0 (kHz)	82.479	14.7	1254.8
Q	7.1	4.5	43.8
ω_{Cmin} (kHz)	54.2	3.9	995.2
ω_{Cmax} (kHz)	97.2	25.5	1323.5
Q_{Cmin}	5.3	0.8	4.72
Q_{Cmax}	73.6	34.6	226.8

Table 4.1: Resume of the different dynamic properties obtained throughout the experiments

Finally, to demonstrate the validity of the FFM methodology for an use in different applications the environment and type of actuation of the experiments were considered. Since a lot of the mentioned applications are in the life-sciences domain, the control of the oscillators has to be performed in a suitable environment: liquid. However, the capacitive actuation would make impossible the application of high force gradients in this media. To address this, the FFM methodology was tested with a different type of actuation perfected for liquid media: the photothermal excitation.

The photothermal excitation is a relatively new adaptation to the conventional AFM [72]. In it, a laser is directed to the cantilever backside, in addition to the common measurement laser. The power of this second laser can be modulated, and is used in AFMs to vibrate the cantilever at the desired frequency. The NMO was mounted on a commercial Cypher^{TM} AFM

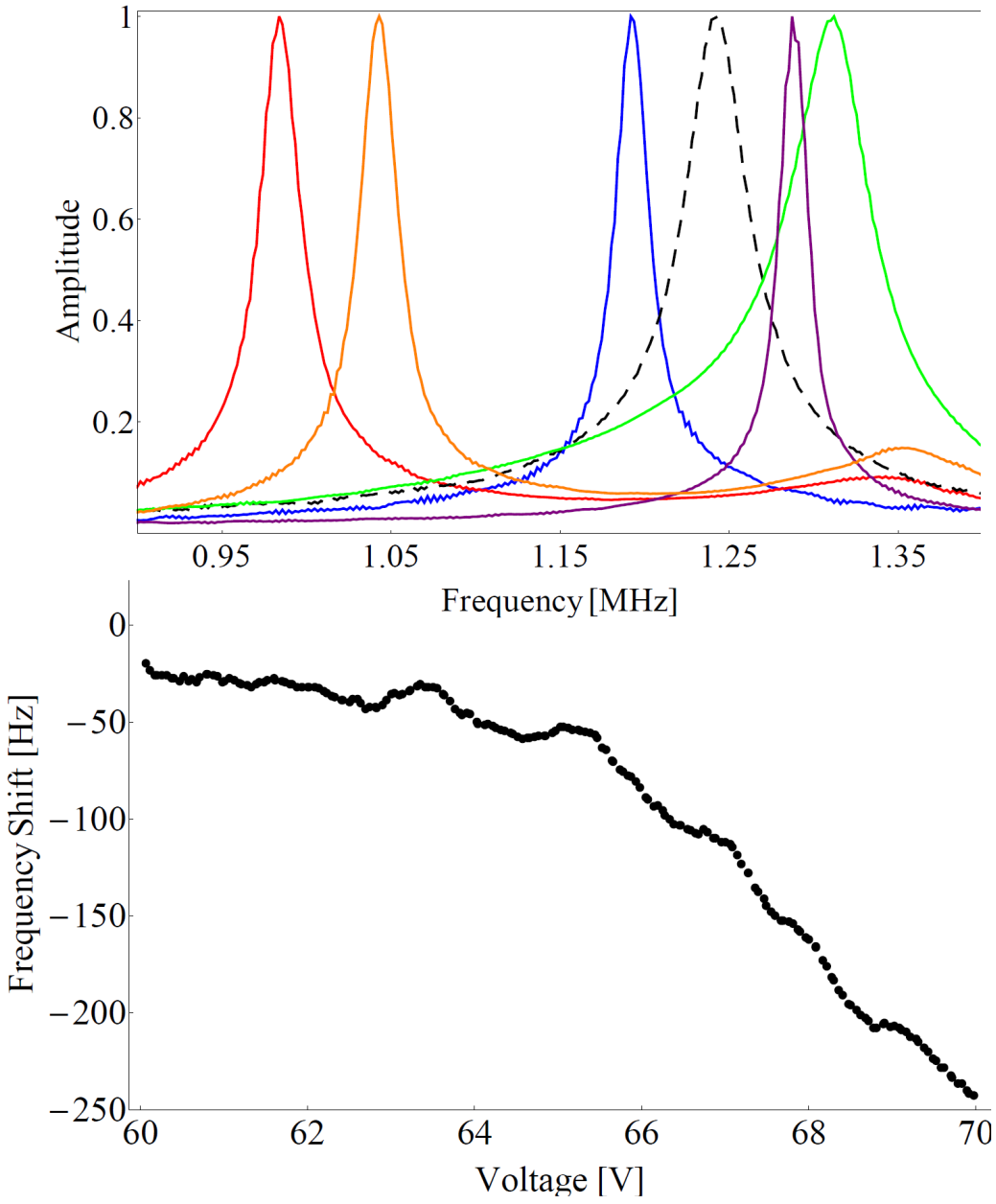

Figure 4.4: Tuning of the dynamic parameters of the high-frequency NMO. Top: normalized frequency response for an ensemble of control gains. Bottom: dependence of the frequency shift with the static voltage V_0 applied on the cantilever.

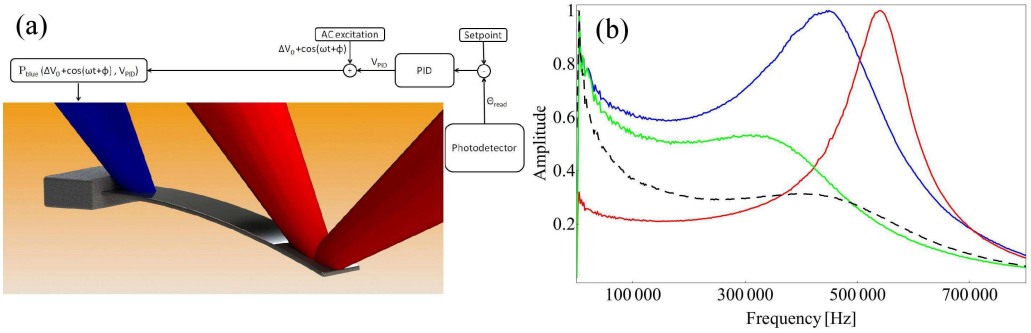

Figure 4.5: Tuning of an NMO in liquid. On the left, the operational scheme of the photothermal control of the cantilever is presented. On the right, different frequency sweeps can be seen. Dashed black: original resonance curve of the cantilever; Blue: effect of the Q-control ($g_P = 0$); Red: effect of the proportional control ($g_P > 0$); Green: effect of the proportional control ($g_P < 0$).

of Asylum Research - Oxford Instruments. The photothermal excitation is provided by the Bluedrive^{TM} technology of this microscope, named after the color of the second laser used to excite the cantilevers. In this AFM the measurement is done in the beam deflection scheme. The PID controller was employed through a proportional controller, with input of a setpoint and the beam deflection output voltage. Its output was connected to the power of the blue laser. The differential gain was performed using the Q-control mechanism of the microscope, an equivalent strategy for applying a differential excitation. Figure 4.5 presents the operational scheme and four different frequency sweeps performed for different control parameters.

As it can be seen the frequency and the quality factor can indeed be tuned. Furthermore, the presence of Q-Control/derivative gain does not mask the much higher tuning range when employing a proportional control. The effect of the Q-control is clearly seen with the increase of the Q-factor of the oscillator, comparing with the original curve (note that when in liquid the resonance curve of the oscillator is reduced to about half of its value in air). But the red and green curves, performed with different proportional gains and the same differential gain, present much larger positive and negative shifts of the frequency. Also noticeable is a peak in every curve for $\omega \longrightarrow 0$. This is due to the nature of the photothermal actuation. It is not constant in frequency and will attenuate high-frequency signals [72]

The results establish the FFM as a valid method to control the dynamic parameters of an oscillator. Compared with previous work this method provides much larger range of the dynamic shifts, and also bi-directionality (ab-

sent in static actuation), room temperature operating conditions and fairly simple instrumentation. It was also demonstrated that it works for different media, making it suitable for applications related to the life-sciences, and opening up a wide range of applicability to the most diverse fields.

Chapter 5

Conclusions and Outlook

Over the last chapters we followed the building of a novel instrument: from the conception, project and design phase, to the commissioning and use of said instrument. As the project reached, at least for the author, an apparent intermission, it is important to finish this text detailing what is the current state of the instrument, how it can be improved to achieve better performance and what is the outlook into its future use and applications of the technology created here.

The HSX-AFM is now capable of routinely achieve high resolution imaging of biological matter. This was demonstrated by imaging monolayers of POPC phospholipids and DNA deposited on mica. Also, the capability of the AFM was shown by imaging Lamellibrachia's chitin, retrieving the same information as it would be done with a commercial instrument. Furthermore, high speed imaging was also performed on biological matter, achieving the electronic limit of 0.6 Images/second. The instrument follows the requirements for ex-situ functioning proposed at the beginning.

However, this is not an ex-situ AFM. Despite the fact that the incorporation of the instrument into the beamline is outside of the scope of the initial project, one should analyze which might be the setbacks that should be addressed before and once it is transported into the beamline.

Currently there are three main areas that need/can be optimized to perfect the HSX-AFM. These were unveiled throughout the last chapter, during the mounting of the AFM. In the following we will analyzed each one:

- *Drift and alignment*: the AFM measurements performed in the last chapter were all done with the HSX-AFM in an incomplete state. As it was predicted, the impossibility of using the correct motor set for the movement of the cantilever had a great impact on all of the measurements. Besides the constant drift, seized to make the first dynamic

experiment with the AFM, in all the experiments a big amount of time had to be spent on the angular alignment of cantilever and laser beam. This behavior has to be solved incorporating the correct motor assembly.

- *Scan size*: the maximum scan area and height changed significantly while testing the instrument. During the commissioning of the microscope two of the lateral piezoactuators cracked while performing measurements. This was probably caused by an excessive pre-loading of the piezoactuators in question, localized in a very specific point, the contact between screw and piezoactuator. The scanner should be revised to include some sort of protection between the scanner frame and the actuators. Towards the end of this project, steel bands were cut to this effect, and the piezoactuators replaced.

  Meanwhile, the maximum scan height exhibited large variations throughout the project. The maximum piezoactuator displacement is 2 µm, so smaller values are expect when the actuator is driving a load. Displacements of 1-1.5 µm were observed in the commissioning. The scan size depends greatly on the placement of the piezotube responsible for this movement and how tight it is screwed. Despite this, provided the same conditions are kept this maximum height remains the same. A detailed study should be carried out to figure out the best possible position for the piezoactuator, in order to improve the scanner performance. Only once this is done, can routine measurements be done more easily and in more demanding conditions.

- *Signal to noise ratio*: to perform high speed measurements of soft matter, extremely small cantilevers have to be used. Consequently, light has to be focused to a spot size equivalent to the cantilever backside. The detection variables of the AFM measurement were successfully detected for this small cantilever, and images of POPC monolayers at high speed can already be performed. This indicates that at least a big quantity of the light emitted is reflected in the cantilever back side and couples back to the fiber. However, it is still possible to observe that some of the light is not reflected, and the images still contain extra noise that prevents an even sharper and fast measurement. This problem has to be solved.

  The reason the spot size is not as predicted is related to the fiber placement. Since the fiber is displaced by approximately 1 cm from its supposed position, it means that light is not completely focused in the cantilever. However, by retracting the fiber from this configuration, the

location of the minimum spot is unreachable by the cantilever, which makes the focusing impossible. Reviewing the optical system the reason for this error was found: an error was made in the design of the optical assembly. The piece that held the lenses was designed by taking the back focal distance, measured from one of the surfaces, to be the same as the effective one, measured from the center of the lens. This caused a shift in the focal position and consequently, due to trying to correct the situation by offsetting the focal point, an increased spot size.

To solve this situation the new optical system has to be adapted with a new set of lenses with back focal lengths equal to the ones predicted in the assembly. Lens 1 requires an effective focal length of 30 mm (*#49-662* from *Edmund Optics*). This places the focus at about 2 mm downstream of the fiber original position. Lens 2 requires an effective focal length of about 22 mm. This would require a custom-made lens as it can not be found in the catalog of any of the major optical elements provider. Another possibility is to opt for an effective focal length of 20 mm (*#49-659* from *Edmund Optics*). The focal point of this lens 2 mm short of the predicted position. To solve this mismatch the lens positioner would have to be moved, in relation to the fiber and to the rest of the assembly. The position of the first lens (and consequently the fiber) also has to be change downstream. To note is the fact that the character of the lenses chosen will reduce the spot size will beyond the required, as the ratio of the lenses' focal lengths is now bigger, implying a bigger demagnification. However, this system would oblige a larger attention to be given to the alignment of the different parts, since the pre-machined references are now useless. Figure 5.1 shows the model in the new designed configuration.

The project, as it can be inferred from what was detailed until now, has been completely oriented towards the achievement of the different goals in terms of the object of measurement (acquiring interference fringes and resonance curves in the different cantilevers) and testing it out in different samples. This was due to the specificity of the context of the work performed, a short-termed internship of the author. Despite being a long term project, it was important to establish the functioning of the instrument before the end of the internship period. This fact made mandatory the sacrifice of some of the normal tasks when commissioning a new AFM. Thus, besides the issues that were addressed before, there are still some important points that need to be tackled before the full operation of the instrument can be done. Firstly, a calibration of the instrument has to be done. Using the interferometry scheme already present in the microscope, it is possible to characterize the

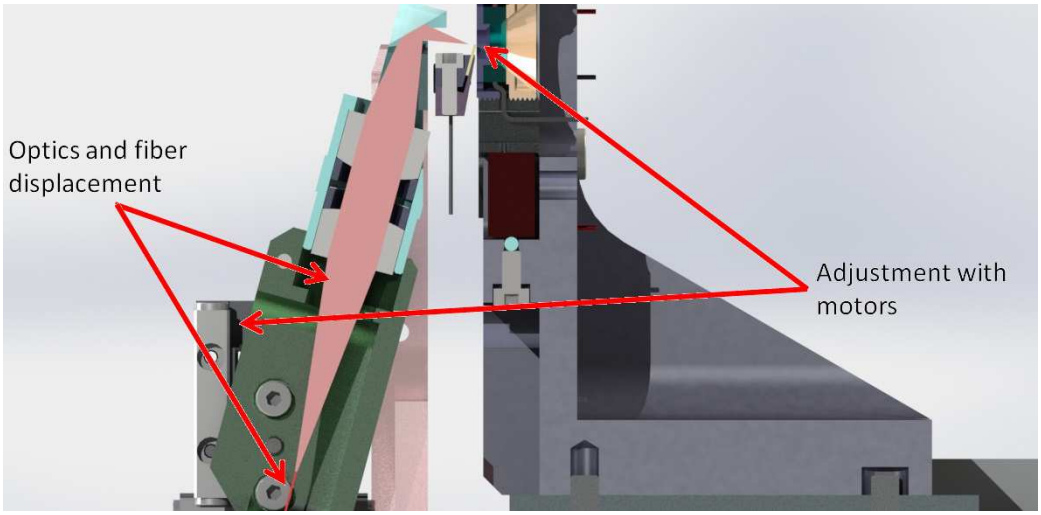

Figure 5.1: Modified optical system taking into account the new focal lengths chosen. Adjustment in the position of the optics and the fiber would be necessary to place the focus at its predicted location.

scanner in terms of maximum scan speed, maximum scan size, resolution and linearity. These parameters improve the performance of the microscope or at least make it easier to operate. For instance, the non linear movement of the piezoactuators can be solved by adapting the voltage signals fed to them. It would be academically interesting to compare the performance results with the ones modeled in the simulation stage of the project.

This improvements constitute a first upgrade phase that is necessary before the move to the beamline. This entails another series of tests and calibrations necessary before it is possible to perform a scientific experiment. Imaging with and without the beam and developing alignment procedures making use of the components of the beamline are difficult and crucial tasks.

After these a reliable experiment can be carried out using both X-Rays and AFM. The quantity of different opportunities available for testing this new instrument is impressive. Filming the effect of radiation in biologic and soft matter tissues is the most direct one. While illuminating the sample with the X-Rays one can look, for instance, at their effect on a living cell, or inspect at which time scales does radiation damage occur in bone tissue (this would have direct consequences on day-to-day activities like going to the doctor or catching an airplane!). Thermally driven phenomena could also be investigated with this AFM, simultaneously with X-Ray probing. Another possible future experiment would be to investigate the deformation of a sample, by performing coherent diffraction imaging and indenting with

the AFM tip. This X-Ray technique allows for the 3D mapping of every atom in the sample, and by pushing it with the tip one could check where and how it would deform. The functioning of the X-Ray experiment would also be made easier, offering the possibility of a continuous alignment between the beam and the sample making use of the cantilever or one of the OSAs embedded in this system.

The beginning of the experimental phase does not mean the improvement of the microscope is over. A second upgrade phase can be thought. Several improvements to the microscope should be implemented. For being too time demanding and somewhat less crucial to the performance than others these were not carried out during the internship, but they can contribute greatly to the perfecting of the microscope. Some have already been mentioned in this text. For instance, one can apply the new electronics and control schemes that were developed by other scientists to increase the scan speed of their instrument, by employing active damping, dummy scanner stages, or dynamic PID schemes. One other possibility that should be looked at is the inclusion or modification of the detection methodology to include the optical beam deflection scheme. Only once the stability of the microscope is increased the current detection scheme can be completely evaluated, but some attention should also be given to the easier to use character of the beam deflection scheme. This is ultimately an AFM to be used in beamlines and ideally by the own personnel of the beamline, that are not AFM specialists. The user-friendly character is then determinant for a wide spread use beyond the AFM community, and the wide spread use should be one of the priorities of an instrument. To perform measurements in liquids the humidity controlled chamber will have to be installed. The humidity has to be kept at a certain value so the small amount of liquid required for this experiment does not evaporate. Finally, the possibility of building an alternative scanner should also be looked upon. A larger scan size would be extremely useful for some experiments (like imaging cells), even if this comes sacrificing the scan speed (especially since the current scanner outperforms the electronics). With the know-how acquired in this thesis it could be possible to produce fast and cheaply a new version adapted to the HSX-AFM frame. This would provide the future user with a better control of the characteristics of the image desired in a particular experiment.

The project detailed here, can only be looked at with optimism. In little more than 7 months a completely new instrument was developed, passing through the idealization and conception, to the design, mounting, commissioning and first tests. Despite the errors and lacks of performance here detailed, I am confident, and hopeful, that this will, in the future, be a case of a successfully made tool that can cause at least a significant and useful

change in Science. The exciting possibilities opened by the instrument are, in my view, rewarding enough of the time, energy and effort spent on it by those who participated, directly or indirectly, in its conception. To all of them I, once again, warmly thank.

Bibliography

[1] T. Ando. High-speed atomic force microscopy coming of age. *Nanotechnology*, 23(6), 2012.

[2] G. E. Fantner, G. Schitter, J. H. Kindt, T. Ivanov, K. Ivanova, R. Patel, N. Holten-Andersen, J. Adams, P. J. Thurner, I. W. Rangelowb, and P. K. Hansma. Components for high speed atomic force microscopy. *Ultramicroscopy*, 106:881–887, 2006.

[3] Georg Schitter, K.J. Astrom, B. DeMartini, Georg E. Fantner, K. Turner, P.J. Thurner, and Paul K. Hansma. Design and modeling of a high-speed scanner for atomic force microscopy. In *American Control Conference, 2006*, pages 6 pp.–, June 2006.

[4] Richard P. Feynman. Plenty of room at the bottom.

[5] G. Binnig, H. Rohrer, Ch. Gerber, and E. Weibel. Surface studies by scanning tunneling microscopy. *Phys. Rev. Lett.*, 49(1), 1982.

[6] G. Binnig, C. F. Quate, and Ch. Gerber. Atomic force microscope. *Phys. Rev. Lett.*, 56(9), 1986.

[7] R. P. Feynman, R. B. Leighton, and M. Sands. *The Feynman Lectures on Physics*. Addison-Wesley, 1964.

[8] H. Butt, B. Cappella, and M. Kappl. Force measurements with the atomic force microscope: Technique, interpretation and applications. *Surf. Sci. Rep.*, 59(1-152), 2005.

[9] J. N. Israelachvili. *Intermolecular and Surface Forces*. Academic Press, 3^{rd} edition, 2011.

[10] M. S. Rodrigues, L. Costa, J. Chevrier, and F. Comin. Why do atomic force microscopy force curves still exhibit jump to contact? *App. Phys. Lett.*, 101(203105), 2012.

[11] Luca Costa. *The Force Feedback Microscope: an AFM for soft condensed matter*. PhD thesis, Université Joseph Fourier, 2014.

[12] L. Gross, F. Mohn, N. Moll, B. Schuler, A. Criado, E. Guitián, D. Pena, A. Gourdon, and G. Meyer. Bond-order discrimination by atomic force microscopy. *Science*, 337(1326), 2012.

[13] S. Sievers, K. Braun, D. Eberbeck, S. Gustafsson, E. Olsson, H. W. Schumacher, and U. Siegner. Quantitative measurement of the magnetic moment of individual magnetic nanoparticles by magnetic force microscopy. *Small*, 8(9), 2012.

[14] J. Ubbink and P. Schär-Zammaretti. Probing bacterial interactions: integrated approaches combining atomic force microscopy, electron microscopy and biophysical techniques. *Micron.*, 36(4), 2005.

[15] Y. Martin, C. C. Williams, and H. K. Wickramasinghe. Atomic force microscope-force mapping and profiling on a sub-100-a scale. *J. Appl. Phys.*, 61(10), 1987.

[16] T. R. Albrecht, P. Grütter, D. Horne, and R. Rugar. Frequency modulation detection using high-q cantilevers for enhanced force microscopy sensitivity. *J. Appl. Phys.*, 69(2), 1991.

[17] F. Giessibl. Atomic resolution of the silicon (111)-(7x7) surface by atomic force microscopy. *Science*, 267(5194), 1995.

[18] Ricardo García. *Amplitude Modulation Atomic Force Microscope*. Wiley-VCH, 2010.

[19] Y. Sugawara, M. Ohta, H. Ueyama, and S. Morita. Defect motion on an InP(110) surface observed with noncontact atomic force microscopy. *Science*, 270(5242), 1995.

[20] H. Hansma, D. Laney, M. Bezanilla, R. Sinsheimer, and P. Hansma. Applications for atomic force microscopy of dna. *Biophys. J.*, 68(1672-1677), 1995.

[21] T. Junno, S.-B. Carlsson, H. Xu, L. Montelus, and L. Samuelson. Fabrication of quantum devices by ångström-level manipulation of nanoparticles with an atomic force microscope. *Appl. Phys. Lett.*, 72(5), 1998.

[22] R. García and R. Perez. Dynamic atomic force microscopy methods. *Surf. Sci. Rep.*, 47(197-301), 2002.

[23] F. Giessibl. Advances in atomic force microscopy. *Rev. Mod. Phys.*, 75(3), 2003.

[24] T. Ando, T. Uchihashi, and S. Scheuring. Filming biomulecular processes by high-speed atomic force microscopy. *Chem. Rev.*, 114(6), 2014.

[25] A. Raman, S. Trigueros, A. Cartagena, A. P. Z. Stevenson, M. Susilo, E. Nauman, and S. A. Contera. Mapping nanomechanical properties of live cells using multi-harmonic atomic force microscopy. *Nat. Nanotechnol*, 6(809), 2011.

[26] T. R. Rodrígues and R. García. Compositional mapping of surfaces in atomic force microscopy by excitation of the second normal mode of the microcantilever. *Appl. Phy. Lett.*, 84(449), 2004.

[27] L. Costa, M. S. Rodrigues, E. Newman, C. Zubieta, J. Chevrier, and F. Comin. Imaging material properties of biological samples with a force feedback microscope. *J. Mol. Recognit.*, 26(689-693), 2013.

[28] A. Compton. The intensity of x-ray reflection, and the distribution of the electrons in atoms. *Phys. Rev. Lett.*, 9(29), 1917.

[29] Stamp Collecting Project. Short history of protein crystallography.

[30] Mário Manuel Silveria Rodrigues. *Bringing Light into the Nanoworld - What can you do with an atomic force microscope on top of you synchrotron radiation sample holder*. PhD thesis, Université Joseph Fourier, 2009.

[31] International Union of Crystalography. Nobel prize winners associated with crystalography.

[32] J. K. Gimzewski, R. Berndt, and R. R. Schlittler. Observation of local photoemission using a scanning tunneling microscope. *Ultramicroscopy*, 42-44(366), 1991.

[33] J. Stangl, C. Mocuta, A. Diaz, T.H. Metzger, and G. Bauer. X-ray diffraction as a local probe tool. *Chem. Phys. Chem,*, 10(2923), 2009.

[34] A. Saito, J. Maruyama, K. Manabe, K. Kitamoto, K. Takahashi, K. Takami, M. Yabashi, Y. Tanaka, D. Miwa, M. Ishii, Y. Takagi, M. Akai-Kasaya, S. Shin, T. Ishikawa, Y. Kuwahara, and M. Aono. Development of a scanning tunneling microscope for in situ experiments with a synchrotron radiation hard-x-ray microbeam. *J. Synchrotron Rad.*, 13(216), 2006.

[35] S. Suzuki, Y. Koike, K. Fujikawa, W.-J. Chun, M. Nomura, and K. Asakura. A possibility of xanam (x-ray aided non-contact atomic force microscopy). *Chem. Lett.*, 33(636), 2004.

[36] S. Suzuki, Y. Koike, K. Fujikawa, N. Matsudaira, M. Nakamura, W.-J. Chun, M. Nomura, and K. Asakura. An approach to nano-chemical analysis through nc-afm technique. *Catal. Today*, 117(80), 2006.

[37] T. Eguchi, T. Okuda, T. Matsushima, A. Kataoka, and A. Harasawa. Element specific imaging by scanning tunneling microscopy combined with synchrotron radiation light. *Appl. Phys. Lett.*, 89(243119), 2006.

[38] M. S. Rodrigues, O. Dhez, S. Le Denmat, , J. Chevrier R. Felici, and F. Comin. Local detection of x-ray spectroscopies with an in-situ afm. *JINST.*, 3(P12004), 2008.

[39] M. S. Rodrigues, T. W. Cornelius, T. Scheler, C. Mocuta, A. Malachias, R. Magalhães-Paniago, O. Dhez, F. Comin, T. H. Metzger, and J. Chevrier. In situ observation of the elastic deformation of a single epitaxial sige crystal by combining atomic force microscopy and micro x-ray diffraction. *J. Appl. Phys*, 106(103525), 2009.

[40] T. Scheler, M. S. Rodrigues, T. W. Cornelius, C. Mocuta, A. Malachias, R. Magalhães-Paniago, F. Comin, J. Chevrier, and T. H. Metzger. Probing the elastic properties of individual nanostructures by combining in situ atomic force microscopy and micro-x-ray diffraction. *Appl. Phy. Lett.*, 94(023109), 2009.

[41] I. Schmid, J. Raabe, B. Sarafimov, C. Quitamann, S. Vranjkovic, Y. Pellmont, and H.J. Hug. Coaxial arrangement of a scanning probe and an x-ray microscope as a novel tool for nanoscience. *Ultramicroscopy*, 110(1267), 2010.

[42] N. Pilet, J. Raabe, S. E. Stevenson, S. Romer, L. Bernard, C. R. McNeil, R. H. Fink, H. J. Hug, and C. Quitmann. Nanostructure characterization by a combined x-ray absorption/scanning force microscopy system. *Nanotechnology*, 23(475708), 2012.

[43] F. Hang, D. Lu, R. J. Bailey, I. Jimenez-Palomar, U. Stachewicz, B. Cortes-Ballesteros, M. Davies, M. Zech, C. Bödefeld, and A. H. Barber. In situ tensile testing of nanofibers by combining atomic force microscopy and scanning electron microscopy. *Nanotechnology*, 22(365708), 2011.

[44] S. Rackwitz, I. Faus, B. Lägel, J. Linden, J. Marx, E. Oesterschulze, K. Schlage, H.-C. Wille, S. Wolff, J. A. Wolny, and V. Schünemann. Installation of a combined raman and afm microscope as a sample environment for nuclear resonance scattering at p01, petra iii. *Hyperfine Interactions*, 2014.

[45] D. Müller and Y. Dufrêne. Atomic force microscopy as a multifunctional molecular toolbox in nanobiotechnology. *Nat. Nanotechnol*, 3(261), 2008.

[46] D. Müller, J. Helenius, D. Alsteens, and Y. Dufrêne. Force probing surfaces of living cells to molecular resolution. *Nat. Chem. Biol.*, 5(6), 2009.

[47] D. Müller and Y. Dufrêne. Atomic force microscopy: a nanoscopic window on the cell surface. *Trends Cell Biol.*, 21(8), 2011.

[48] B. Brown, L. Picco, M. J. Miles, and C. F. J. Faul. Opportunities in high-speed atomic force microscopy. *Small*, 9(19), 2012.

[49] B. G. Audenis, M. Boilot, P. Bernard, A. Panzarella, L. Costa, M. S. Rodrigues, and F. Comin. High speed x-atomic force microscope for beamlines. *updatethis*.

[50] T. Fukuma, M. J. Higgins, and S. P. Jarvis. Direct imaging of individual intrinsic hydration layers on lipid bilayers at ångström resolution. *Biophys. J.*, 92:3603–3609, 2007.

[51] H. Asakawa, K. Ikegami, M. Setou, N. Watanabe, M. Tsukada, and T. Fukuma. Submolecular-scale imaging of a-helices and c-terminal domains of tubulins by frequency modulation atomic force microscopy in liquid. *Biophys. J.*, 101:1270–1276, 2011.

[52] T. R. Rodrígues and R. García. Theory of q control in atomic force microscopy. *Appl. Phy. Lett.*, 82(4821), 2003.

[53] T. Fukuma, Y. Okazaki, N. Kodera, T. Uchihashi, and T. Ando. High resonance frequency force microscope scanner using inertia balance support. *App. Phys. Lett.*, 92, 2008.

[54] G. E. Fantner, P. Hegarty, J. H. Kindt, G. Schitter, G. A. G. Cidade, and P. K. Hansma. Data acquisition system for high speed atomic force microscopy. *Rev. Sci. Instrum.*, 76, 2005.

[55] N. Kodera, M. Sakashita, and T. Ando. Dynamic proportional-integral-differential controller for high-speed atomic force microscopy. *Rev. Sci. Instrum.*, 77, 2006.

[56] D. Rugar, H. J. Mamin, R. Erlandsson, J. E. Stern, and B. D. Terris. Force microscope using a fiber-optic displacement sensor. *Rev. Sci. Instrum.*, 59(11), 1988.

[57] D. Rugar, H. J. Mamin, and P. Guethner. Improved fiber-optic interferometer for atomic force microscopy. *Appl. Phys. Lett.*, 55(258), 1989.

[58] B. W. Hoogenboom, P. L. T. M. Fredrix, J. L. Yang, S. Martin, Y. Pellmont, M. Steinacher, S. Zäch, E. Langenbach, H.-J. Heimbeck, A. Engel, and H. J. Hug. A fabry-perot interferometer for micrometer-sized cantilevers. *Appl. Phys. Lett.*, 86(074101), 2005.

[59] Z. Jianyong, S. Guangyi, G. Weitao, and Y. Junen. A novel optical beam deflection detection system based on aspheric lens for high-speed atomic force microscope. In *Proc. of SPIE*, volume 8557, pages 855723–855723–7, 2012.

[60] C. Pruss, E. Garbusi, and W. Osten. Testing aspheres. *Optics and Photonics News*, 19:24–29, 2008.

[61] S. W. Hui, R. Viswanathan, J. A. Zasadzinski, and J. N. Israelachvili. The structure and stability of phospholipid bilayers by atomic force microscopy. *Biophys. J.*, 68:171–178, 1995.

[62] Y. F. Dufrêne, W. R. Barger, J.-B. D. Green, and G. U. Lee. Nanometer-scale surface properties of mixed phospholipid monolayers and bilayers. *Langmuir*, 13:4779–4784, 1997.

[63] M.S. Rodrigues, L. Costa, J. Chevrier, and F. Comin. System analysis of force feedback microscopy. *J. Appl Phys.*, 115(054309), 2014.

[64] L Costa, M. S. Rodrigues, N. Benseny-Cases, V. Mayeux, J. Chevrier, and F. Comin. Spectroscopic investigation of local mechanical impedance of living cells. *PLOS One*, 9, 2014.

[65] M. V. Vitorino, S. Carpentier, L. Costa, and M.S. Rodrigues. Force feedback microscopy based on an optical beam deflection scheme. *Appl. Phys. Lett.*, 105(013106), 2014.

[66] Thomas P. Burg, Michel Godin, Scott M. Knudsen, Wenjiang Shen, Greg Carlson, John S. Foster, Ken Babcock, and Scott R. Manalis. Weighing of biomolecules, single cells and single nanoparticles in fluid. *Nature*, 446(7139):1066–1069, April 2007.

[67] G Longo, L Alonso-Sarduy, L Rio Marques, A Bizzini, A Trampuz, J Notz, G Dietler, and S Kasas. Rapid detection of bacterial resistance to antibiotics using afm cantilevers as nanomechanical sensors. *Nat Nano*, 8(7):522–526, July 2013.

[68] K. L. Ekinci, Y. T. Yang, X. M. H. Huang, and M. L. Roukes. Balanced electronic detection of displacement in nanoelectromechanical systems. *Applied Physics Letters*, 81(12):2253–2255, 2002.

[69] Christian Peters, Dominic Maurath, Wolfram Schock, Florian Mezger Mezgerl, and Yiannos Manoli. A closed-loop wide-range tunable mechanical resonator for energy harvesting systems. *Journal of Micromechanics and Microengineering*, 19(9):094004, 2009.

[70] Quirin P. Unterreithmeier, Eva M. Weig, and Jorg P. Kotthaus. Universal transduction scheme for nanomechanical systems based on dielectric forces. *Nature*, 458(7241):1001–1004, April 2009.

[71] Nicola Manca, Luca Pellegrino, Teruo Kanki, Syouta Yamasaki, Hidekazu Tanaka, Antonio Sergio Siri, and Daniele MarrÃƒÂ©. Programmable mechanical resonances in mems by localized joule heating of phase change materials. *Advanced Materials*, 25(44):6430–6435, 2013.

[72] D. Ramos, J. Tamayo, J. Mertens, and M. Calleja. Photothermal excitation of microcantilevers in liquids. *Journal of Applied Physics*, 99:–, 2006.

[73] T. W. Cornelius, D. Carbone, V. L. R. Jacques, T. Schüli, and T. H. Metzger. Three-dimensional diffraction mapping by tuning the x-ray energy. *J. Synchrotron Rad.*, 18(413), 2011.

[74] T. W. Cornelius, A. Davydok, V. L. R. Jacques, R. Grifone, T. Schü li, M.-I Richard, G. Beautier, M. Verdier, T. H. Metzger, U. Pietsch, and O. Thomas. In situ three-dimensional reciprocal-space mapping during mechanical deformation. *J. Synchrotron Rad.*, 19(688), 2012.

[75] R. García and E. Herruzo. The emergence of multifrequency force microscopy. *Nat. Nanotechnol*, 7(217-26), 2012.

[76] N. Kodera and T. Ando. The path to visualization of walking myosin v by high-speed atomic force microscopy. *Biophys. Rev.*, pages 1–24, 2014.

[77] J. Marx, H. Huang, I. Faus, S. Rackwitz, J. A. Wolny, K. Schlage, R. Ulber, H.-C. Wille, and V. Schünemann. Simultaneous characterization of protein coated iron oxide nanoparticles with nuclear inelastic scattering and atomic force microscopy. *Hyperfine Interactions*, 2013.

[78] I. Schmid, J. Raabe, S. Wenzel, R. Fink, and H. Hug. Nanoxas - the in situ combination of scanning transmission xray and scanning probe microscopy. In *AIP Conf. Proc. 1365(449)*, 2011.

Appendix A

Datasheets and references of various components

6-Axis Miniature Hexapod

HIGH PRECISION IN A SMALL PACKAGE

H-810

- Most compact standard Hexapod in the PI portfolio
- Travel ranges to 40 mm / 60°
- Load capacity to 5 kg
- Actuator resolution 40 nm
- Min. incremental motion to 0.5 µm
- Repeatability to ±0.1 µm

Reference-class 6-axis positioning system
Parallel-kinematic design for six degrees of freedom making it significantly more compact and stiff than serial-kinematic systems, higher dynamic range, no moved cables: Higher reliability, reduced friction

Direct drive with brushless DC motors (BLDC) and long-life ball screws
High precision, velocity and lifetime

Powerful digital controller, open software architecture
User-defined, stable pivot point, software-selectable. Positions commanded in Cartesian coordinates. Macro programming. Open source LabVIEW driver set. Work space simulation software. Virtual Hexapod machine software. Optional: Collision avoidance software (external obstacles).

H-810.xx1 includes C-887.11, 6D vector motion controller plus 2 additional servo axes. Options:

- Analog interfaces/photometer cards for visible light (F-206.VVU) or the infrared light range (F-206.iiU)
- F-206.NCU fast piezo nano-alignment system for alignment with nanometer precision

H-810.xx2 includes C-887.21 compact 6D vector motion controller

Fields of application
Research and industry. For micromanipulation, laser and optics alignment, biotechnology, tool control

PICMA® Stack Multilayer Piezo Actuators

CERAMIC-INSULATED HIGH-POWER ACTUATORS

P-882 – P-888

- Superior lifetime
- High stiffness
- UHV-compatible to 10^{-9} hPa
- Microsecond response
- Sub-nanometer resolution
- Large choice of designs

Patented PICMA® Stack multilayer piezo actuators with high reliability

Operating voltage -20 to 120 V. Ceramic insulation, polymer-free. Humidity resistance. UHV-compatible to 10^{-9} hPa, no outgassing, high bakeout temperature. Encapsulated versions for operation in splash water or oil

Custom designs with modified specifications

- For high operating temperature up to 200°C
- Special electrodes for currents of up to 20 A
- Variable geometry: Inner hole, round, rectangular
- Ceramic or metal end pieces in many versions
- Applied SGS sensors for positional stability

Fields of application

Research and industry. Cryogenic environment with reduced displacement. For high-speed switching, precision positioning, active and adaptive systems

Suitable drivers

E-610 Piezo Amplifier / Controller
E-617 High-Power Piezo Amplifier
E-831 OEM Piezo Amplifier Module

Valid patents

German Patent No. 10021919C2
German Patent No. 10234787C1
German Patent No. 10348836B3
German Patent No. 102005015405B3
German Patent No. 102007011652B4
US Patent No. 7,449,077
Japan Patent No. 4667863
China Patent No. ZL03813218.4

Order number*	Dimensions A x B x L [mm]	Nominal displacement [µm] (0 – 100 V)	Max. displacement [µm] (0 – 120 V)	Blocking force [N] (0 – 120 V)	Stiffness [N/µm]	Electrical capacitance [µF] ±20%	Resonant frequency [kHz] ±20%
P-882.11	3 × 2 × 9	6.5 ±20%	8 ±20%	190	24	0.15	135
P-882.31	3 × 2 × 13.5	11 ±20%	13 ±20%	210	16	0.22	90
P-882.51	3 × 2 × 18	15 ±10%	18 ±10%	210	12	0.31	70
P-883.11	3 × 3 × 9	6.5 ±20%	8 ±20%	290	36	0.21	135
P-883.31	3 × 3 × 13.5	11 ±20%	13 ±20%	310	24	0.35	90
P-883.51	3 × 3 × 18	15 ±10%	18 ±10%	310	18	0.48	70
P-885.11	5 × 5 × 9	6.5 ±20%	8 ±20%	800	100	0.6	135
P-885.31	5 × 5 × 13.5	11 ±20%	13 ±20%	870	67	1.1	90
P-885.51	5 × 5 × 18	15 ±10%	18 ±10%	900	50	1.5	70
P-885.91	5 × 5 × 36	32 ±10%	38 ±10%	950	25	3.1	40
P-887.31	7 × 7 × 13.5	11 ±20%	13 ±20%	1700	130	2.2	90
P-887.51	7 × 7 × 18	15 ±10%	18 ±10%	1750	100	3.1	70
P-887.91	7 × 7 × 36	32 ±10%	38 ±10%	1850	50	6.4	40
P-888.31	10 × 10 × 13.5	11 ±20%	13 ±20%	3500	267	4.3	90
P-888.51	10 × 10 × 18	15 ±10%	18 ±10%	3600	200	6.0	70
P-888.91	10 × 10 × 36	32 ±10%	38 ±10%	3800	100	13.0	40

* For optional solderable contacts, change order number extension to .x0 (e. g. P-882.10).
Piezo ceramic type: PIC 252.
Standard electrical interfaces: PTFE-insulated wire leads, 100 mm, P-882, P-883: AWG 32 (Ø 0.49 mm); P-885, P-887, P-888: AWG 30 (Ø 0.61 mm).
Recommended preload for dynamic operation: 15 MPa.
Maximum preload for constant force: 30 MPa.
Resonant frequency at 1 V_{pp}, unloaded, free on both sides. The value is halved for unilateral clamping.
Capacitance at 1 V_{pp}, 1 kHz, RT.
Operating voltage: -20 to 120 V.
Operating temperature range: -40 to 150°C.
Custom designs or different specifications on request.

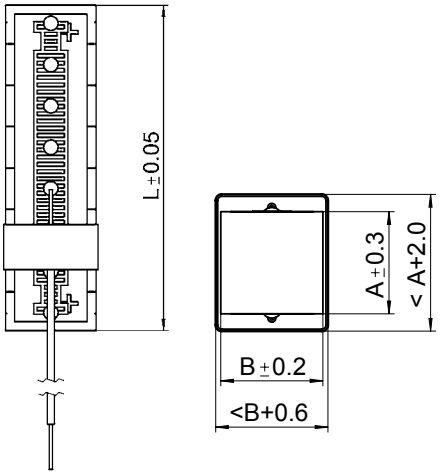

PICMA® Stack actuators, L, A, B see table

PICMA® Chip Actuators

MINIATURE MULTILAYER PIEZO ACTUATORS

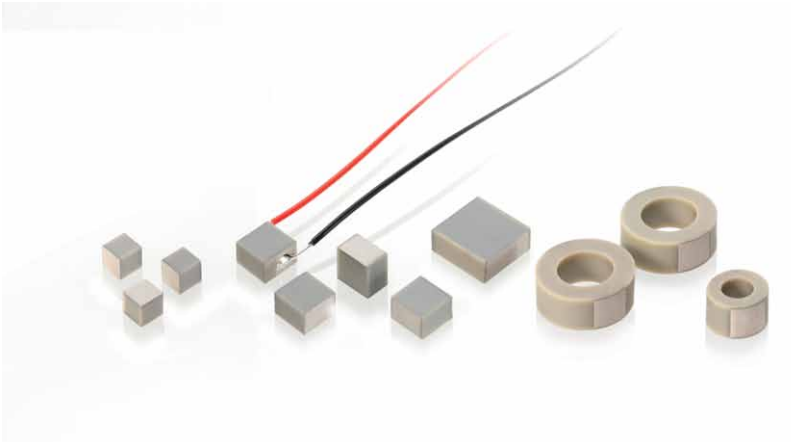

PLOxx • PDOxx

- Superior lifetime
- Ultra-compact: From 2 × 2 × 2 mm
- Ideal for dynamic operation
- Microsecond response
- Sub-nanometer resolution
- Large choice of designs

Piezo linear actuator with PICMA® multilayer technology

Operating voltage -20 to 100 V. Ceramic insulation, polymer-free. Humidity resistance. UHV-compatible to 10^{-9} hPa, no outgassing, high bakeout temperature. Versions with rectangular or annular cross-section

Available options

PTFE-insulated wire leads. Various geometric shapes, inner hole. Precision-ground ceramic end plates

Fields of application

Research and industry. For laser tuning, micro-dispensing, life science

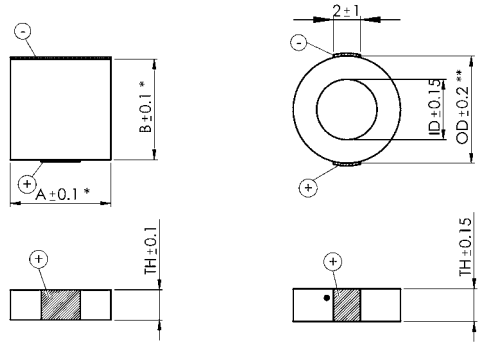

PICMA® Chip miniature piezo actuator, A, B, TH see table. Tolerances A, B for PL022, PL033 ±0.10 mm, for PL055 ±0.15 mm, for PL088 ±0.20 mm. Tolerance OD for PD080 ±0.30 mm

Suitable drivers

E-610 Piezo Amplifier / Controller
E-617 High-Power Piezo Amplifier
E-831 Piezo Driver

Order Number*	Dimensions A × B × TH [mm]	Displacement** [µm] ±20% (0 – 100 V)	Blocking force [N] (0 – 100 V)	Electrical capacitance [nF] ±20%	Axial resonant frequency [kHz]
PL022.30	2 × 2 × 2	2.2	>120	25	600
PL033.30	3 × 3 × 2	2.2	>300	85	600
PL055.30	5 × 5 × 2	2.2	>500	250	600
PL088.30	10 × 10 × 2	2.2	>2000	1100	600

Order Number*	Dimensions OD × ID × TH [mm]	Displacement [µm] ±20% (0 – 100 V)	Blocking force [N] (0 – 100 V)	Electrical capacitance [nF] ±20%	Axial resonant frequency [kHz]
PD050.30	5 × 2.5 × 2.45	2.0	>400	110	500
PD080.30	8 × 4.5 × 2.45	2.0	>1000	300	500

* Optionally equipped with 100 mm PTFE-insulated wire leads, AWG 32 (Ø 0.49 mm); change order number extension to 1 (e. g. PL022.31).
** The values refer to the free component and can be lower when glued on.
Piezo ceramic type: PIC 252.
Standard connections: Solderable contacts.
Recommended preload for dynamic operation: 15 MPa.
Maximum preload for constant force: 30 MPa.
Axial resonant frequency at 1 V_{pp}, unloaded, unclamped. The value is halved for unilateral clamping. Lateral resonant frequencies can be lower than the axial one, depending on the installation situation.
Capacitance at 1 V_{pp}, 1 kHz, RT.
Operating voltage: -20 to 100 V.
Operating temperature range: -40 to 150°C.
Ask about custom designs!

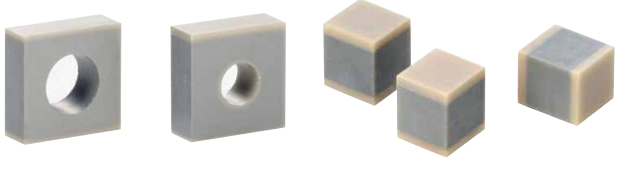

On request PICMA® Chip piezo actuators can be manufactured with ceramic-insulated inner hole (left) or with precision-ground ceramic end plates (right)

NOTES:

1. ALLOWABLE OPTICAL MATERIAL: GRADE A FINE ANNEALED
   ELEMENT A: SCHOTT: N-LAK8 713/538
   ELEMENT B: SCHOTT: N-SF57 847/238
2. CENTERING TOLERANCE (AT 587.6nm):
   BEAM DEVIATION: 3-5 arc min.
3. COATING (APPLY ACROSS COATING APERTURE)
   S1: VIS 0° [425-675nm]
   Rave ≤ 0.4% 425-675nm
   S2: NONE
   S3: NONE
   S4: NONE

△4. FINE GROUND SURFACE

5. FOCAL LENGTH TOLERANCE: ± 1%

△6. ELEMENTS TO BE CEMENTED WITH NORLAND OPTICAL ADHESIVE NOA 61

7. HYBRID ASPHERE APPLIED TO S4 OF ACHROMAT:
   MATERIAL: n_d=1.517, V_d=52.0
   CENTER THICKNESS: 0.060mm ADDED ONTO S4
   CLEAR APERTURE: ∅7.5

$$Z(Y)= \frac{CY^2}{1 + SQRT\{1-(1+k)C^2Y^2\}} + D*Y^2 + E*Y^4 + F*Y^6 + G*Y^8 + H*Y^{10} + J*Y^{12} + L*Y^{14}$$

C= -0.00306755
K=0
D=0
E= 1.006099E-004
F= -7.1352097E-007
G=0
H=0
J=0
L=0

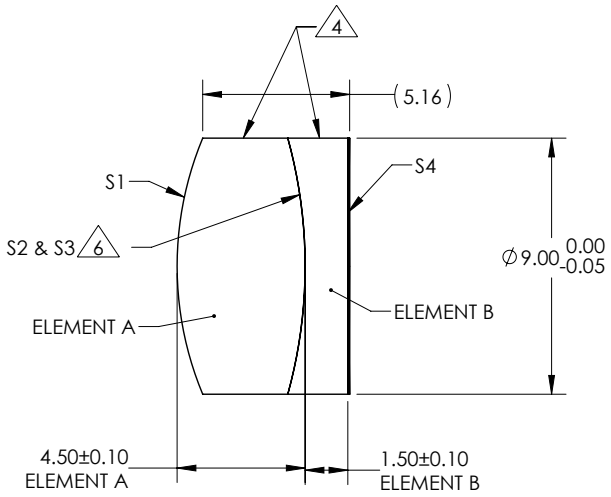

FOR INFORMATION ONLY:
DO NOT MANUFACTURE PARTS TO THIS DRAWING

	ELEMENT A		ELEMENT B	
	S1	S2	S3	S4
SHAPE	CONVEX	CONVEX	CONCAVE	PLANO
RADIUS	11.70	16.90	16.90	INFINITY
SURFACE QUALITY	40-20	40-20	40-20	40-20
CLEAR APERTURE	∅8.1	∅8.1	∅8.1	∅8.1
BEVEL MAX FACE	0.25mm x 45°	0.25mm x 45°	0.25mm x 45°	0.25mm x 45°

EFL (AT 587.6nm)	(18.00)	Edmund Optics®	
BFL (AT 587.6nm)	(14.29)	TITLE	9mm Diameter x 18mm EFL Aspherized Achromatic Lens
ALL DIMS IN	mm	DWG NO	49657

NOTES:

1. ALLOWABLE OPTICAL MATERIAL: GRADE A FINE ANNEALED
   ELEMENT A: SCHOTT: N-LAK8 713/538
   ELEMENT B: SCHOTT: N-SF57 847/238
2. CENTERING TOLERANCE (AT 587.6nm):
   BEAM DEVIATION: 3-5 arc min.
3. COATING (APPLY ACROSS COATING APERTURE)
   S1: VIS 0° [425-675nm]
   Rave ≤ 0.4% 425-675nm
   S2: NONE
   S3: NONE
   S4: NONE

△4. FINE GROUND SURFACE

5. FOCAL LENGTH TOLERANCE: ± 1%

△6. ELEMENTS TO BE CEMENTED WITH NORLAND OPTICAL ADHESIVE NOA 61

7. HYBRID ASPHERE APPLIED TO S4 OF ACHROMAT:
   MATERIAL: n_d=1.517, V_d=52.0
   CENTER THICKNESS: 0.080mm ADDED ONTO S4
   CLEAR APERTURE: ∅11.0

$$Z(Y)= \frac{CY^2}{1 + SQRT\{1-(1+k)C^2Y^2\}} + D*Y^2 + E*Y^4 + F*Y^6 + G*Y^8 + H*Y^{10} + J*Y^{12} + L*Y^{14}$$

C= -0.0037345
K=0
D=0
E= 2.77599E-005
F= -8.6915827E-008
G=0
H=0
J=0
L=0

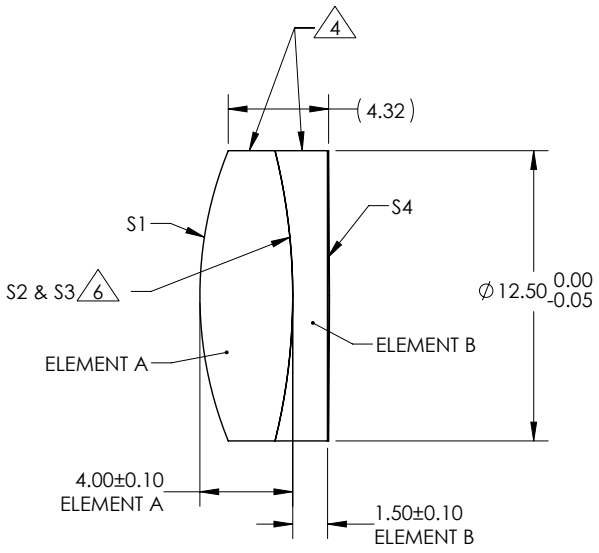

FOR INFORMATION ONLY:
DO NOT MANUFACTURE PARTS TO THIS DRAWING

	ELEMENT A		ELEMENT B	
	S1	S2	S3	S4
SHAPE	CONVEX	CONVEX	CONCAVE	PLANO
RADIUS	16.60	26.00	26.00	INFINITY
SURFACE QUALITY	40-20	40-20	40-20	40-20
CLEAR APERTURE	∅11.25	∅11.25	∅11.25	∅11.25
BEVEL MAX FACE	0.25mm x 45°	0.25mm x 45°	0.25mm x 45°	0.25mm x 45°

EFL (AT 587.6nm)	(25.00)	Edmund Optics®	
BFL (AT 587.6nm)	(21.66)	TITLE	12.5mm Diameter x 25mm EFL Aspherized Achromatic Lens
ALL DIMS IN	mm	DWG NO	49660

TECHSPEC 5mm Enhanced Aluminum Coated, N-BK7 Right Angle Mirror

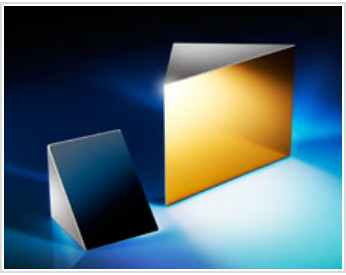

Stock No. #45-591 In Stock: IN STOCK

$56.50

- 1 - 5 for $56.50
- 6 - 25 for $45.20
- 26 or more Request Quote

Quantity 1 ADD TO CART REQUEST QUOTE

View Product Family | Add to Wish List

Specifications

Length of Hypotenuse (mm)	7.0
Length of Legs (mm)	5.00
Clear Aperture CA (mm)	4.5 x 6.3
Dimensional Tolerance (mm)	±0.1
Surface Accuracy (λ)	1/8
Surface Quality	40 - 20
Angle Tolerance (arcminutes)	±2
Bevel	Protective bevel as needed
Substrate	N-BK7
Coating Specification	R_{avg} >95% @ 450 - 650nm
Coating	Enhanced Aluminum
Typical Energy Density Limit	0.2 J/cm^2 @ 532nm, 10ns
Wavelength Range (nm)	450 - 650
RoHS	Compliant (View Certificate)

Technical Images

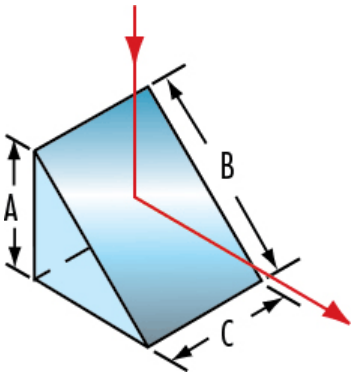

Related Documents

Metallic Mirror Coatings

Related Products

Edmund Lens Cleaner

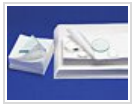

Edmund Optics Lens Tissue - Industrial Grade

Dust-Off® Plus

Piezo LEGS® Linear Twin 20N

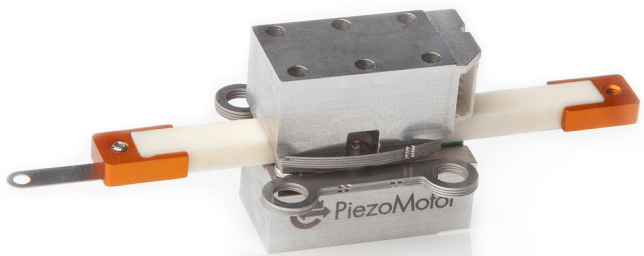

- **Direct drive - backlash free**
- **Nanometer resolution**
- **Simple drive electronics**
- **No power draw in hold position**
- **Quick response and high speed**

The Piezo LEGS 20N linear motor is intended for a large range of OEM applications. Design focus has been for ease of integration. The very high speed dynamics and nanometer resolution makes it ideal for numerous applications.

The LEGS technology is characterized by its outstanding precision. Fast speed and quick response time, as well as long service life are other benefits. In combination with the nanometer resolution the technology is quite unique.

The motor is ideally suited for move and hold applications or for automatic adjustments. When the motor is in hold position it does not consume any power. The drive technology is direct, meaning no gears or lead screws are needed to create linear motion. This means the motor has no mechanical play or backlash. The Piezo LEGS 20N linear motor is available in a standard version and a vacuum version.

Mechanical and electrical connection

The motor is easily integrated in your application using the drive rod mechanical adapter. Drive rods are supplied in different lengths (30, 40, 50, 60, 70 and 101.8 mm).

The motor has two electrical connectors which are connected in parallel to the driver.

Operating modes

The motor can move in full steps (wfm-steps), or partial steps (microsteps) giving positioning resolution in the nanometer range. Speed is adjustable from single microsteps per second up to max specified.

Controlling the motor

PiezoMotor offers a range of drivers and controllers. The most basic one is a handheld push button driver. Another option is an analogue driver that regulates the motor speed by means of an ±7 V analogue interface. One of the more advanced alternatives is the PMD101 Microstep Driver/Controller. This product enables the user to vary the waveform as well as speed. The PMD101 is equipped with encoder signal inputs for close loop control. The microstepping feature divides full step cycle into maximum 2048 increments which results in microsteps as small as two nanometers.

PMD101

Design your own driver

Some customers prefer to design their own driver for ease of integration or for even higher waveform resolution (sub-nanometer range). In this case PiezoMotor can provide information to assist in the design.

Ordering information	
Motor	
LT2010A-	Standard version, stainless steel
LT2010B-	Vacuum version, stainless steel
Drivers and Controllers	
PMCM21-01	Handheld push button driver
PMCM31-01	Analogue driver
PMD101	Microstepping driver
Accessories	
LEGS-LT CONNECT	Twin connect board
102431-05	Motor cable 0.5 m
102431-15	Motor cable 1.5 m

150020-02

Technical Specification

Type	LT2010A (standard version)	LT2010B (vacuum version)	Unit	Note
Maximum Stroke	80 (L−20.8)	80 (L−20.8)	mm	100.8 mm drive rod, no mechanical adapter
Speed Range	0-10	0-10	mm/s	recommended, no load
Step Length	0.001[a]-4	0.001[a]-4	µm	no load, microsteps up to full wfm-steps
Resolution [a]	< 1	< 1	nm	
Recommended Operating Range	0-10	0-10	N	for best microstepping performance and life time
Stall Force	20	20	N	
Holding Force	22	22	N	
Vacuum	-	10^{-7}	torr	
Maximum Voltage	48	48	V	
Connector	2 x JST BM05B-SRSS-TB	soldered cable with 2 x JST 05SR-3S		
Mechanical Size	22 x 21 x 10.8	22 x 21 x 10.8	mm	see drawing for details
Material in Motor Housing	Stainless Steel	Stainless Steel		
Weight	29	29	gram	approximate
Operating Temp.	−20 to +70	−20 to +70	ºC	

a. Driver dependant

Item no. LT2010 _ - _ _ _ _ _

Stall Force
20 = 20 N

Version

Motor type
A = SS / Stainless Steel
B = SSV / Stainless Steel Vacuum

Drive rod (standard lengths)
030 = 30 mm
040 = 40 mm
050 = 50 mm
060 = 60 mm
070 = 70 mm
101 = 100.8 mm

Mechanical adapter
A0 = No adapter
D1 = One adapter - Front
D2 = One adapter - Back
E1 = Two adapters - Front and back

Connector
A = JST connectors - for motor type A
B = Teflon cables PTFE AWG28 with JST connectors - for motor type B

Cable Options
00 = No cables (JST connectors only) - for motor type A
05 = 2 x 0.5 m - for motor type A
10 = 2 x 1.0 m - for motor type B
15 = 2 x 1.5 m - for motor type A

Twin connect board is sold separately, see accessory list on page 1.

Example:
LL2010A-050D1A05: LEGS Linear, 20N, version 10, stainless steel, 50 mm drive rod, one mechanical adapter front end, JST connector with 0.5 m cable

Note: All combinations are **not** possible!

Note: All specifications are subject to change without notice.

Visit our website for application examples, CAD files, videos and more...

www.piezomotor.com

PiezoMotor

PiezoMotor Uppsala AB
Stålgatan 14
SE-754 50 Uppsala, Sweden

Telephone: +46 18 489 5000
Fax: +46 18 489 5001

info@piezomotor.com
www.piezomotor.com

Axmo Précision, 15 rue du Roussillon, ZI de la Moinerie, 91220 Brétigny/Orge Tél. : 01 60 84 90 75 | Fax : 01 60 85 31 55 | E-mail : info@axmo.fr

Glissières type NKL

oduits
oles
to-Mécanique
mposants de dages
à Billes
ntrôle d'axe
mmandes Moteurs
leries Photos

rques
mo
neeberger
oud
rax
l Hipp
C
T

léchargement
talogues et CGV
hiers CAO
otes et Utilitaires

Descriptif

Exécution à **un seul axe**
Exécution légère, parties de la table en aluminium
4 séries
Avec **cages à rouleaux ou à billes** AC
Longueur : 25 à 410 mm
Course : 10 à 280 mm
Pour les **accélérations plus hautes** avec FORMULA-S

Matière

Aluminium

Exécutions standard

Les tables sur roulements type NKL se composent d'une partie supérieure et d'une partie inférieure de même longueur ainsi que de rails de guidage correspondants du type R. Toutes les séries sont équipées de cages à rouleaux type AC et de plaques terminales type GB. Le montage peut être vertical ou horizontal. Les trous de fixation normalisés sont présents dans les deux parties (inférieure et supérieure). Pour la version standard la face opposée aux vis de réglage des jeux peut être utilisée comme référence. La limitation de la course est identique à celle des tables du type NK. Avec FORMULA-S ces vis ne sont plus nécessaires, grâce au système de la cage assistée.

Exécutions spéciales

Cages à billes type AK (-AK)
pour une réduction de la sensibilité aux impuretés avec toutefois une diminution de la capacité de charge

Cages à rouleaux type EE (-EE)
matière synthétique PE, seulement pour série 6 comme étanchéité contre la saleté et la poussière.
Fonctionnement légèrement entravé

Cage assistée integrée (-KS)
pour haute dynamique et toutes positions d'assemblage

Tableau dimensions

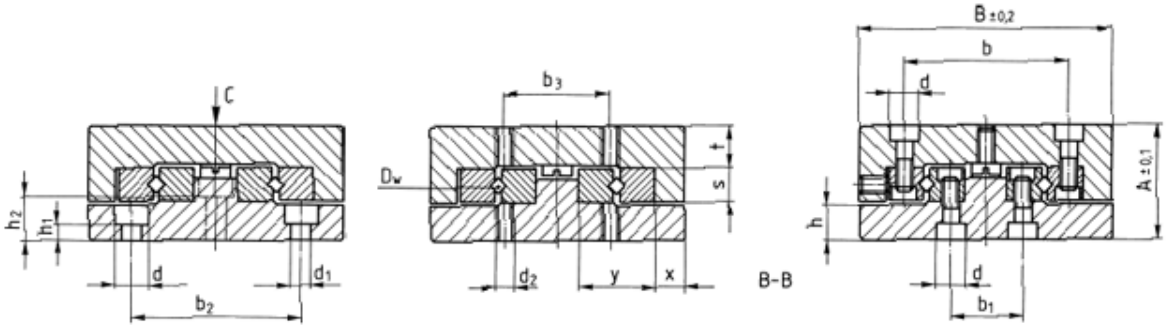

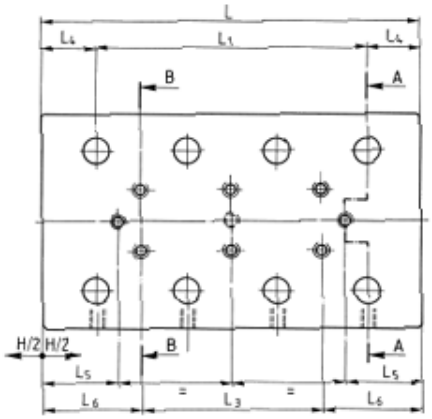

Disposition des trous de fixation normalisés dans la partie inférieure

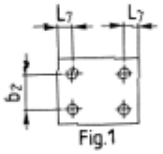

Fig.1

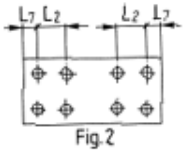

Fig.2

No de réf.	A	B	Dw	H	L	L1	L2	L3	L4	L5	L6	L7	b	b1	b2	b3
NKL 1-25	13	30	1.5	10	25	1x10	10	-	7.5	3.0	12.5	3.5	18.4	8.6	22	10
NKL 1-35	13	30	1.5	18	35	2x10	10	1x10	7.5	4.5	12.5	3.5	18.4	8.6	22	10
NKL 1-45	13	30	1.5	25	45	3x10	10	2x10	7.5	6	12.5	3.5	18.4	8.6	22	10
NKL 1-55	13	30	1.5	32	55	4x10	10	3x10	7.5	7.5	12.5	3.5	18.4	8.6	22	10
NKL 1-65	13	30	1.5	40	65	5x10	10	4x10	7.5	8.5	12.5	3.5	18.4	8.6	22	10
NKL 1-75	13	30	1.5	45	75	6x10	10	5x10	7.5	11	12.5	3.5	18.4	8.6	22	10
NKL 1-85	13	30	1.5	50	85	7x10	10	6x10	7.5	13.5	12.5	3.5	18.4	8.6	22	10
NKL 2-35	21	40	2	18	35	1x15	15	-	10	3	17.5	5	25	11	30	15
NKL 2-50	21	40	2	30	50	2x15	15	1x15	10	4.5	17.5	5	25	11	30	15
NKL 2-65	21	40	2	40	65	3x15	15	2x15	10	7	17.5	5	25	11	30	15
NKL 2-80	21	40	2	50	80	4x15	15	3x15	10	9.5	17.5	5	25	11	30	15
NKL 2-95	21	40	2	60	95	5x15	15	4x15	10	12	17.5	5	25	11	30	15
NKL 2-110	21	40	2	70	110	6x15	15	5x15	10	14.5	17.5	5	25	11	30	15
NKL 2-125	21	40	2	80	125	7x15	15	6x15	10	17	17.5	5	25	11	30	15

No de réf.	d	d1	d2	h	h1	h2	s	t	x	y	C en N	ML en Nm	MQ en Nm	Poids en kg	Fig.
NKL 1-25	4.1	2.55	M2	4.1	1.6	-	4	4.5	4	8.5	250	1.20	1.69	0.04	1
NKL 1-35	4.1	2.55	M2	4.1	1.6	-	4	4.5	4	8.5	350	1.80	2.36	0.05	1
NKL 1-45	4.1	2.55	M2	4.1	1.6	-	4	4.5	4	8.5	450	2.40	3.04	0.06	1
NKL 1-55	4.1	2.55	M2	4.1	1.6	-	4	4.5	4	8.5	550	3.00	3.71	0.075	2
NKL 1-65	4.1	2.55	M2	4.1	1.6	-	4	4.5	4	8.5	650	3.60	4.39	0.09	2
NKL 1-75	4.1	2.55	M2	4.1	1.6	-	4	4.5	4	8.5	750	4.20	5.06	0.105	2
NKL 1-85	4.1	2.55	M2	4.1	1.6	-	4	4.5	4	8.5	900	5.10	6.08	0.12	2
NKL 2-35	6	3.5	M3	6.7	3.2	-	6	8	5	12	425	2.72	3.83	0.11	1
NKL 2-50	6	3.5	M3	6.7	3.2	-	6	8	5	12	595	4.08	5.36	0.15	1
NKL 2-65	6	3.5	M3	6.7	3.2	-	6	8	5	12	850	6.12	7.65	0.19	1
NKL 2-80	6	3.5	M3	6.7	3.2	-	6	8	5	12	1020	7.48	9.18	0.23	2
NKL 2-95	6	3.5	M3	6.7	3.2	-	6	8	5	12	1275	9.52	11.48	0.27	2
NKL 2-110	6	3.5	M3	6.7	3.2	-	6	8	5	12	1445	10.88	13.01	0.31	2

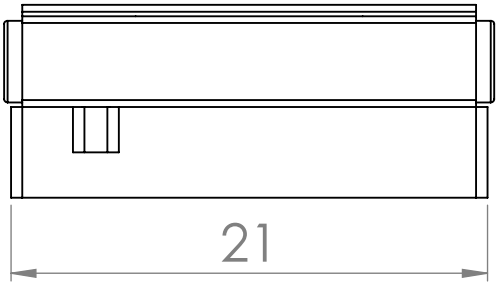

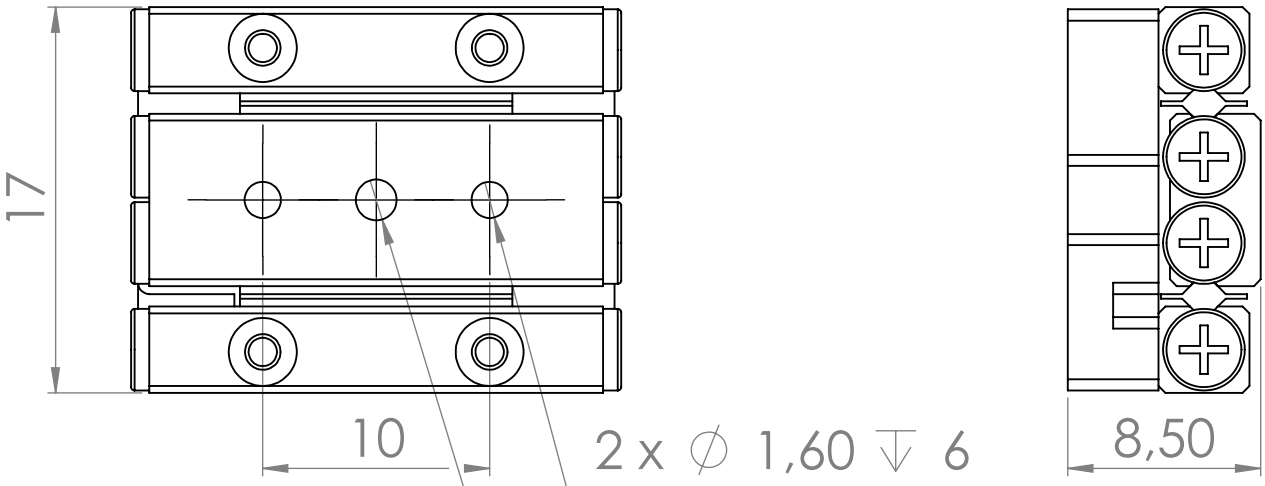

Bottom View

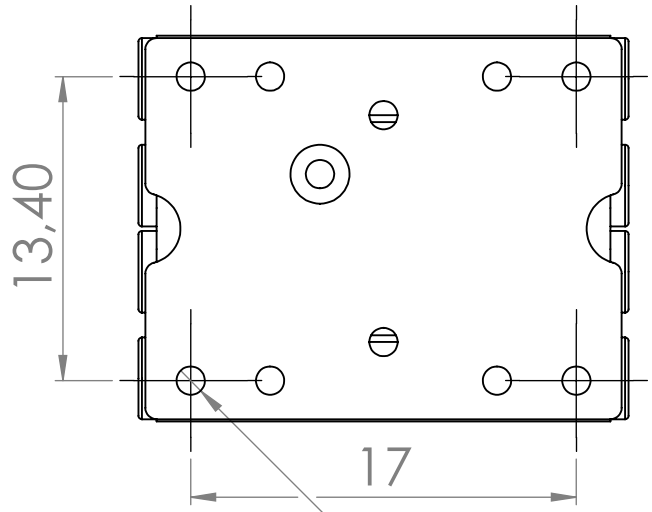

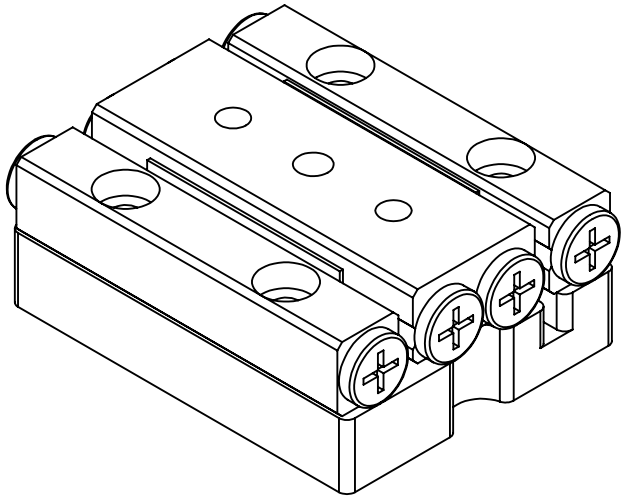

WENN NICHT ANDERS DEFINIERT: BEMASSUNGEN SIND IN MILLIMETER OBERFLÄCHENBESCHAFFENHEIT: TOLERANZEN: LINEAR: WINKEL:	OBERFLÄCHENGÜTE:	ENTGRATEN UND SCHARFE KANTEN BRECHEN	ZEICHNUNG NICHT SKALIEREN	ÄNDERUNG		
	NAME	SIGNATUR	DATUM			BENENNUNG:
GEZEICHNET						
GEPRÜFT						
GENEHMIGT						
PRODUKTION						
QUALITÄT				WERKSTOFF:	ZEICHNUNGSNR. SLC-1720	A4
				GEWICHT:	MASSSTAB:3:1	BLATT 1 VON 1

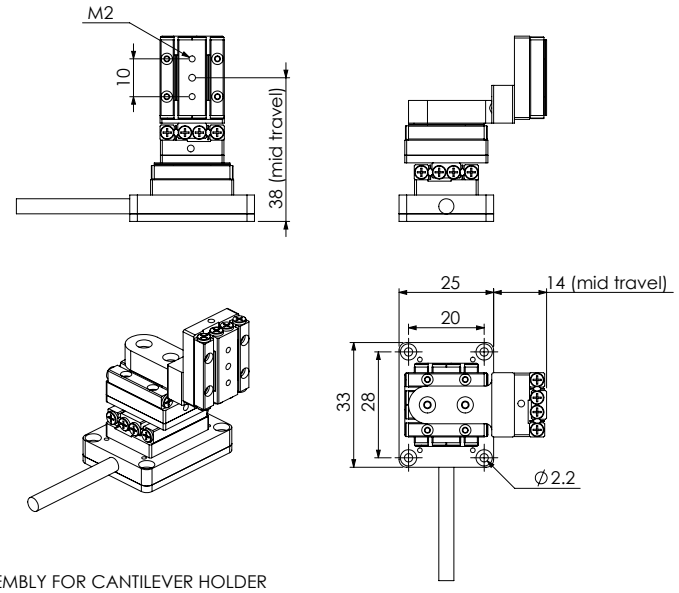

ASSEMBLY FOR CANTILEVER HOLDER

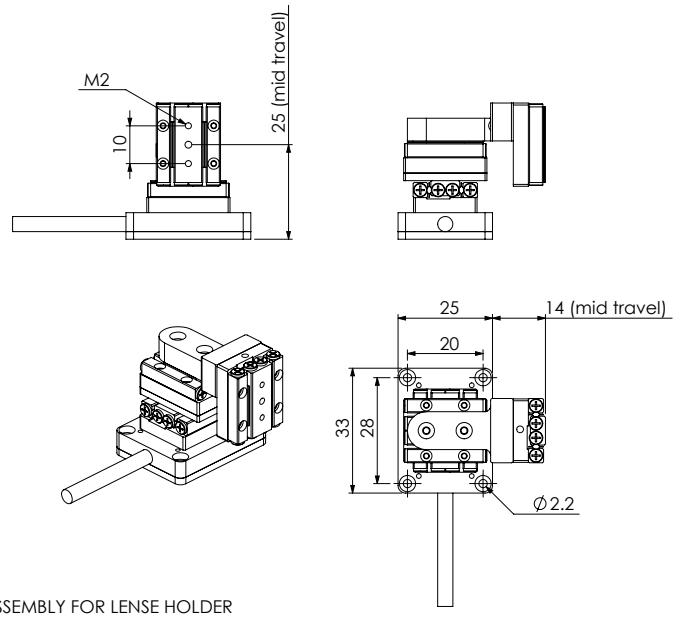

ASSEMBLY FOR LENSE HOLDER

Smaract XYZ stage.
- 3 x SLC1720 stages + connecting plates

ITEM	DRAWING N.	QTY	DESCRIPTION / REMARKS	MATERIAL	W./Kg
					0.08

SCALE: 1/ 1

0 mm 100

	NAME	DATE
DRN.	A.Harris	30/06/14
CKD.	A.HARRIS	
APPD.	P.BERNARD	

ID13 HS X-AFM
GENERAL ASSEMBLY
Smaract XYZ

ISO STANDARD
GEN. SURFACE FINISH : N7
GEN. LINEAR TOL. : Js12
GEN. ANGULAR TOL. : ±0,5°

EUROPEAN SYNCHROTRON RADIATION FACILITY
BP 220 38043 GRENOBLE CEDEX-FRANCE
TEL. 04-76-88-20-00 FAX 04-76-88-20-20

A3

ASSY. 00.90.1487

00.90.1564

MOD	DATE	DRND.	APPD.	DESCRIPTION

Design Méca

SolidWorks

Schäfter + Kirchhoff

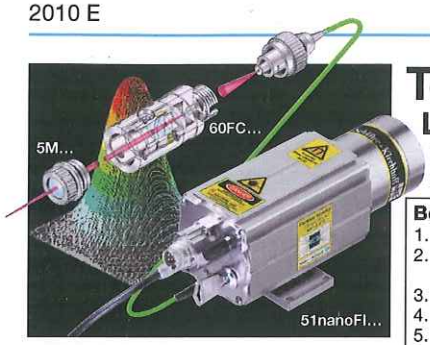

Technical Information

Laser diode beam source 51nanoFl... with faraday isolator and singlemode fiber

• HF-modulated • short coherence length • reduced speckle contrast

Before Operation: Read this information sheet completely.

1. **Adhere to laser safety regulations**!
2. Turn the key switch **OFF**.
   Otherwise take care that the power supply used is turned off.
3. Connect cable to power supply.
4. Connect modulation input or interlock (optional)
5. Turn on power supply.
6. Turn key switch to ON.
7. **Protect Laser against shock! Do not disassemble!**
   Fiber bending radius must be greater than 25 mm!

Laser Safety!

The module is an OEM product.

This means that the actual regulations and documentations for laser safety (e.g., DIN/EN 60825, ANSI Z136.2) must be strictly applied before any usage, assembly into further systems or reselling to other customers.

Electrical Data

Electronic	9761, 9762, 9763	
Laser diode operation mode	constant power	
Supply Voltage	+5V DC (±0.2V)	
Internal RF-Modulation	300 MHz	
Max. operating current	< 260 mA	
Ambient temperature range	15 - 35 °C	
Laser power adjustm. range	< 5-100%*	
Modulation input	U_{Analog}	U_{TTL}
Min. / Max. Voltage	0V / +5V	0V / +5V
Input Impedance	22 kΩ	22 kΩ
Max. Modulation Frequency	100 kHz	100 kHz
Modulation delay ON/OFF	<2µs/1µs	<2µs/1µs
Rise / fall time max.	1 µs/1 µs	1 µs/1 µs
Laser 'ON' at U_{mod}	+2.5V AND TTL high	
Laser P_{out} <1 - 100% at U_{mod}	0-2.5V AND TTL high	
Laser 'OFF' at U_{mod}	0V AND TTL low	
	0-2.5V AND TTL low	
	0V AND TTL high	
	n.c. AND n.c.	

* Dependend on Laser diode

CE This product meets the requirement of the EC directive 89/336/E.E.C. The requirements of DIN EN 61326 are fullfilled.

Pin Description X1

Cable (1.5 m): AWG 26 C UL 3 x 0,14 mm² (tense protected)	1 Round connector Lumberg SV30 IEC-60130-9	front view (male)
black	1	GND
red	2	+ 5V DC
brown	3	n.c.
Cable shield	Shield	Laser housing

Laser housing and cable shield are connected. Electronics and laser diode are insulated from the module housing.

Connector X2 for Modulation/Interlock

2 Connector 6 pin male Lumberg SFV60 IEC-60130-9	front view (male)
1	GND
2	+ 5V out
3	Interlock out (GND)
4	Interlock in
5	U_{mod} analog
6	U_{mod} digital (TTL)

For laser operation Pin 3 and 4 (Interlock) must be connected. **Attention:** The modulation inputs are not galvanically decoupled, transients may damage the laser diode!

Adjustment of Laser Power

With the potentiometer, the desired output power is adjustable from $P_{min} \approx 0.01\ P_0$ up to P_0. The actual values P_0 depend on the laser diode used.

Increased operating current I_O may indicate imminent laser break down. See application note: "Observe laser operating current consumption"!

Power Supply

The operating voltage(5V DC) has to be free of electronic fast transients. Transients arising from a wide variety of sources (e.g. lightning, poor power conditioning, switched power supplies, or other electronic equipment) have to be kept off by an isolation transformer and/or filters in the power line.
To reduce electromagnetic interference we recommend an EMI-Filter 1 as included in the 3 pin connector by **Schäfter+Kirchhoff**.
Shielded cable and a separate switch between the module and the supply is recommended. This is turned on **after** the supply voltage, and turned off **before** the supply voltage.

Grounding

To prevent laser diode damage, system grounding is necessary. **Ground** connection has to be restricted to **a single point of the system**. This should either be the laser housing or the shielding of the connection cable.
Using a floating output power supply it is recommended to connect the 0V-Level of the supply with the ground level.

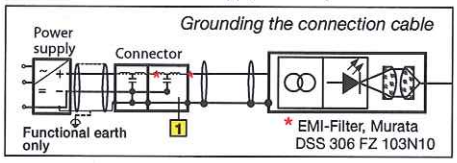

Modulation

The laser provides two modulation inputs U_{analog} 5 and U_{TTL} 6 using AND Logic. If one of the inputs is not connected the laser will be OFF. So if you are going to use one input only, please connect the other one to +5V DC. The digital input 6 may be used for additional modulation (see timing diagram).

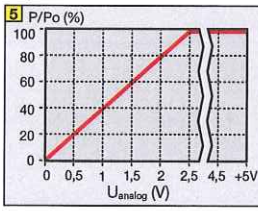

Connecting analog voltage (U_{analog} ranging from 0 to 2.5V) to modulation input 5 gives linear control of the laser output power from approximately zero to the power level given by the potentiometer setting (see plot).

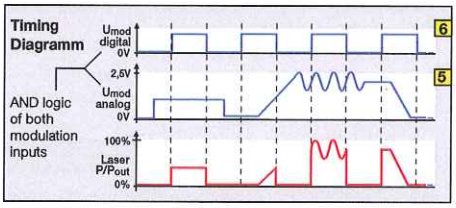

Modulation and Interlock

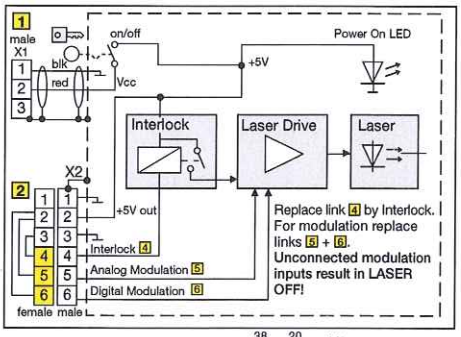

Case Type	L1	L2
A	141	195
B	111	165
C	126	180
D	118	172

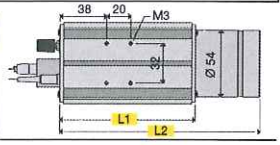

Configurations

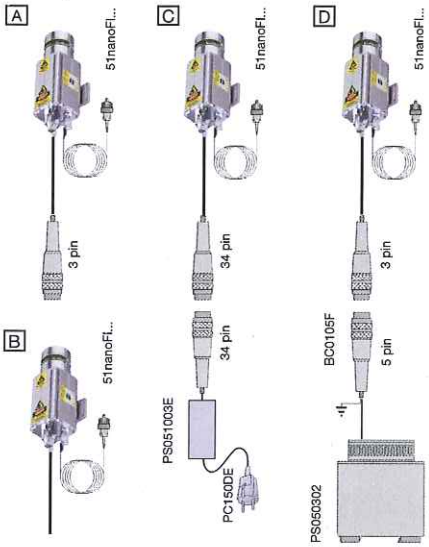

Type 51nanoFl- 660 - 6 - M01 - P - 5 - 2 - 1 8 - C - 150 - **Order** 508323 **S/N** 10108

(Nominal values: Wavelength / Power / LD Code / Mode / Volt / Electr./El. Cable / SM/PM PC/APC / O/C / Fiber length / Option)

						Config.
Wavelength:	659 nm	**Pmin:**	0.0004 mW	**Accessories included:**		
Laser class:	3B	**Po:**	6.07 mW	Power Supply PS050302	☐	A ☒
Test temperature:	25 °C	**Io*:**	140 mA	Power Supply 051003E	☐	B ☐
Fiber cable:	Single mode ☒	PM Singlemode	☐	Power Supply 120516E	☐	C ☐
Connector:	FC-PC ☐ FC-APC (8°) ☒	.....	☐	Power Supply L05B	☒	D ☐
Fiber cable length:	Standard 1.5 m ☒	..... m	☐	Connector BC0106F	☐	
MFD/NA:	4.3 µm / 0.11	**Case Type:**	.....	Connector BC0105F	☐	
Electronics:	9763 ☐ 9762 ☒		9761 ☐	Connector	☐	
LD operation mode:	Constant power ☒	Constant current	☐	Power Cord PC150	☒ DE ☐ US ☐ UK	
El. Cable:	Standard 1.5 m ☒	..... m	☐	Poti knob (standard)	☒	
Connector:	without ☐ 3 pin ☒	.....	☐	Protection cap	☐	

Notes:

ILA: 128	IMA: 389 391	PA: 42.9 23.8	OD: A3.1-02 A3.1-02	FIB: S6-10	Date: 05.11.2013	Operator: JL

51FI_H_Telnfo_ED

Schäfter + Kirchhoff GmbH
Kieler Straße 212, D-22525 Hamburg • Tel: (+49) 40 85 39 97-0 • Fax: (+49) 40 85 39 97-79 • eMail: info@SuKHamburg.de • Web: www.SuKHamburg.de

Single Mode Fiber: 633 / 680 nm

SM600

Description

Thorlabs' specialty single mode fibers are engineered for a variety of applications including biotechnology, laser delivery, and telecommunications. These fibers offer enhanced bend-insensitivity as well as reduced splice loss while providing excellent resistance to bend induced loss similar to that of conventional type fibers.

Specifications

Geometrical & Mechanical	
Cladding Diameter	125 ± 1 µm
Coating Diameter	245 µm ± 5%
Core-Clad Concentricity	<1.0 µm
Coating / Clad Offset	≤5 µm
Coating Material	Dual Acrylate
Proof Test Level	100 kpsi (1%)

Optical	
Numerical Aperture (nominal)	0.10 – 0.14
Attenuation[1]	<15 dB/km
Design Wavelength[2]	633 / 680 nm
Cut-Off Wavelength	500 – 600 nm
Mode Field Diameter[3]	4.3 µm @ 633 nm 4.6 µm @ 680 nm

[1]Attenuation is a worst-case value, quoted for the shortest design wavelength.
[2]The Design Wavelength is the wavelength (or wavelengths) at which the fiber is typically used. In practice, the fiber will transmit the TEM_{00} mode at wavelengths of up to approximately 200 nm longer than the cut-off wavelength. At the design wavelengths of 633 nm and 680 nm, the launched power must be considered carefully as these fibers have germanosilicate cores and as such as susceptible to color center generation.
[3]The Mode Field Diameter is a nominal, calculated value, estimated at the operating wavelength(s) using typical value of numerical aperture and cut-off wavelength.

Appendix B

Frequency Study of Scanner Motion

Surface Science Laboratory - ESRF
71 Rue de Martyrs, 38000 Grenoble, France

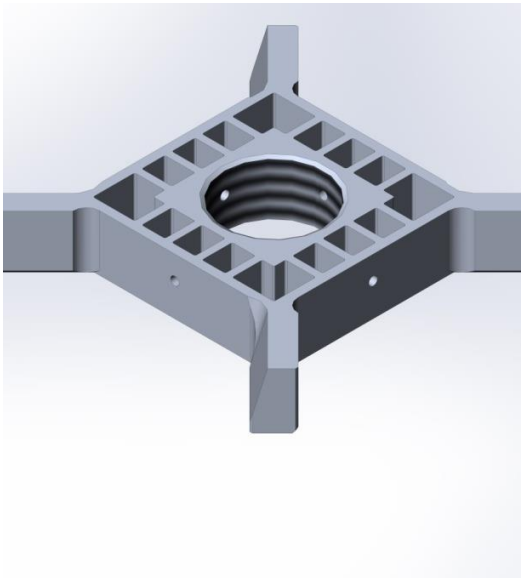

Simulation of the central scanner frame

Date: Friday 18 July 2014
Designer: Miguel Vargas Vitorino
Analysis type: Frequency

Table of Contents

Description

Frequency analysis of the inner frame of the scanner for the HSX-AFM

Model Information

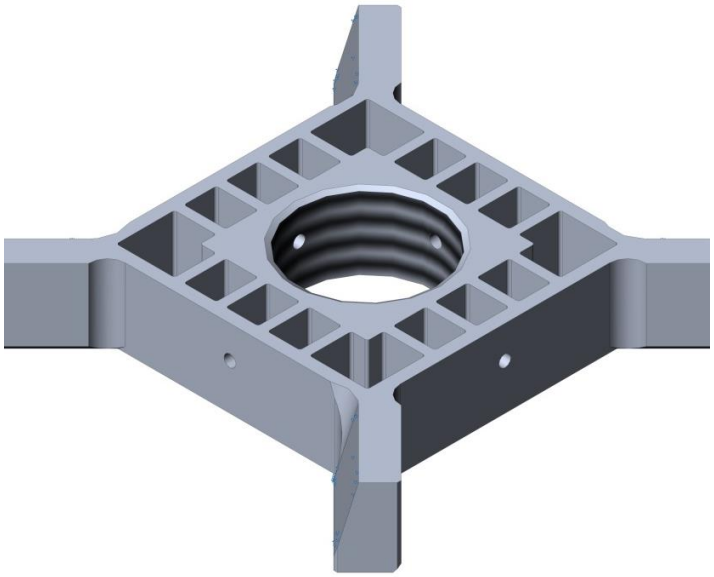

Model name: Scanner Inner Frame

Solid Bodies

Document Name and Reference	Treated As	Volumetric Properties	Document Path/Date Modified
Chanfrein2 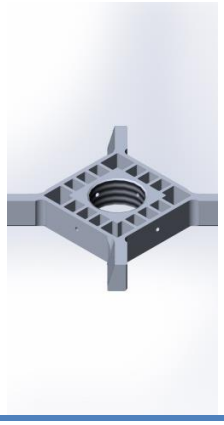	Solid Body	**Mass:0.00600705 kg** **Volume:2.22483e-006 m^3** **Density:2700 kg/m^3** **Weight:0.0588691 N**	**C:\Users\opssl\Desktop\Miguel\HS X-AFM dossier 1 july 14\00901511.SLDPRT** Jul 01 15:57:47 2014

Study Properties

Analysis type	Frequency
Mesh type	Solid Mesh
Number of frequencies	5
Solver type	FFEPlus
Soft Spring:	Off
Incompatible bonding options	Automatic
Thermal option	Include temperature loads
Zero strain temperature	298 Kelvin
Include fluid pressure effects from SolidWorks Flow Simulation	Off

Units

Unit system:	SI (MKS)
Length/Displacement	mm
Temperature	Kelvin
Angular velocity	Rad/sec
Pressure/Stress	N/m^2

Material Properties

Model Reference	Properties	Components
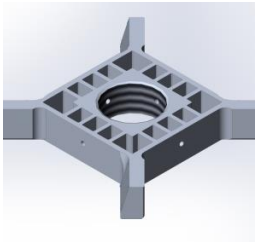	**Name:** 6063-T6 **Model type:** Linear Elastic Isotropic **Default failure criterion:** Unknown **Yield strength:** 2.15e+008 N/m^2 **Tensile strength:** 2.4e+008 N/m^2 **Mass density:** 2700 kg/m^3 **Elastic modulus:** 6.9e+010 N/m^2 **Poisson's ratio:** 0.33 **Thermal expansion coefficient:** 2.3e-005 /Kelvin	SolidBody 1(Chanfrein2)(00901511)
Curve Data:N/A		

Loads and Fixtures

Fixture name	Fixture Image	Fixture Details
Fixed-1	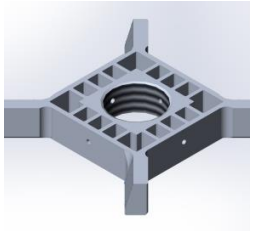	**Entities:** 4 face(s) **Type:** Fixed Geometry

Comments:
Fixed faces as they are predicted in the assembly.

Mesh Information

Mesh type	Solid Mesh
Mesher Used:	Standard mesh
Jacobian points	4 Points
Element Size	0.653016 mm
Tolerance	0.0326508 mm
Mesh Quality	High

Mesh Information - Details

Total Nodes	108373
Total Elements	67224
Maximum Aspect Ratio	19.436
% of elements with Aspect Ratio < 3	98.6
% of elements with Aspect Ratio > 10	0.0298
% of distorted elements(Jacobian)	0
Time to complete mesh(hh;mm;ss):	00:00:09

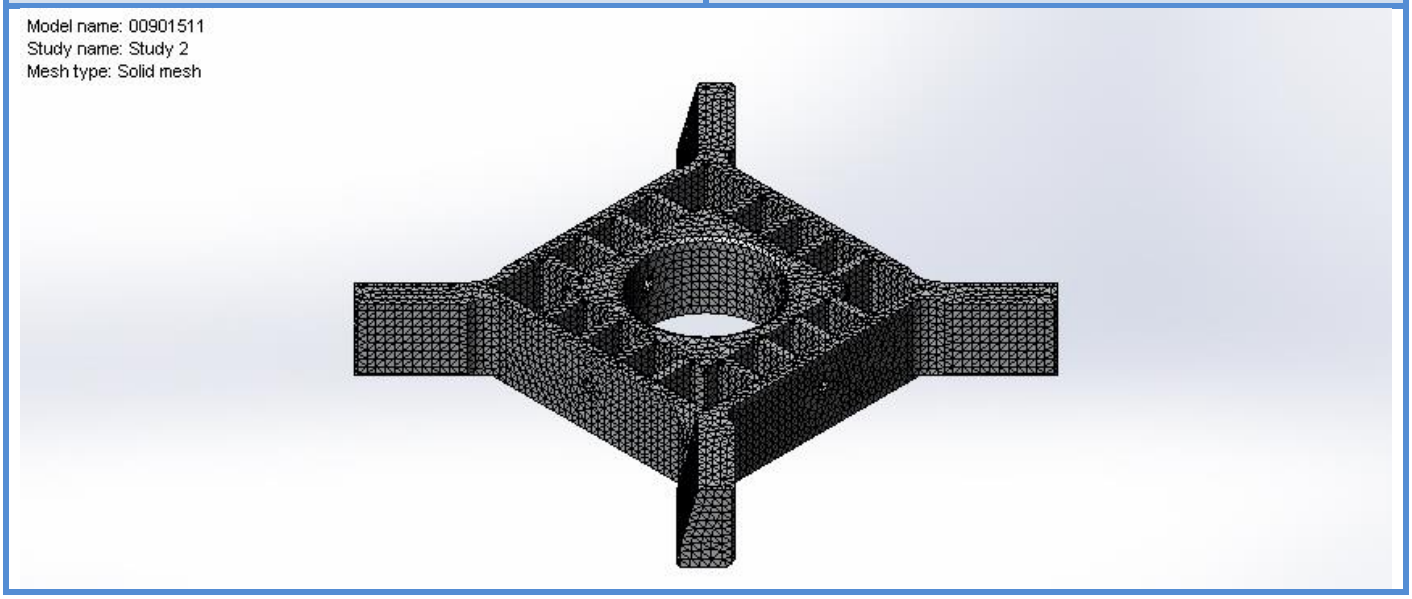

Study Results

Name	Type	Min	Max
Displacement1	URES: Resultant Displacement Plot for Mode Shape: 1(Value = 18363.4 Hz)	0 mm Node: 1109	21391.6 mm Node: 89213

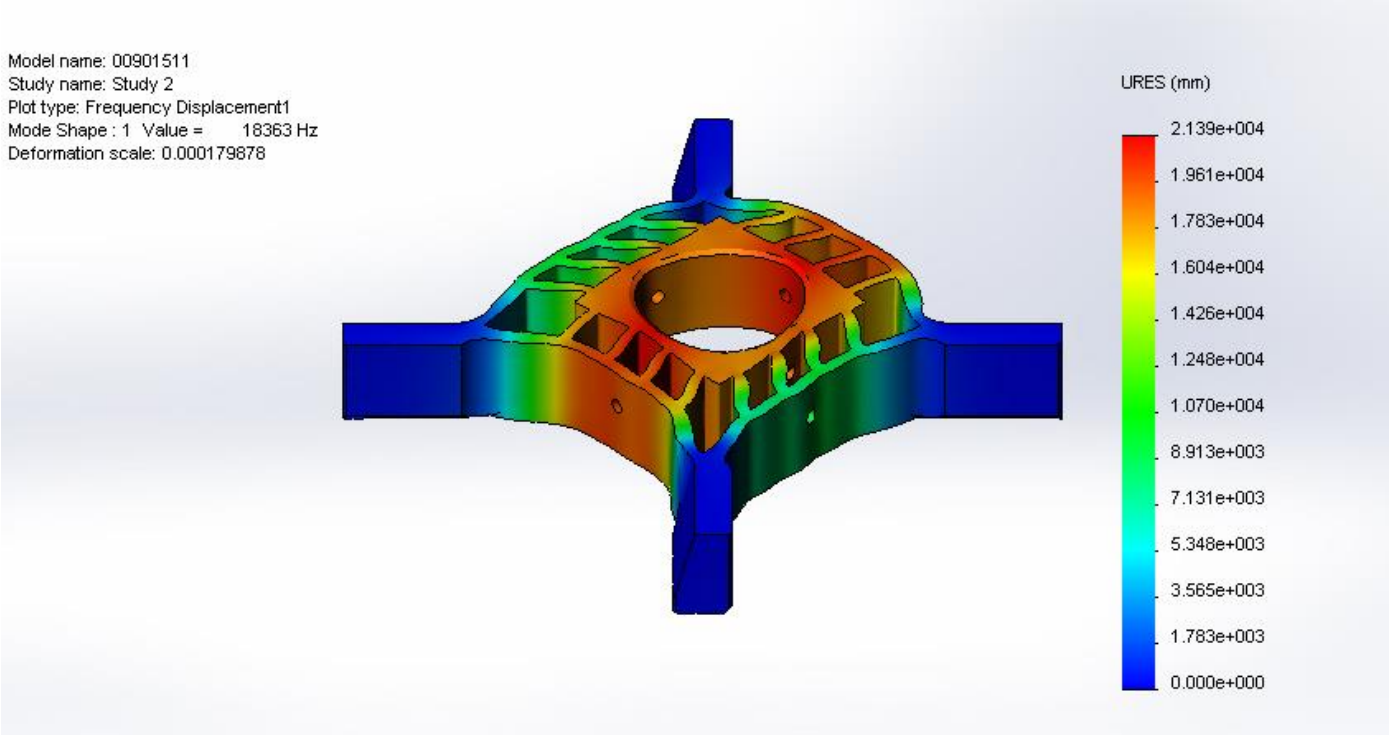

00901511-Study 2-Displacement-Displacement1

Name	Type	Min	Max
Displacement2	URES: Resultant Displacement Plot for Mode Shape: 2(Value = 18370 Hz)	0 mm Node: 1109	21421.1 mm Node: 40

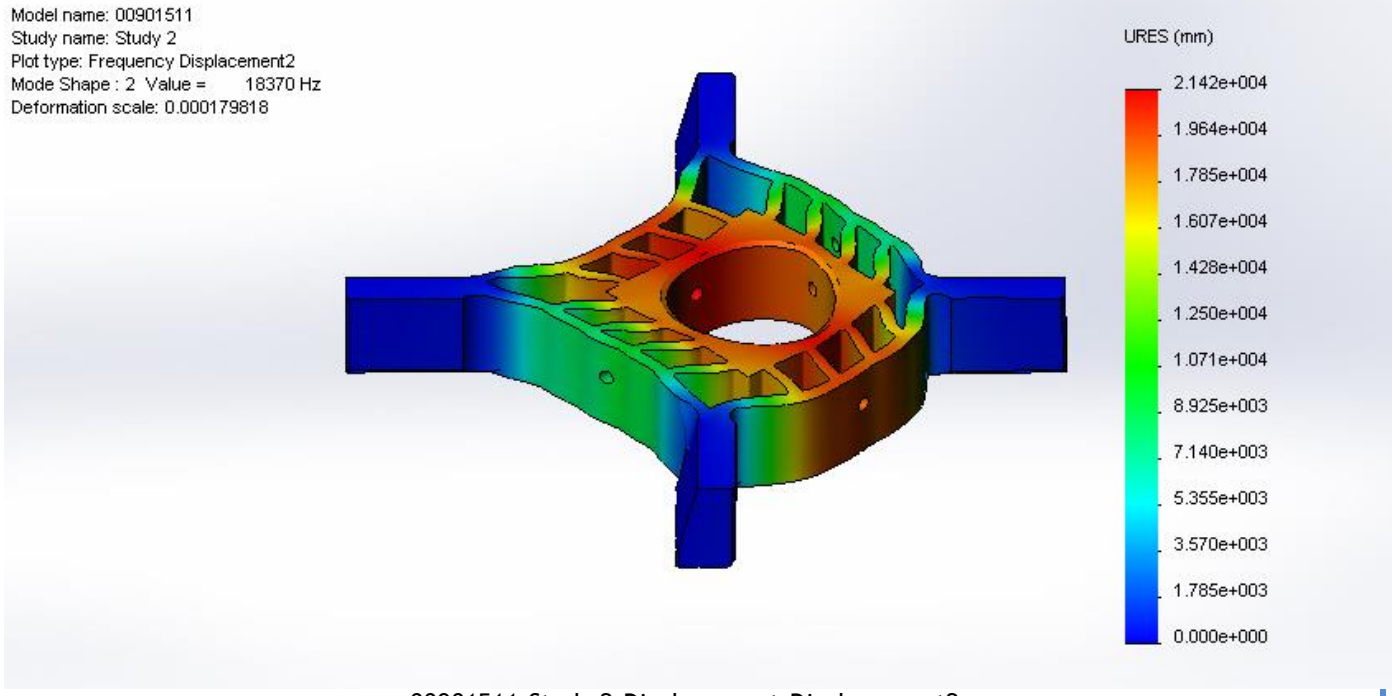

00901511-Study 2-Displacement-Displacement2

Name	Type	Min	Max
Displacement3	URES: Resultant Displacement Plot for Mode Shape: 3(Value = 20750 Hz)	0 mm Node: 1109	21514.4 mm Node: 190

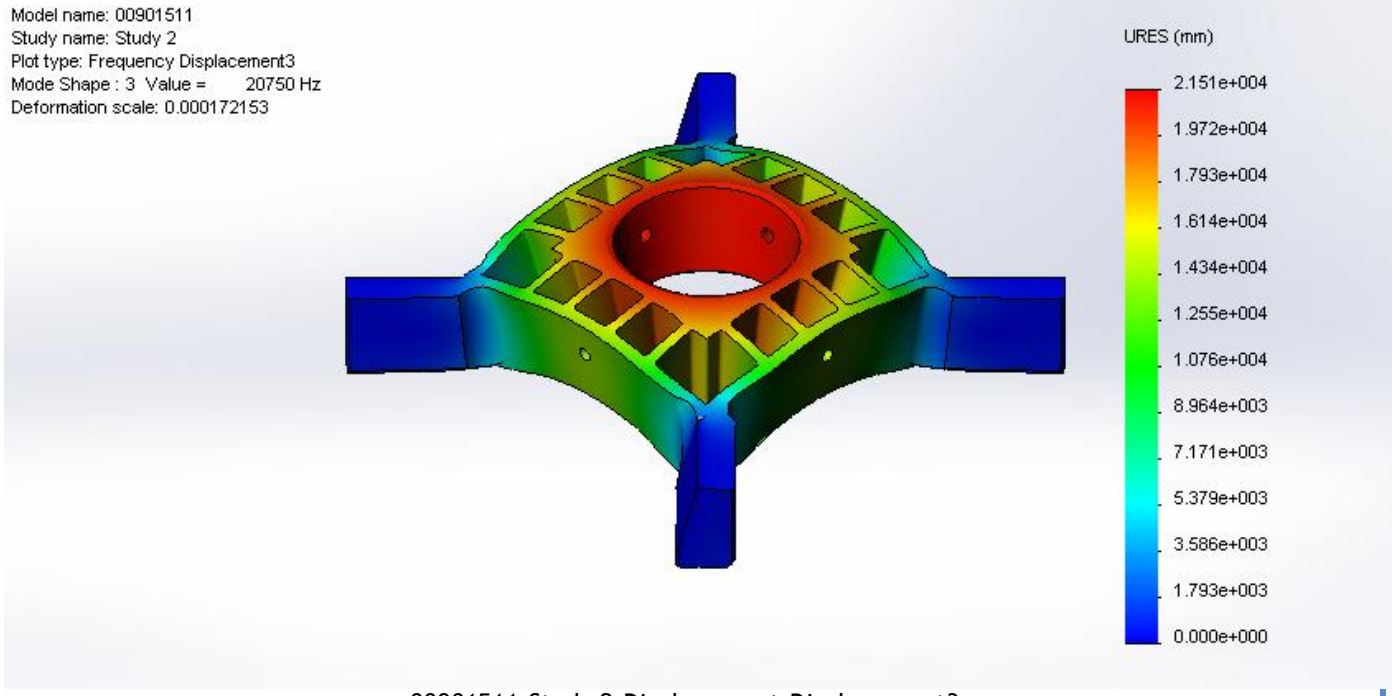

00901511-Study 2-Displacement-Displacement3

Name	Type	Min	Max
Displacement4	URES: Resultant Displacement Plot for Mode Shape: 4(Value = 28076.8 Hz)	0 mm Node: 1109	27416.8 mm Node: 107912

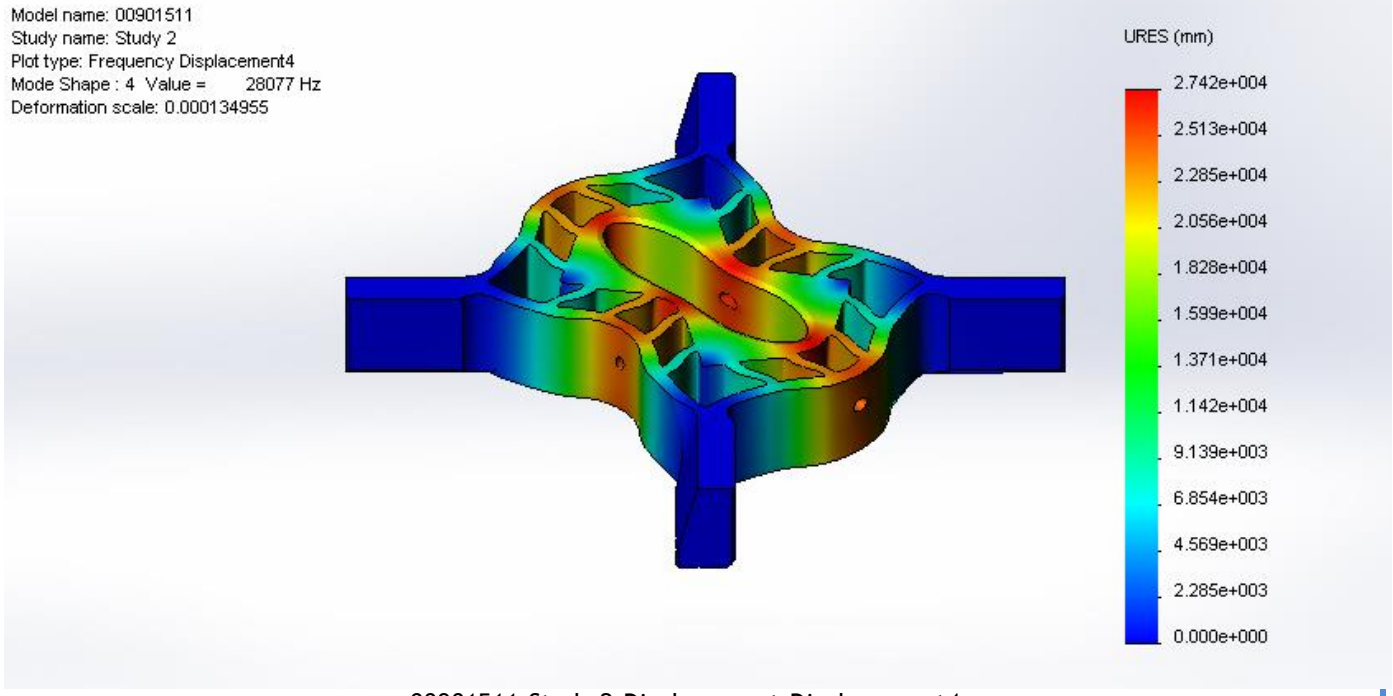

00901511-Study 2-Displacement-Displacement4

Name	Type	Min	Max
Displacement5	URES: Resultant Displacement Plot for Mode Shape: 5(Value = 29994.9 Hz)	0 mm Node: 1109	30632.4 mm Node: 100109

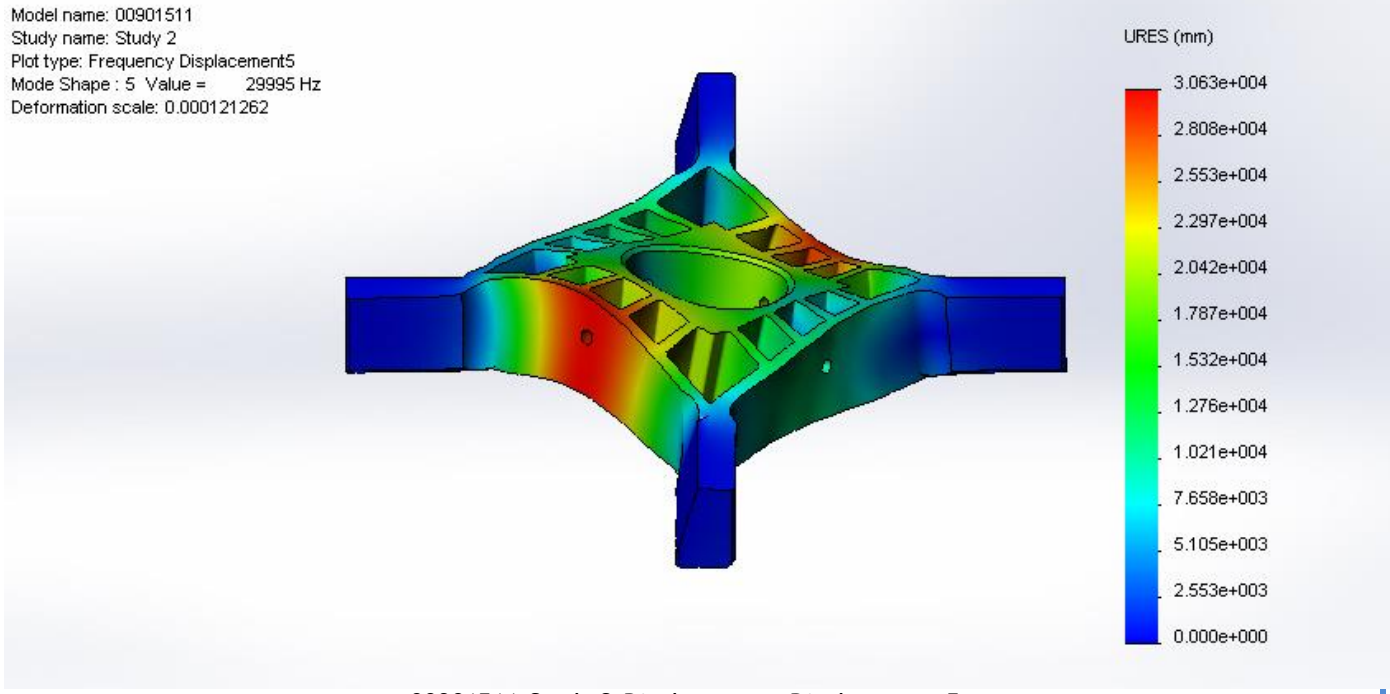

00901511-Study 2-Displacement-Displacement5

Mode List

Frequency Number	Hertz
1	18363
2	18370
3	20750
4	28077
5	29995

Mass Participation (Normalized)

Mode Number	Frequency(Hertz)	X direction	Y direction	Z direction
1	18363	0.082802	0.00010142	0.42638
2	18370	0.42549	0.00050577	0.082976
3	20750	0.00059609	0.58039	1.523e-008
4	28077	9.581e-006	1.6304e-007	8.2455e-009
5	29995	1.9444e-006	1.9623e-005	2.0924e-005
		Sum X = 0.5089	Sum Y = 0.58101	Sum Z = 0.50938

Conclusion

Comments:

The predicted lateral resonances are on the order of 18kHz, and the first vertical mode has a frequency of 20kHz. This model then exceeds the minimum specifications in terms of scanner speed

Appendix C

Fast Switch for Stick *and* Slip Scanner

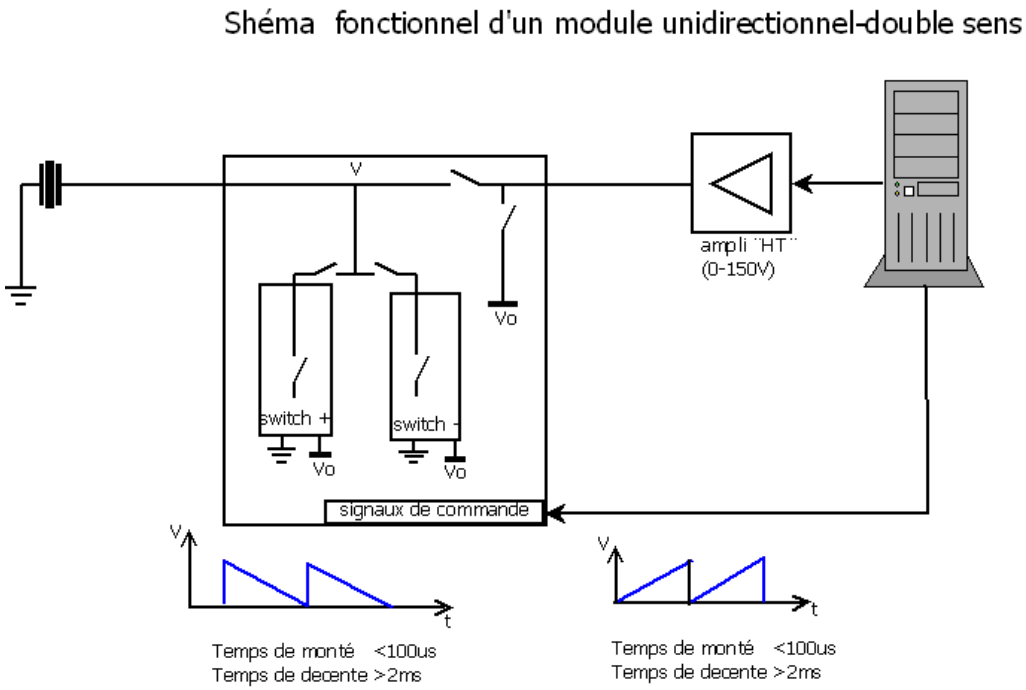

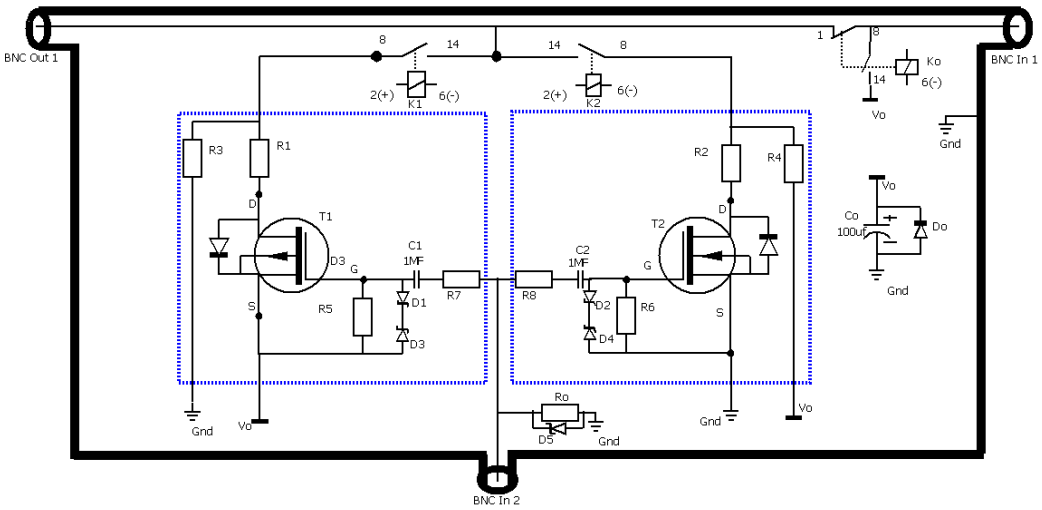
BNC Out 1
BNC In 1
BNC In 2
8
14
14
8
2(+)
K1
6(-)
2(+)
K2
6(-)
1
8
Ko
14
6(-)
Vo
Gnd
R3
R1
D
T1
D3
G
S
C1
1MF
R5
D1
R7
D3
R2
R4
D
T2
G
S
C2
1MF
R8
D2
R6
D4
Vo
Co
100uF
Do
Gnd
Gnd
Vo
Ro
D5
Gnd
Gnd
Vo